Lawrence Berkeley National Laboratory
Recent Work

Title
STUDIES IN NUCLEAR SPECTROSCOPY BY TWO-NUCLEON TRANSFER REACTIONS

Permalink
https://escholarship.org/uc/item/18p664f8

Author
Pehl, Richard H.

Publication Date
1963-08-28

University of California

Ernest O. Lawrence Radiation Laboratory

STUDIES IN NUCLEAR SPECTROSCOPY BY TWO-NUCLEON TRANSFER REACTIONS

DISCLAIMER

UNIVERSITY OF CALIFORNIA

STUDIES IN NUCLEAR SPECTROSCOPY BY TWO-NUCLEON TRANSFER REACTIONS

Richard H. Pehl

(Ph.D. Thesis)

August 28, 1963

STUDIES IN NUCLEAR SPECTROSCOPY BY TWO-NUCLEON TRANSFER REACTIONS

Contents

STUDIES IN NUCLEAR SPECTROSCOPY BY TWO-NUCLEON TRANSFER REACTIONS

Richard H. Pehl

Lawrence Radiation Laboratory
University of California
Berkeley, California

August 28, 1963

ABSTRACT

Alpha particle energy spectra from (d,α) reactions on Li^6, Be^9, C^{12}, N^{14}, and O^{16} have been obtained using 24-MeV deuterons. The development of a high-resolution semiconductor $E - \frac{dE}{dx}$ counter telescope made possible the observation of alpha particle groups arising from the formation of final states of higher excitation than previously studied by this reaction. Angular distributions corresponding to resolvable final states are presented.

Marked variation in the relative cross sections of final states was observed in most of the alpha particle energy spectra. In an effort to explain the nature of this preferential population these final states are correlated, where possible, with their expected configurations. The removal of two nucleons from the target nucleus should favorably excite levels whose configuration is two holes relative to the target configuration. Experimentally, however, formation of levels that require additional nucleon excitation are not appreciably inhibited in some cases. Possibly more than one reaction mechanism should be considered. The present evidence predominantly favors a pickup mechanism over knockout, but the relatively large cross section to several levels can be explained more easily by invoking a knockout mechanism.

The difficulties involved in using the (d,α) reaction to test the validity of the isotopic-spin selection rule are discussed. An extensive review of the $O^{16}(d,\alpha)N^{14*}$ (2.31-MeV) transition over a range of bombarding energies is presented.

A fairly extensive distorted-wave Born-approximation analysis has been carried out for several of the (d,α) transitions studied. Good fits to the alpha particle angular distributions were obtained. The outstanding characteristic of this analysis was the strong preference for L=2 transitions relative to L=0 transitions.

I. INTRODUCTION

Studies of both the relative and absolute values of the differential cross sections for various direct nuclear reactions have given insight into the detailed nature of nuclear structure. Single-nucleon transfer reactions, such as (p,d) and (d,p), have been used for a number of years as a method to obtain spectroscopic information. (See for example reference 1 and references contained therein.) Two-nucleon transfer reactions such as (d,α), (α,d), (He^3,n), (t,p), and (α,Li^6) are also of interest. These reactions can reach states that have two holes or particles excited relative to the ground state, so that additional states not excited in single-nucleon transfer reactions can be investigated. For sufficiently high bombarding energies these reactions have the general features of a direct reaction: they are (a) strongly selective in the levels that are excited, and (b) the angular distributions of the outgoing particles corresponding to the formation of the strongly excited levels are peaked at forward angles.[2,3,4] Hence, these reactions may prove to be another valuable tool for studying nuclear structure.

Previous attempts to analyze two-nucleon transfer reactions have made use of plane-wave Born-approximation (PWBA) calculations. However, to obtain a detailed agreement between theory and experiment it is necessary to take proper account of the interactions in the entrance and exit channels. That is to say the scattering and partial absorption of the incident particle, before the actual reaction event, and the emitted particle after, can have an important effect on the differential cross section. As shown by Tobacman[5] these distorted-wave Born-approximation (DWBA) calculations give superior fits to the angular distributions of single-nucleon transfer reactions. Thus a DWBA calculation should be superior for two-nucleon transfer reactions also. To investigate the possibility of spectroscopic identification of levels through

fitting the alpha particle angular distribution from a (d,α) reaction, a fairly extensive DWBA analysis has been carried out for several of the (d,α) reactions studied in this work, using the program developed by Glendenning.[6]

A measurement of the relative cross sections to the levels in a given nucleus made by different reactions — e.g., $C^{12}(\alpha,d)N^{14}$, $N^{14}(\alpha,\alpha')N^{14}$, and $O^{16}(d,\alpha)N^{14}$ — can give information concerning both the configuration of the level and the reaction mechanisms involved. It should be emphasized that these two facets are inherently tied together. Several such comparisons are discussed in this work.

Direct (d,α) reactions can make only final states having the same isotopic spin as the target nucleus if nuclear forces are charge-independent. Since the isotopic-spin operator does not commute with the nuclear Coulomb-force operator, the resultant isotopic-spin impurity means that the isotopic-spin selection rule is not strictly obeyed. Thus this reaction can be used to test the validity of the isotopic-spin slection rule.[7]

There has also been considerable speculation whether reactions such as (d,α) proceed by a pickup or knockout mechanism.[8,9] Although it is very unlikely that one could learn anything about the reaction mechanism from fitting angular distributions, a comparison of the magnitudes of the cross sections for (d,α) reactions on different targets might be valuable.

In order to investigate the above possibilities, (d,α) reactions on Li^6, Be^9, C^{12}, N^{14}, and O^{16} were studied using 24-MeV deuterons. For a comparison of final states the $B^{10}(\alpha,d)C^{12}$ reaction was also investigated.

II.   EXPERIMENTAL PROCEDURES

A.   Machine and External-Beam Facilities

The 24-MeV deuterons and 48-MeV alpha particles that initiated the reactions studied were obtained by using the external beam of the Crocker Laboratory 60-inch cyclotron. As shown in Fig. 1 the beam was brought out through a long iron pipe, focused by a quadrupole magnet, and directed by a small steering magnet through a 3/16-in.-diameter graphite collimator and a 3/16-in-diameter tantalum baffle collimator into a 36-in.-diameter scattering chamber.

After passing through the chamber the beam was collected in a Faraday cup and integrated. Two remotely controlled twelve-position foil wheels — located between the scattering chamber and the Faraday cup, and containing various thicknesses of Al absorber — were used to determine the mean energy of the beam. A plot of beam intensity at the Faraday cup vs. thickness of Al absorber was used to determine the absorber corresponding to one-half the maximum beam intensity. These ranges in Al were converted into energies by means of range-energy tables[10] based on experimental proton range-energy data.[11]

The particle detectors were mounted on a remotely controlled table that comprised the bottom of the scattering chamber,[12,13,14] and could be rotated to any desired angle. However, the edge of the detector holder intercepted part of the beam when measurements were made at less than 6 deg or greater than 174 deg (laboratory system). A remotely controlled target holder was suspended from the lid of the chamber. The scattering chamber was evacuated by a local pumping system, which consisted of a water-cooled 6-in. diffusion pump backed by a mechanical pump.

A twelve-position foil wheel containing various thicknesses of Al absorber, which could be operated by remote control, was placed immediately in front of the detectors. This allowed one to vary the
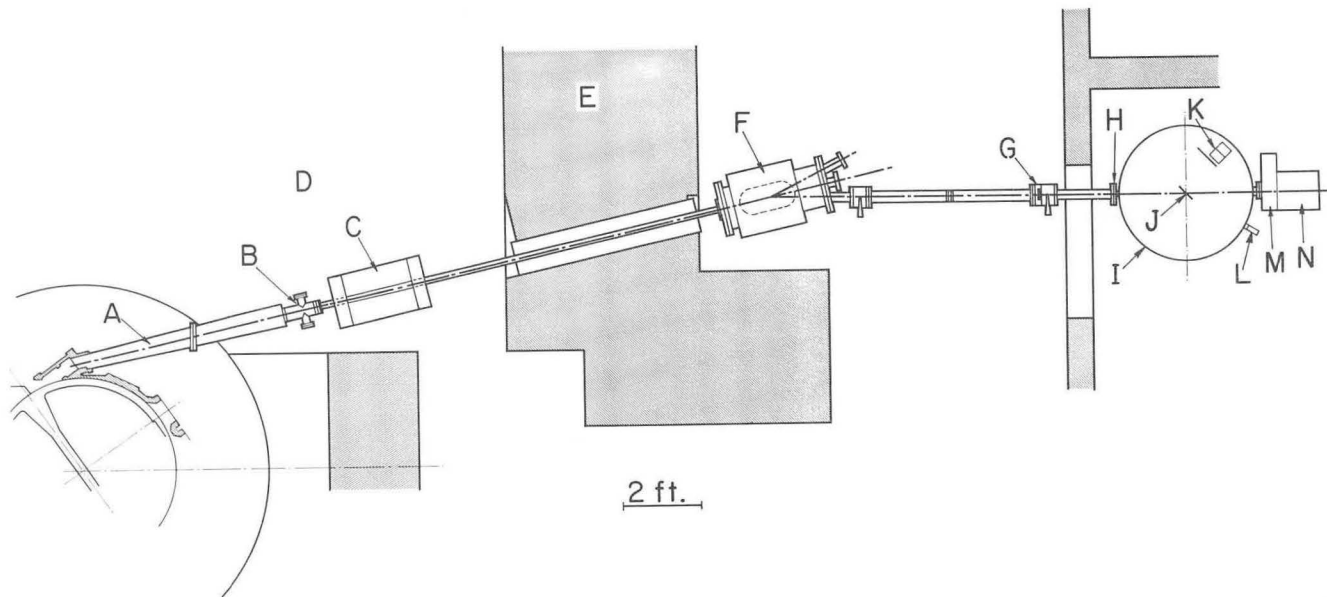
Fig. 1. Experimental arrangement: A, iron pipe; B, adjustable
slit; C, quadrupole focusing magnet; D, cyclotron vault;
E, shielding wall; F, steering magnet; G, 3/16-in.-diameter
graphite collimator; H, 3/16-in.-diameter tantalum baffle
collimator; I, 36-in. scattering chamber; J, target; K,
counter telescope and foil wheel; L, monitor; M, foil
wheel for measuring beam energy; and N, Faraday cup.

MUB-2118

energy of the particles incident on the detectors, which was useful for energy calibrations and for adjusting the analog pulse multiplier, as described later. In addition a Th^{228} alpha source, which was used for checking counters and for energy calibrations, was attached to the foil wheel.

During some of the runs a monitor, consisting of a CsI (Tl) crystal mounted outside the scattering chamber and separated from it by a thin Al window, detected the elastically scattered beam particles at a fixed angle (approx 20 deg). The monitor was useful in determining whether the target thickness had changed during the course of a run and as a check on the stability of the Faraday cup and integrating electrometer.

B. Detectors and Electronics

1. Particle Identification

In the energy region above a few MeV, simple single-counter detecting systems generally cannot be employed because of the many side reactions which obscure the reaction of interest. For example, when 24-MeV deuterons interact with a C^{12} target the following reactions occur:

$$C^{12}(d,\alpha)B^{10},$$
$$C^{12}(d,He^3)B^{11},$$
$$C^{12}(d,t)C^{11},$$
$$C^{12}(d,d)C^{12},$$
$$C^{12}(d,p)C^{13}.$$
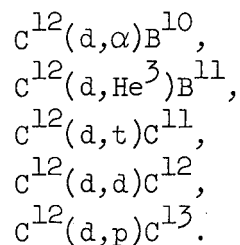
In each of these reactions the outgoing reaction particles have energies corresponding to the energy levels of the final nuclei. All of these reactions occur with approximately equal probability at high energy, and a detector will produce pulses corresponding to protons, deuterons,

tritons, He^3, and alpha particles from each of the above reactions. When two or more particle groups are superimposed it is extremely difficult to tell much about the reaction.

During the course of the experimental work several methods were used to separate the various particle groups so that they could be observed independently. The first (d,α) results were obtained using a single p-n junction silicon detector. (A more detailed description of the detectors is given in the following section.) The discrimination of alpha particles from protons, deuterons, and tritons depended on the fact that the high-energy charge-one particles completely penetrated the detector and thus expended only part of their energy in the depletion region of the detector. Since the depth of the depletion region is proportional to the square root of the applied reverse bias voltage,[15] the detector was operated with a voltage that produced a depletion region corresponding to the range of the maximum energy of the measured alpha particles. However, the "background" of charge-one particles obscured the observation of low-energy alpha particles corresponding to highly excited levels of the residual nucleus. In addition, He^3 ions could not be distinguished from alpha particles.

The removal of some of the charge-one-particle background was accomplished by placing a lithium-drifted p-i-n junction silicon detector behind the first counter. The Li-drifted detector was connected in anticoincidence with respect to the first counter; i.e., a particle that traversed the first counter and also produced a pulse in the second counter was not recorded.

The method used for the (α,d) work and for the later (d,α) results made use of a transmission counter which measured an energy loss ΔE proportional to the rate of energy loss dE/dx and a stopping counter which measured the remaining energy, E. Pulses from these counters were fed into an analog pulse multiplier,[16,17] the output of which is proportional to the product of the mass of the particle times the square of its charge.

The principle of operation of the multiplier arises from the approximate relationship obtained from the nonrelativistic equation for the rate of energy loss of charged particles as they pass through matter. This equation can be stated[18]

$$\frac{dE}{dx} = \frac{C_1 M Z^2}{E} \ln C_2 \frac{E}{M} ,$$

where M, Z, and E are the mass, charge, and energy of the particle, respectively, and C_1 and C_2 are products of constants. It has been shown[17] that the addition of a properly selected constant, E_0 , to the total energy of a particle will partially compensate for the ln factor in the above equation so that — over a wide range of energies — the product of $(E + E_0)$ and dE/dx will be closely proportional to the product of the mass of the particle times the square of its charge. Since the measurement of dE/dx introduces a finite energy loss, ΔE, it is necessary to add to the measured energy from the stopping counter a certain amount of ΔE as KΔE, so that E and dE/dx will correspond to the same particle energy (in first approximation K would be 1/2). The final expression is then

$$M Z^2 \approx (E + E_0 + K\Delta E) \Delta E .$$

The computer circuit utilizes the ΔE and E pulses to perform the multiplication

$$(A + B)^2 - (A - B)^2 = 4 AB ,$$

where A = $E + E_0 + K\Delta E$ and B = ΔE. The squaring is performed by two Raytheon QK-329 square-law tubes.

In actual operation K and E_0 are left as adjustable parameters used to optimize the particle separation. Since E_0 is introduced as a dc bias on the deflectors of the squaring tubes, one can have spurious

output pulses arising from the product of E_0 and ΔE when particles stop in the ΔE detector. These spurious pulses are eliminated in the multiplier spectra by requiring a coincidence between an E pulse and this output pulse.

2. Detector System for (d,α) Reactions

The advantages of semiconductor dE/dx transmission and E counters have been described by Wegner.[19] However, slices of silicon thin enough to be used as transmission counters for (d,α) reactions initiated by 24-MeV deuterons (≈ 2 mils) are brittle and break easily. Therefore, a hole was lapped in the center of a 10- to 14-mil silicon slice to give a thin central region supported by a thicker outer ring where contacts could safely be made (see Fig. 2).

Starting with a phosphorous-diffused 2000 ohm-cm p-type silicon mesa-type counter,[20] a hole was lapped into the back side of the counter to such a depth as to leave approximately 1 mil more than the desired thickness in the central region.

The holes were lapped by using grooved brass laps 5/32 or 7/32 in. in diameter rotated 1/32 in. off center at a rate of 120 rpm. The crystal, cemented with wax to an optically flat glass plate, was rotated in the opposite direction at 120 rpm and lapped with 6-μ diamond compound. The lapped side was then etched in CP-4, a hydrofluoric nitric acetic acid etch, to obtain the final thickness.

To complete the counter, a 1000-$\overset{\text{o}}{\text{A}}$ thickness of Al metal was evaporated onto the back surface and alloyed with the silicon at the eutectic temperature, 577°C. If the junction edge was damaged during the grinding operation the junction was reetched.

Thickness profiles were obtained by using a metallurgical microscope at a magnification of 500. The top surface of a glass microscope slide, on which the face of the counter rested, was used as the reference for measurement. Figure 3 shows a typical profile after etching, for the 5/32-in. lapped hole.

Phosphorous diffused
surface

0.012in.

p-type silicon

Al-Si eutectic over entire
back surface

0.800in.
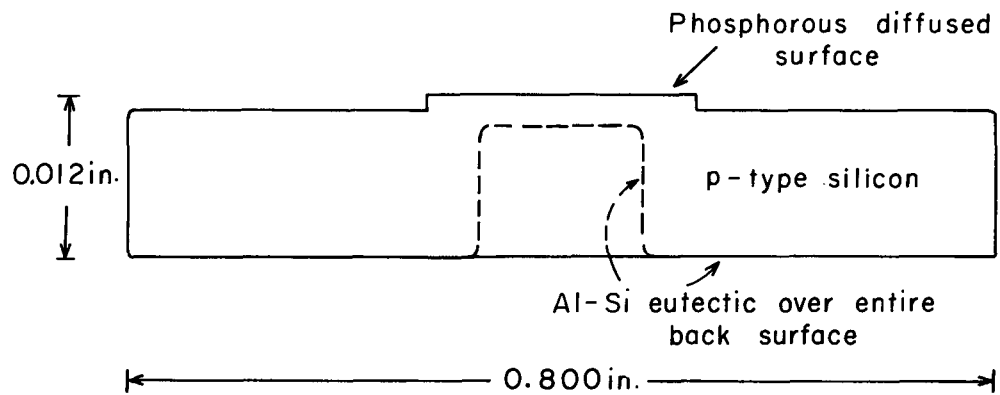
MU-25670

Fig. 2. Diagram of transmission counter.

Fig. 3. Typical thickness profile after etching. Two sections at right angles are shown.

Both Au- and Al-alloyed back contacts were tried. Counters with Au backings showed greater reverse bias currents (Fig. 4). A decrease in the slope of the current-voltage plot at voltages higher than requi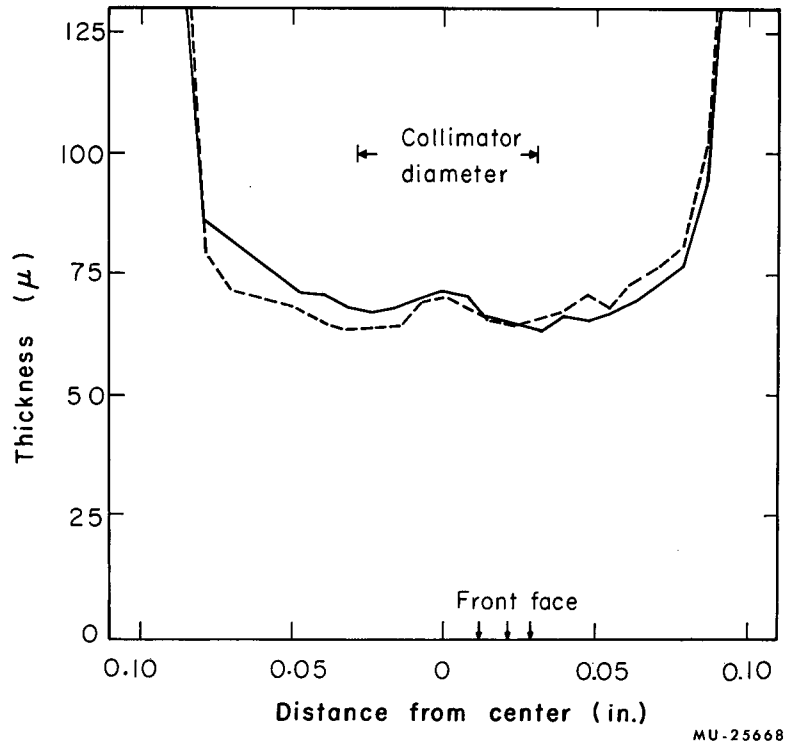red to fully deplete the thin central region was not observed. Such a decrease would be expected if a large portion of the leakage current was due to charge-carrier injection from the back surface.[21]

The counters were tested with 5.477-MeV alpha particles from Am[241] collimated by a 60-mil-diameter aperture. Pulses were observed, as expected, when the particles entered the front, because of the "built in" field of the junction located at the front face. A broad peak was also observed for particles entering the back of the counter, where some of the charge was collected by diffusion. The peak height increased only slightly after 5-V bias and appeared in the same channel whether particles entered the front or the back face (Fig. 5), indicating that the depletion layer was driven all the way to the back surface of the thin section, with essentially no dead layer. The resolution of the alpha particles was 35 keV, full width at half maximum (FWHM).

The resolution of a 2.7-mil-thick transmission counter for incident 48-MeV alpha particles was about 15%. The thickness variation alone within the 60-mil-diameter collimated area could cause a 12% spread if equal cross section is assumed for each thickness. The statistical fluctuation of energy loss in a uniform 2.7-mil-thick absorber, in which the energy loss is 1.92 MeV, is 12.5% (FWHM).[22] Of course for the lower-energy alpha particles arising from the (d,α) reactions studied the statistical fluctuation is much smaller.

A schematic drawing of the holders used for these counters, and all the other semiconductor detectors discussed later, is shown in Fig. 6.

Two different types of semiconductor E detectors were used. The first was a phosphorous-diffused p-type silicon mesa-type counter[20] (similar to the ΔE counter before the hole was lapped). This detector had a depletion thickness of 66.7 mg/cm^2, which corresponds to 23.2-MeV
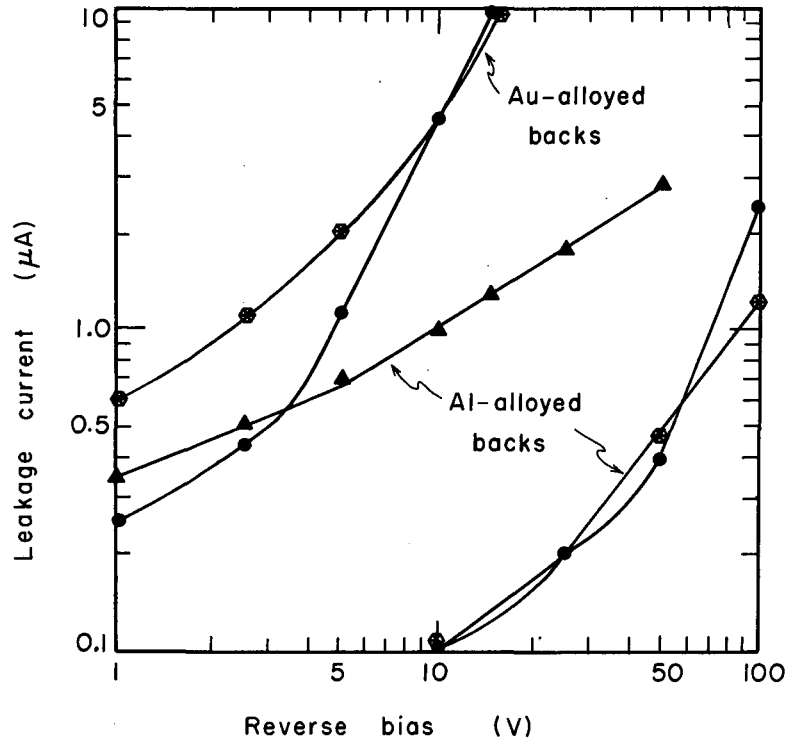
Fig. 4. Typical reverse bias currents for Al- and Au-alloyed
back contacts.
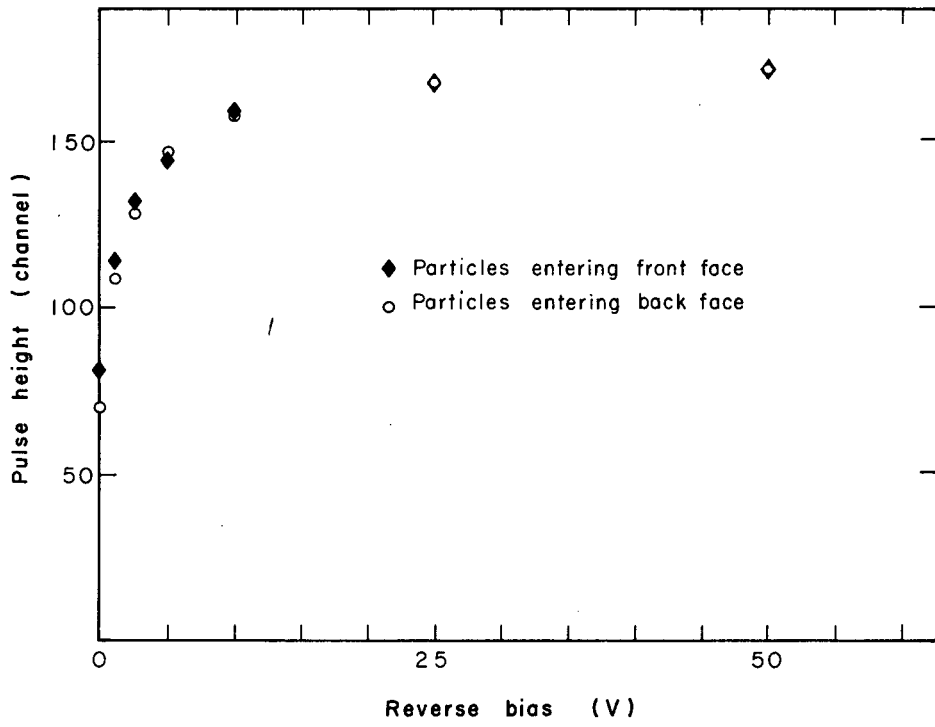
Fig. 5. Pulse height vs bias voltage.

BNC connection

Modified alligator clip

Signal

Steel wire front contact

Lucite plate

Silver washer on which detector rests (connected to ground on BNC)
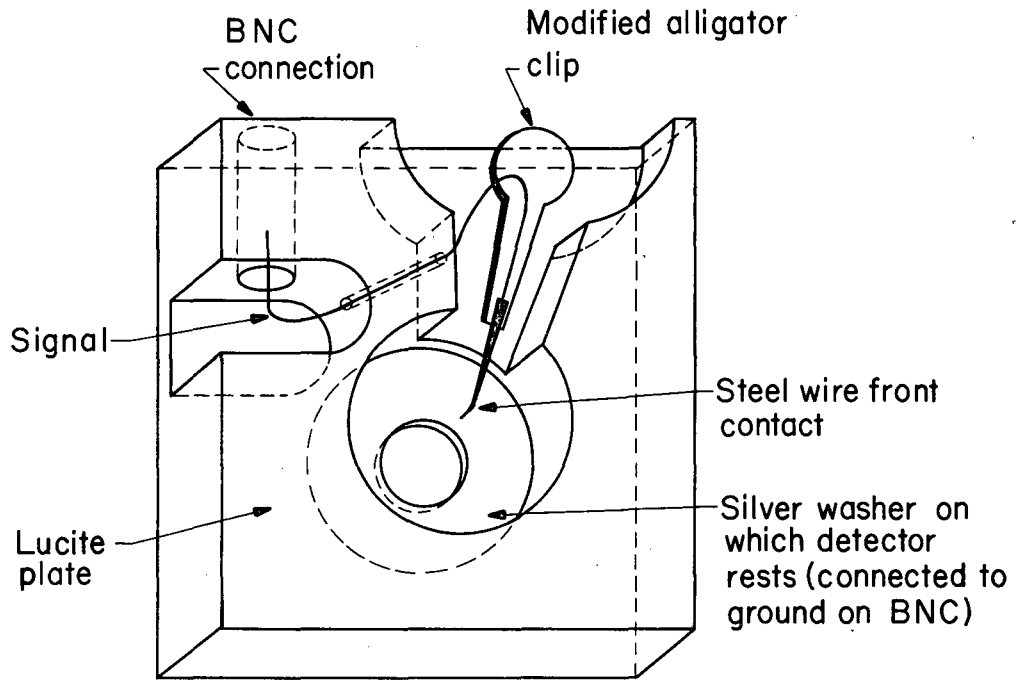
MU-32057

Fig. 6. Diagram of counter holder.

alpha particles, when a 240-V reverse bias was applied. Lithium-drifted p-i-n junction detectors[23] of various thicknesses were used when studying (d,α) reactions that produced alpha particles above 23 MeV.

The counter system was placed so that the tantalum baffle collimator, which preceded the ΔE detector and defined the solid angle, was 8 to 12.5 in. from the target. The collimator diameter, which could be easily varied, was 60 mils when the thin transmission counter was used, because of the small thin area. This was replaced by a 125-mil-diameter collimator when the ΔE counter was not used.

The loss of resolution in the E counter due to the nonuniform transmission counter was compensated by adding the pulses from the two counters in the appropriate ratio. The optimum resolution of the added pulses was about 240 keV for solid targets. The resolution was limited by the approximately 0.75% energy spread in the cyclotron beam. The simple passive pulse-adder circuit is shown in the electronic block diagram, Fig. 7.

3. Detector System for (α,d) Reactions

The ΔE counter was the p-n junction detector used as an E counter for (d,α) reactions. Its resolution for 20.5-MeV incident deuterons was 10.9% for a 2.1-MeV energy drop. A 150-mil-thick Li-drifted p-i-n junction detector[23] served as the E counter. The optimum resolution of the system was about 350 keV when a 30-mil-thick Li-drifted detector was used for the ΔE counter.

The general electronic circuitry was the same as for the (d,α) reactions (Fig. 7).

4. Pulse-Height Analyzers

A Penco 100-channel pulse-height analyzer and a RIDL 400-channel pulse-height analyzer were used to analyze the pulses from the detectors and the multiplier. These analyzers have a coincidence circuit, so that signal pulses can be required to possess a corresponding trigger pulse. The use of variable upper and lower discriminators permitted "single-channel" analysis of the trigger pulses.
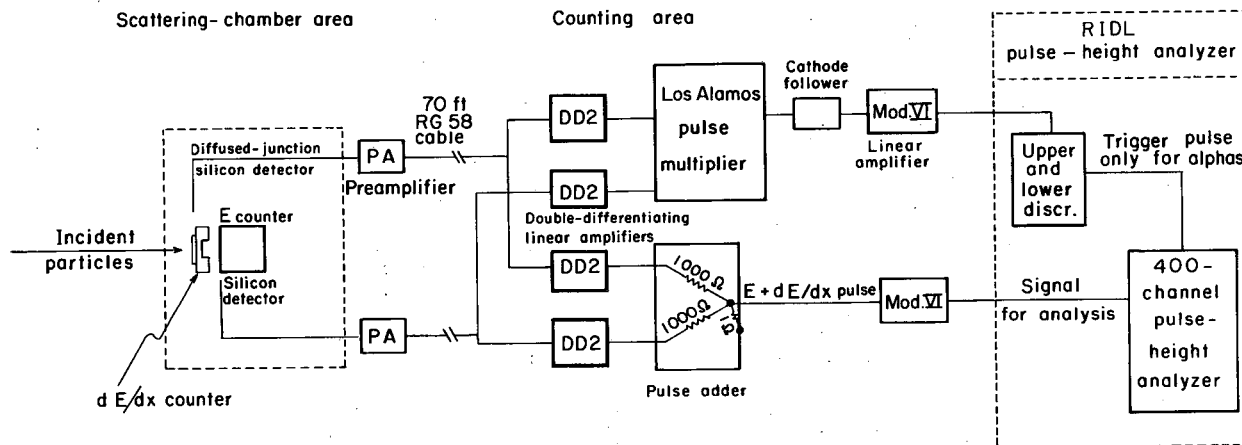
Fig. 7. The passive pulse-adder circuit, shown with complete
    electronics block diagram.

MU-26089

C.   METHOD OF OPERATION

1.   Pulse-Adder Adjustment

The 33.4-MeV alpha particles obtained by elastic scattering of 48-MeV alpha particles from a thin carbon foil at 62 deg (lab) were observed, and the size of the ΔE and E signals adjusted to give pulse heights in the same ratio as the energy calculated to be deposited by the alpha particles in the respective detectors. Small changes in the ΔE amplifier gain were then made to optimize the resolution of the pulse-adder output. These changes invariably proved to be very slight.

The adjustment was checked by moving the counter telescope to a smaller angle (to increase the counting rate) and varying the energy of the particles incident on the counters by means of Al absorbers. If the pulse adder was properly adjusted a plot of channel number vs energy would be linear.

2.   Multiplier Spectra

The preliminary tuning of the multiplier was done by following the procedure of Briscoe.[16] Only a discussion of the He^3 - He^4 separation will be given here since the adjustment for proton-deuteron-triton separation have been discussed at length elsewhere.[24,25]

The bombardment of an He^3 gas target by 48-MeV alpha particles produced the mixture of He^3 and He^4 ions used for the rough adjustment of the multiplier. The angle of observation was adjusted ($\approx$ 38 deg) to give approximately an equal number of He^3 and He^4 ions as shown by the pulse-adder output displayed on the pulse-height analyzer. The corresponding multiplier output in coincidence with an E trigger was then displayed on the analyzer, and the energy of the particles incident on the counter telescope was varied by means of Al absorbers. This enabled one to adjust the ΔE and E amplifier gains and the values of E_0

and $\bar{K}$ to obtain a multiplier pulse height as nearly energy-independent as possible. Final adjustment of the multiplier was made during the deuteron bombardment of the target to be investigated. A multiplier spectrum with optimum He^3 - He^4 separation is shown in Fig. 8.

Even though the transmission counter was very thin the low-energy alpha particles that left the residual nucleus highly excited dropped a large fraction of their energy in the ΔE detector. However, the multiplier apparently worked properly (i.e., the multiplier output signal remained essentially constant) when as much as 95% of the alpha energy was dropped in the ΔE counter. This knowledge should prove useful to anyone interested in using a multiplier for reactions such as (α, d) or (He^3, p) since much thicker ΔE counters can be used than were previously tried.

3. Energy Spectra

(The method of obtaining the energy spectra from the single-counter experiments will not be discussed in this section since such an operation is self-evident.)

The energy spectra from the various bombardments were obtained by using the pulse from the pulse adder as the signal to the pulse-height analyzer and the appropriately discriminated multiplier pulse as the trigger. This discrimination was determined by using the multiplier output as both signal and trigger to the analyzer, and adjusting the discriminators as follows. For (d, α) reactions the lower discriminator was adjusted to correspond to a pulse height slightly to the left of the He^3 peak and the upper discriminator was adjusted to correspond to a pulse height slightly to the right of the alpha peak. Under these conditions the energy spectra contained peaks arising from both He^3 ions and alpha particles. Generally the He^3 - He^4 separation was not sufficiently clean to permit complete removal of He^3 peaks from the (d, α) spectra without also losing alpha particles. However, several energy
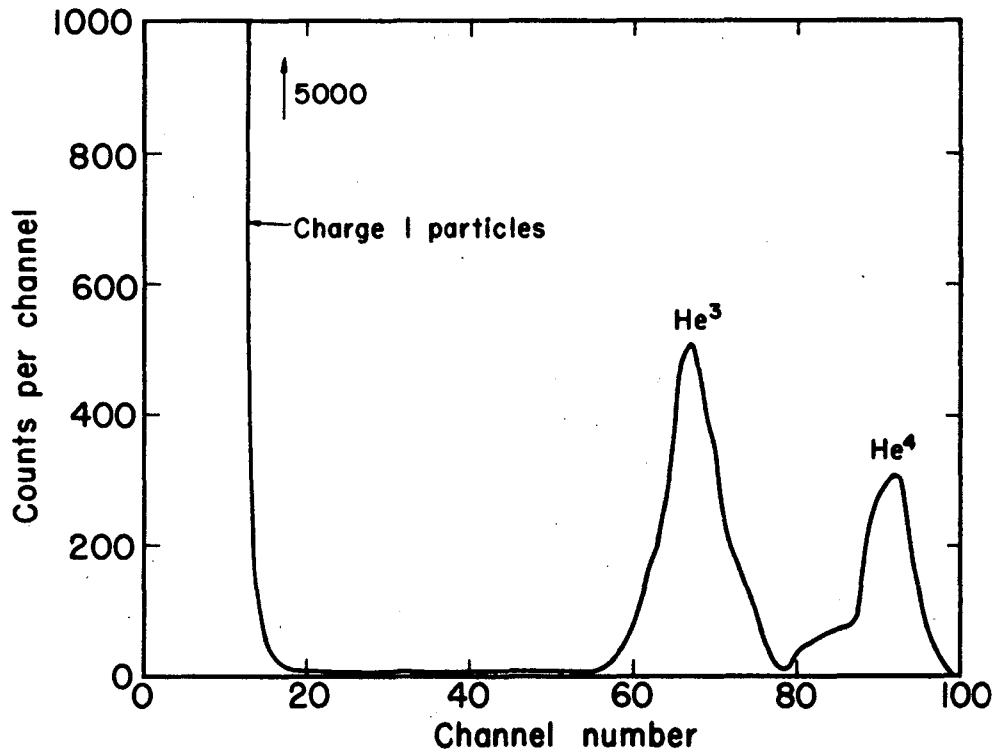
Fig. 8. Multiplier spectrum at a scattering angle of 15 deg (lab) from bombardment of O^{16} with 24-MeV deuterons.

spectra were obtained when the lower discriminator corresponded to the center of the He^3 - He^4 valley. This is discussed more thoroughly in Subsecs. III.C and III.F.1.

For (α,d) reactions the lower discriminator corresponded to the center of the proton-deuteron valley (Fig. 9), and the upper discriminator corresponded to the center of the deuteron-triton valley.

During the measurement of an angular distribution the multiplier spectra were observed and the discriminators reset at about 10-deg intervals.

D. TARGETS

1. Solid Targets

The Li^6 targets were self-supporting foils rolled from 99.3% enriched Li^6 metal (obtained from Oak Ridge National Laboratory). The target thickness was determined to be 10 mg/cm^2 ± 30% by measuring the beam range with the target both in and out and then converting[10,26] this differential range in Al to the range in Li^6. The large uncertainty in the thickness quoted above arises from target nonuniformity.

The Be^9 targets were self-supporting 2.8-mg/cm^2-thick foils obtained from the Brush Beryllium Co. In addition a 0.9-mg/cm^2 foil was made by etching 1-mil Be^9 foils with 1 $\underline{M}$ H_2SO_4.

The B^{10} targets were made as follows: (a) a suspension of B^{10} in 10% ethanol in water was formed, (b) the suspension was allowed to evaporate on a 0.1 mil Au foil, (c) another 0.1-mil Au foil was placed on top of the B^{10} and the resulting sandwhich pressed together under high pressure between two polished stainless steel plates. The targets so obtained varied in thickness between 0.7 and 1.2-mg/cm^2.

The C^{12} targets were prepared by diluting a "Dag" solution (colloidal graphite in isopropyl alcohol and acetone) with ethanol and actone. This solution was poured on a glass mirror and allowed to dry.
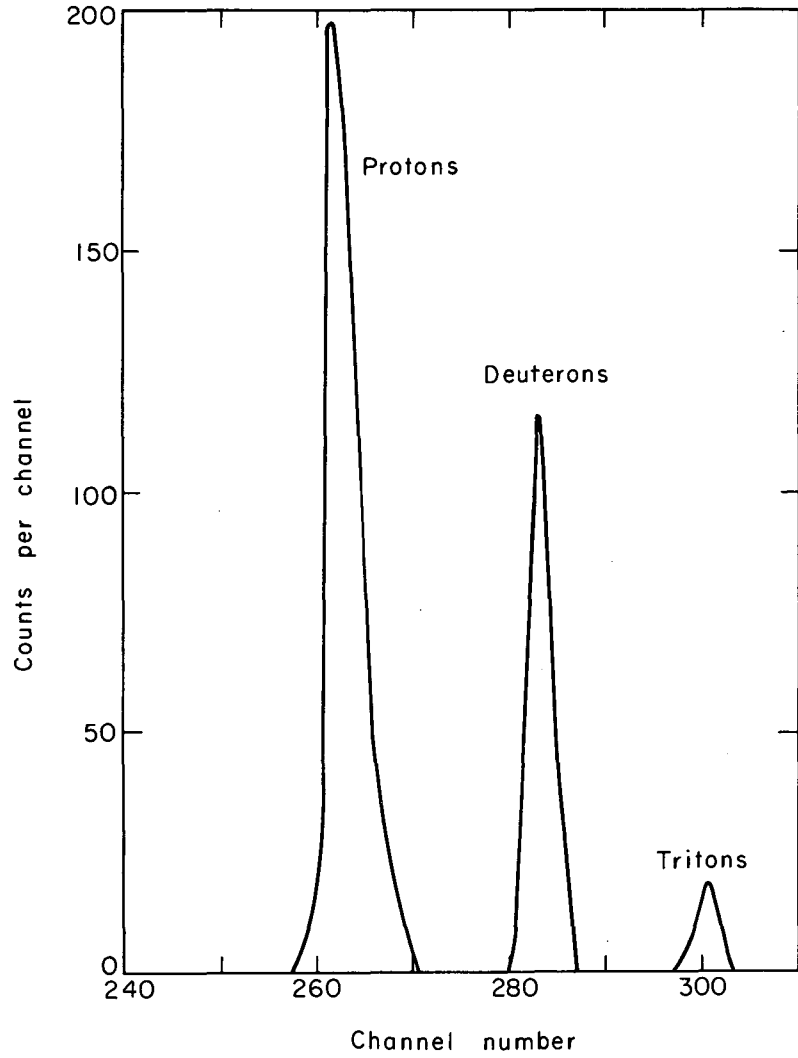
Fig. 9. Multiplier spectrum at a scattering angle of 15 deg (lab) from bombardment of O^{16} with 47-MeV alpha particles.

When the mirror was submerged in water the carbon film would rise to the surface. The film was then collected on cellophane and the water allowed to evaporate. When dry, self-supporting films about 0.2 mg/cm^2 thick and as large as 4 by 4 in. could be peeled from the cellophane. The uniformity of these targets varied by less than ± 10% but they were quite difficult to handle. Any oxygen impurity was almost completely removed by heating the targets to $1400^{\circ}C$ in a vacuum for several hours and then allowing them to cool to below $200^{\circ}C$ before exposure to air. When bombarded, these targets did not produce any peaks that could be attributed to an impurity. Recently these targets have been used for studying the $C^{12}(\alpha,d)N^{14}$ reaction and a small peak arising from an oxygen impurity observed as shown later in Fig. 29. However, the oxygen impurity may have been larger in the recent work because of the length of time (about two years) between target preparation and bombardment. Even if the small oxygen impurity were present at the time of the (d,α) work no peak arising from oxygen would have been observed. (The $O^{16}(\alpha,d)F^{18}$ peak observed is a "giant peak."[27])

Since different carbon targets varied in thickness by large factors, a thicker carbon target, which was prepared by carbonizing circles of Whatman filter paper, was used to determine the effective thickness of the thin carbon foils used for each run. The thickness of the filter paper targets, 2.6 mg/cm^2, was determined by weighing a known area.

2. Gas Targets

Natural nitrogen and oxygen gases were bombarded in a 3-in.-diameter 2.5-in.-high gas holder that was suspended from the target mount inside the scattering chamber. The gas pressures ranged from 45 to 73 cm Hg at about $18^{\circ}C$. An additional 125-mil-wide slit was positioned about 6.4 in. ahead of the counter collimator to define the solid angle. The effective target thicknesses ranged from about 0.4 to 0.6 mg/cm^2 when the beam was viewed at 90 deg and, of course, varied as $1/\sin\theta$, where θ is the angle of observation.

The gas holder had two approximately 120-deg 3/4-in.-high windows made of 1-mil-thick Dural; it could be rotated to permit measurements at any angle. This system was connected to an external manometer and a pumping unit so the gas pressure could be read and the gas changed. The effective deuteron energy was degraded about 0.3 MeV by the gas target.

E. EXPERIMENTAL CHECKS

In order to check the accuracy of the experimental system the following comparisons with previous measurements were made. Polystyrene and "filter paper" carbon targets were used to obtain $C^{12}(p,p)C^{12}$, $C^{12}(p,p')C^{12*}$ (4.43 MeV), and $p(p,p)p$ differential cross sections which agreed to within 8% with previous data.[28,29]

As discussed in more detail in Subsec. IV.B the $N^{14}(d,\alpha)C^{12}$ and $C^{12}(\alpha,d)N^{14}$ differential cross sections at bombarding energies of 23.8 and 48 MeV, respectively, should be very similar. The experimental agreement with the $C^{12}(\alpha,d)N^{14}$ data[3] was excellent.

F. DATA REDUCTION

1. Energy-Level Analysis

To determine the energies of the final states populated, an energy-vs-channel calibration of the pulse-height analyzer was made by systematically varying the energy of elastically scattered alpha particles incident on the counter telescope by means of Al absorbers and by using different angles of observation. A Th^{228} alpha source was used for the low-energy points of the calibration.

Spectra were obtained at a series of angles and the particle energies corresponding to peaks in the reaction spectrum determined. The difference in energy between the peak corresponding to the ground state transition and the other peaks was determined and these differences were then converted to energy separations between the particular excited

states and the ground state of the residual nucleus by means of a computer program which solved the equation[30]

$$E_b^{1/2} = \frac{(m_a m_b E_a)^{1/2} \cos\theta \pm \left\{ m_a m_b E_a \cos^2\theta + (m_y + m_b)\left[m_y Q + (m_y - m_a)E_a \right] \right\}^{1/2}}{m_y + m_b},$$

where E_b = energy of emitted particle in laboratory system,

E_a = energy of incident particle in laboratory system,

θ = laboratory angle of observation,

m_a = mass of incident particle,

m_b = mass of emitted particle,

m_y = mass of residual nucleus,

Q = kinetic energy released or absorbed in the reaction.

2. Differential and Total Cross Sections

The conversion of the number of counts in a specific peak to a differential cross section was done by standard methods (e.g., reference 31). The cross sections of levels that were not cleanly resolved experimentally were obtained by means of a computer program which fit the experimental spectrum by using gaussian-shaped peaks whose width and relative amplitudes were varied to obtain the lowest value of χ^2, where

$$\chi^2 = \sum_{n=1}^{N} \frac{\left[cts^{th}(n) - cts^{ex}(n) \right]^2}{cts^{ex}(n)},$$

where N is the number of channels over which the fit is made.

Total cross sections were obtained by integration of the differential cross sections according to

$$\sigma = 2\pi \int_0^\pi \frac{d\sigma}{d\Omega} \, \sin\theta \, (d\theta) = 2\pi \int_{-1}^1 \frac{d\sigma}{d\Omega} \, d(\cos\theta).$$

In practice, the second expression was evaluated by plotting $d\sigma/d\Omega$ vs $\cos\theta$ and measuring the area under this curve with a planimeter.

III. RESULTS AND DISCUSSION OF SPECIFIC REACTIONS

The reactions that were investigated are discussed separately in this section. The energy levels of the product nuclei observed in these reactions are correlated where possible with their expected configurations in an effort to determine the nature of any preferential population of final states that might arise. The respective angular distributions are included but the corresponding DWBA analysis is not discussed until Subsec. IV.C.3.

A. $\underline{Li^6(d,\alpha)He^4}$

This reaction has been studied previously only at low bombarding energies;[32,33] i.e., $\leq$ 5 MeV, except for brief investigations at 14.8 MeV[34] and 21.6 MeV.[35] In our experiment the angular distribution of the alpha particle group corresponding to the ground state of He^4, shown in Fig. 10, has been measured from 18 to 113 deg (c.m.). A typical energy spectrum at a laboratory scattering angle of 36 deg is shown in Fig. 11. Smooth curves have been drawn through the experimental points for all the energy spectra to be presented. The experimental work on this reaction was completed before the thin ΔE counters were developed and consequently these results were obtained with single counter systems. Counters of different thicknesses had to be used because the alpha particle energy changes rapidly as a function of angle when such a light target is bombarded.

Although the multiplier was not used the alpha particle group corresponding to the ground state of He^4 was well separated at all angles studied. The ground state Q value for the $Li^6(d,\alpha)He^4$ reaction is 22.365 MeV,[*] which is considerably greater than the energy of the

---

[*]Ground state Q values for all reactions discussed were taken from Ashby and Catron.[36]
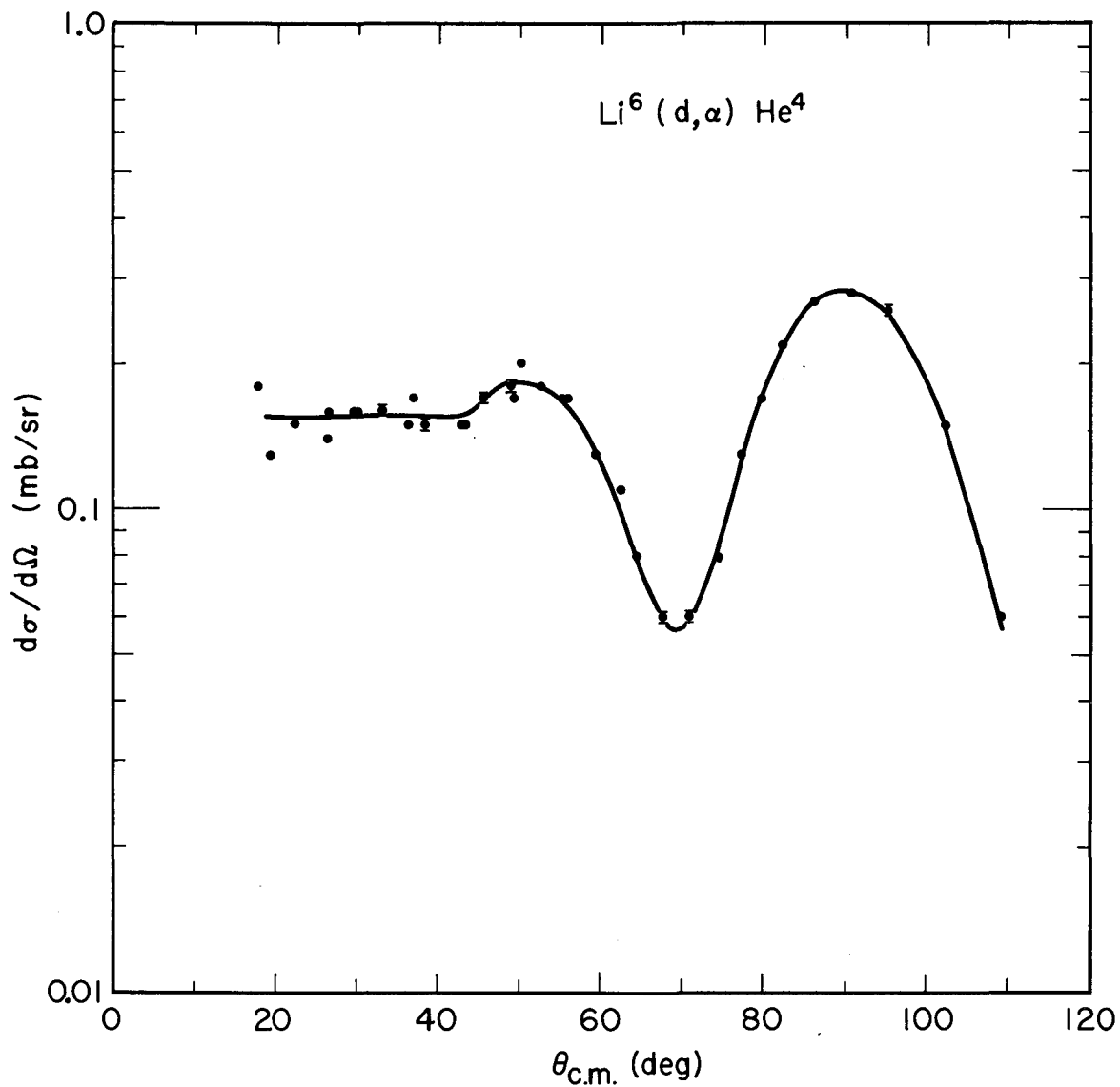
Fig. 10. Angular distribution of alpha particles from the Li[6] (d, α)He[4] transition.
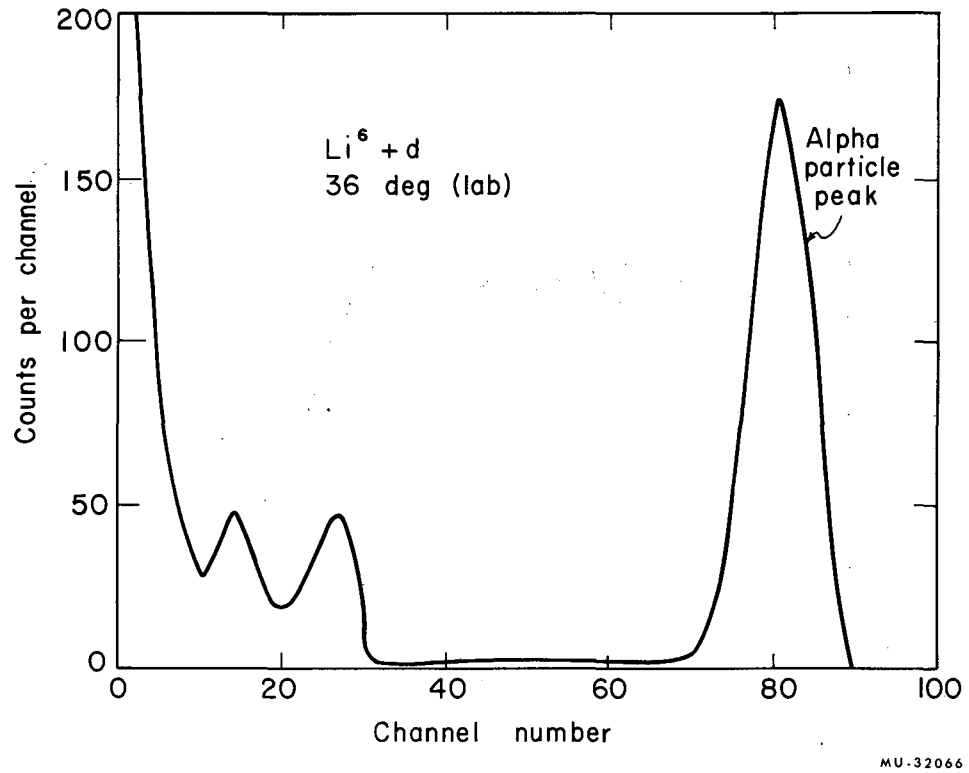
Fig. 11. Energy spectrum of the Li^6 + d reaction.

other charged particles produced by $Li^6 + d$:

$$Li^6 + d \rightarrow Li^7 + p \quad , \quad Q = 5.0267 \text{ MeV}$$
$$\rightarrow He^5 + He^3, \quad Q = 0.8445 \text{ MeV}$$
$$\rightarrow Li^5 + t \quad , \quad Q = 0.8304 \text{ MeV} .$$
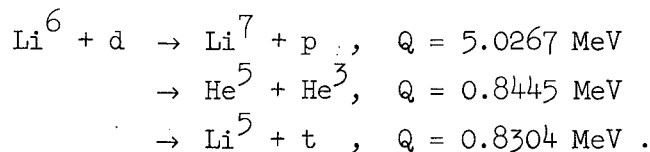
However, these charged particles and the elastically scattered deuterons prevented the observation of any indication of the broad peak that has been observed in other reactions — $t(p,n)He^3$ (references 37 and 38), $t(d,n)He^4$ (reference 39), $He^4(p,p')He^4$ (reference 40) — and interpreted as an indication of a broad excited state in He^4 at $\approx$ 22-MeV excitation.[37]

Sawicki[41] has calculated the angular distribution, assuming the "$\alpha + d$" model for Li^6 and a pickup mechanism. For the incident deuteron energy, 20 MeV, he predicts an angular distribution with a strong diffraction maximum at $\theta_{c.m.} = 40$ deg and minima at $\theta_{c.m.} = 17$ and 68 deg with an absolute value of $(d\sigma/d\Omega)_{\theta=0}$ between 0.2 and 0.4 $\times$ 10^{-3} mb/sr. The experimental angular distribution indicates that Sawicki's reaction mechanism may not be the most important one for 24-MeV deuterons. However, Zeidman and Monahan[35] have rederived the cross section, using the same assumptions and procedures as Sawicki, and find a large discrepancy between their results and Sawicki's, both in absolute magnitude and shape. These differences were not resolved after correspondence with Sawicki. Furthermore, they find approximate agreement with the 21.6-MeV data, both in absolute magnitude and shape. The absolute magnitudes of the experimental cross sections for 14.8-, 21.6-, and 24-MeV deuterons do not differ widely, (factor of two at the most), but the shape of the angular distribution fluctuates markedly. The approximate agreement obtained by Zeidman and Monahan indicates that if Sawicki's reaction mechanism is appropriate his derivation of the theoretical cross section contains an error.

It is interesting to note that the shape of the angular distribution for 46.12-MeV alpha particles scattering from helium[42] is similar to the $Li^6(d,\alpha)He^4$ angular distribution at E_d = 24 MeV except at small angles where one would expect Coulomb scattering to become highly dominant for $He^4 + He^4$. (The relative energy of the two residual alpha particles from the $Li^6(d,\alpha)He^4$ reaction at E_d = 24 MeV is 46.36 MeV; i.e., at 0 deg the "emitted alpha" has an energy of 38.78 MeV and the "recoil alpha" an energy of 7.58 MeV. Since they are moving in opposite directions their relative energy is the sum of their respective energies.)

B. $\underline{Be^9(d,\alpha)Li^7}$

The primary reason for investigating this reaction was to look for the 5/2- state that shell model calculations predict[43] at about 5 MeV in Li^7, but which has not been experimentally observed.[32,44] Early calculations by Wildermuth indicated this "level" was not expected on the basis of the cluster model,[45] and consequently offered a possible test for the relative merit of the two theoretical approaches. However, later cluster model calculations[46] predict a 5/2- state at about 5.6 MeV in Li^7. Calculations by Clegg based on a unified model of Li^7 also predict a 5/2- state at about this excitation.[47]

Previous investigations of this reaction have been carried out at low bombarding energies, except for one observation using 14-MeV deuterons.[48] However, this later work was hampered by poor resolution and an appreciable oxygen impurity in the target.

Neither the predicted level at about 5.5 MeV nor the doubtful level at 6.54 MeV were observed in our work, which covered the angular range between 11 and 45 deg (lab). Additional information indicates that a positive-parity level at about 6.5-MeV excitation in Li^7 does not exist. Hamburger and Cameron[34] searched for this level in the reaction

$Li^6(d,p)Li^7$ and found that the previous observation of a level at 6.54-MeV excitation[49] might arise from a contaminant in the experiment. Theoretical calculations[50] based on the cluster model indicate that the occurrence of a positive-parity state at an excitation energy as low as 6.54 MeV would be hard to explain. Figure 12 shows a typical alpha particle energy spectrum at a laboratory scattering angle of 21 deg. As can be seen there is no indication whatsoever for either of the above mentioned levels or of any oxygen impurity in the target.

The alpha particle continuum that begins at a position corresponding to an excitation in Li^7 of about 2.5 MeV probably arises because of several-body breakup. The various reactions that could produce alpha particles are:

$$Be^9 + d \rightarrow \alpha + Li^7 \qquad Q = 7.153 \text{ MeV},$$
$$\rightarrow \alpha + \alpha \quad + t \quad Q = 4.687 \text{ MeV},$$
$$\rightarrow \alpha + Li^6 + n \quad Q = -0.100 \text{ MeV},$$
$$\rightarrow \alpha + He^5 + d \quad Q = -2.528 \text{ MeV},$$
$$\rightarrow \alpha + He^6 + p \quad Q = -2.832 \text{ MeV}.$$
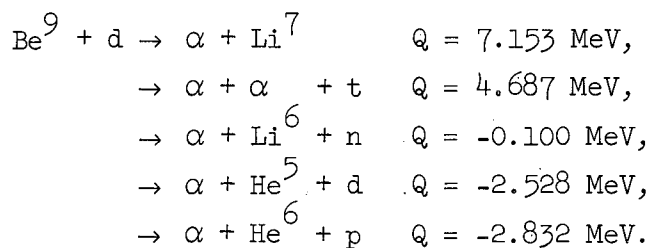
Thus the continuum begins at an alpha energy corresponding to the upper limit from the $Be^9 + d \rightarrow 2\alpha + t$ reaction.

Table I compares the Li^7 energy levels observed with those previously reported. Although there is no indication of any Li^7 levels above the level at 7.47 MeV the large alpha continuum would obscure any level made with a relatively small cross section.

In the cluster model picture the ground state, 0.478-MeV, and 4.63-MeV levels are essentially pure alpha cluster plus triton cluster configurations,[46,51] whereas the 7.47-MeV level is a Li^6 cluster plus neutron configuration.[50] The latter level is made in relatively large amount via the (d,α) reaction. Kunz[52] has been able to describe the Be^9 levels below 11 MeV by an alpha - alpha plus neutron configuration.
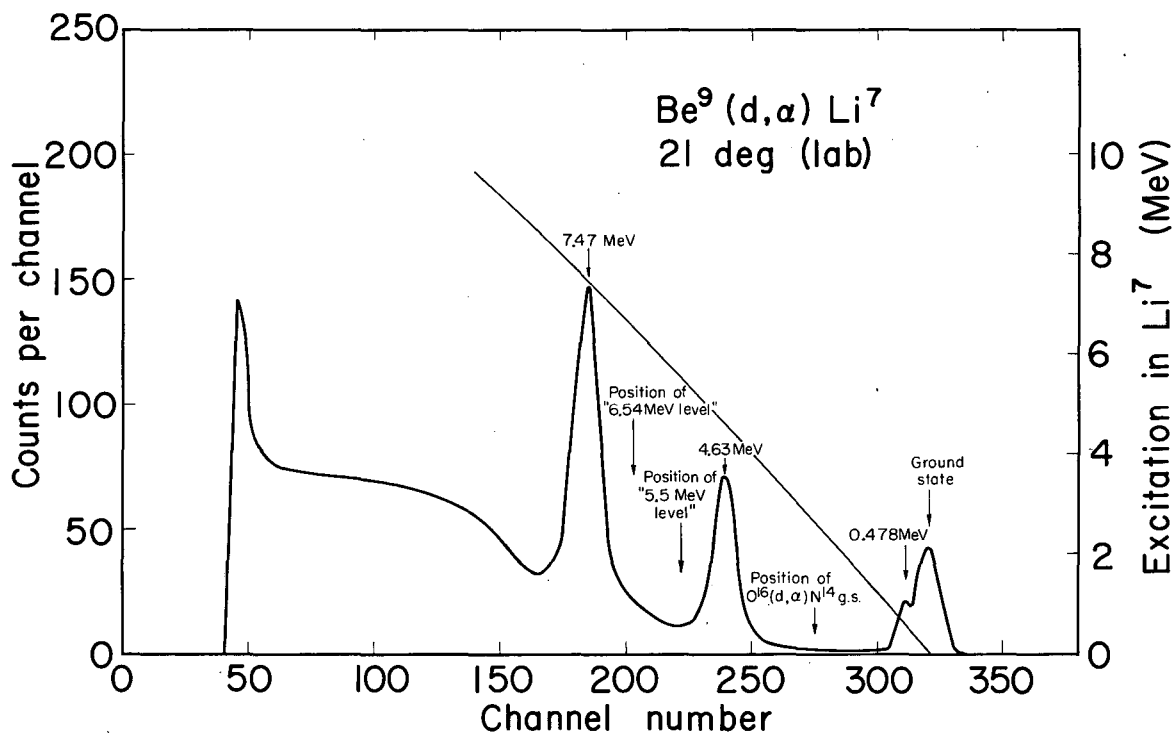
Fig. 12. Alpha particle energy spectrum from the $Be^9(d,\alpha)Li^7$ reaction.

MUB-2125

Table I. Comparison of Li^7 levels observed with those previously reported.[a]

Levels identified (MeV)	Previously reported levels	
	Energy (MeV)	J^{π}
0	0	3/2-
0.48 ± 0.03	0.478	1/2-
4.63 ± 0.03	4.63	(≤ 7/2-)
	(6.54)	
7.47 ± 0.03	7.47	5/2-
	(9.6)	
	(10.8)	
	(12.4)	

[a]References 32 and 44.

If one accepts this picture for the Be^9 target nucleus, and assumes a pickup reaction mechanism the 7.47-MeV level could be formed by picking up a neutron and proton from either of the two alpha clusters. To form an "α + t" level a proton from an alpha particle would have to be picked up along with the "outer" neutron. However, any discussion concerning the reaction mechanism is only conjecture at the present time.

C. $C^{12}(d,\alpha)B^{10}$

Previous investigations of this reaction have been carried out at bombarding energies up to 19 MeV.[32,44] However, most of these studies were done with single counter systems and consequently the observable excitation in B^{10} was restricted to about 5 MeV at the most,[53] and usually no levels above the 3.58-MeV level were resolved. The study at 19 MeV made use of a photographic method,[54] and it was possible to identify alpha tracks that corresponded to up to 6-MeV excitation in B^{10}.

In our work alpha particle energy spectra corresponding to excitation in B^{10} up to about 12 MeV have been obtained. The angular range studied covered from 6.3 to 71.4 deg (lab). Figures 13 and 14 show alpha particle energy spectra at laboratory scattering angles of 45 and 15 deg, respectively. A comparison of the levels of B^{10} observed with those previously reported is presented in Table II.

One of the main purposes for investigating this reaction was to test the isotopic-spin selection rule. Many (d,α) isotopic-spin "forbidden" transitions, primarily at compound-nucleus energies, have been previously investigated. (Reference 55 gives a summary of these and other similar investigations through ca 1956.) Most of the specific transitions studied, however, have been 0+, T=0 → 0+, T=1 (d,α) reactions, and these involve difficulties with angular momentum and parity conservation, in addition to requiring nonconservation of isotopic spin. (See reference 25 for a comprehensive discussion of the selection rules
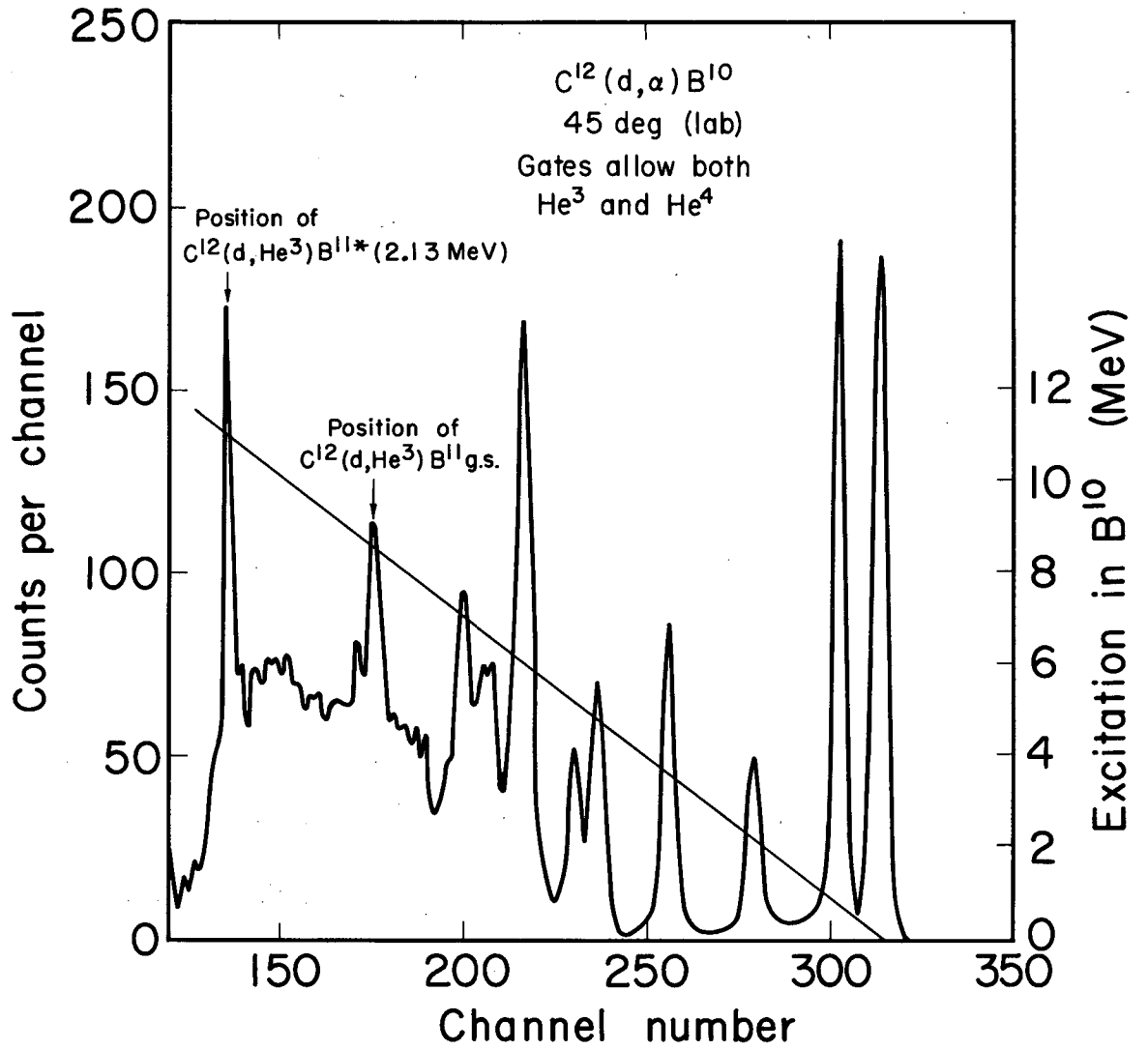
Fig. 13. Alpha particle energy spectrum from the $C^{12}(d,\alpha)B^{10}$ reaction.
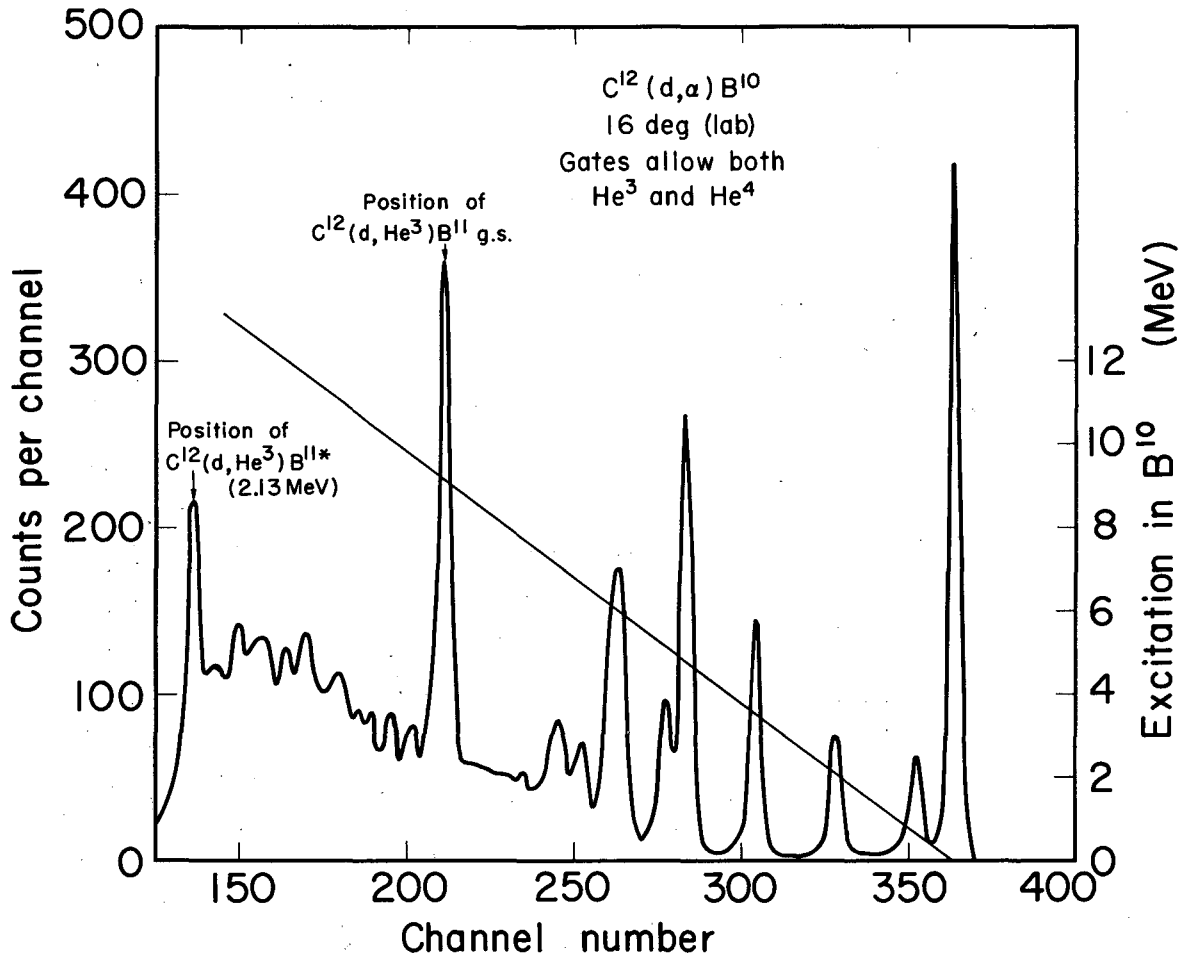
MUB-2126

Fig. 14. Alpha particle energy spectrum from the $C^{12}(d,\alpha)B^{10}$ reaction.

Table II. Comparison of B^{10} levels observed in this experiment with those previously reported.[a]

Levels identified (MeV)	Previously reported levels		
	Energy (MeV)	J^{π}	T
·0	0	3+	0
0.72 ± 0.01	0.717	1+	0
	1.74	0+	1
2.15 ± 0.01	2.15	1+	0
3.59 ± 0.01	3.59	2+	0
4.77 ± 0.02	4.77	(2+)	(0)
	5.11	(2-)	(0)
	5.16	(2+)	(1)
5.18 ± 0.03	5.18	$1^{(+)}$	0
	(5.37)		
	5.58		
6.04 ± 0.03	5.92	2+	
	6.04	4+	
	6.16		
?	6.42		
6.67 ± 0.11	5.57		
	(6.77)		
?	6.88		
7.05 ± 0.10	6.97		
?	(7.19)		
	7.47	2+	
	7.48	2-	1
	7.56	0+	(1)
	7.78	2-	
	(8.07)		
	(8.66)		
	8.89	2+	1
	8.89	(3-)	(1)
	9.7		(1)
	10.7		(1)

[a]References 32 and 44.

arising from angular momentum and parity conservation which are applicable to two-nucleon transfer reactions.) Consequently, if one desires to test the isotopic-spin selection rule via the (d,α) reaction, transitions other than 0+, T=0 → 0+, T=1 should be studied. (A more extensive discussion of isotopic-spin considerations is given in Subsec. III.F.3.).

The transitions to the 2+, T=1 and 3-, T=1 levels at 8.89-MeV excitation in B^{10} satisfy the above conditions and, furthermore, these levels are sufficiently separated from any known T=0 B^{10} levels[44] that their peak in the alpha particle energy spectra would be completely resolved if no complicating factors entered the picture. Unfortunately a peak arising from He^3 ions from the $C^{12}(d, He^3)B^{11}$ ground state reaction falls in the region of interest on the energy spectra, as shown in Figs. 13 and 14. To remove this peak from the energy spectra the lower discriminator on the multiplier pulse was adjusted to correspond to the center of the He^3 - He^4 valley. Figures 15 and 16 show the energy spectra obtained when the gates are adjusted for He^4 and He^3, respectively. The He^3 - He^4 separation obtained with the multiplier was not sufficient to remove completely the He^3 peaks from the alpha energy spectra without also losing a few alpha particles. However, if this had been the only problem the He^3 - He^4 separation undoubtedly could have been improved to the point where the He^3 peaks could be completely removed without any attendant loss of alpha particles. As Fig. 15 illustrates, an alpha particle continuum begins at a position in the energy spectra corresponding to an excitation in B^{10} of about 4.5 MeV. The various reactions that could produce alpha particles via several-body breakup are:

$$
\begin{aligned}
C^{12} + d \;\rightarrow\; &\alpha + B^{10} & Q = -1.34 \;\; \text{MeV}, \\
\rightarrow\; &\alpha + \alpha + Li^6 & Q = -5.80 \;\; \text{MeV}, \\
\rightarrow\; &\alpha + \alpha + \alpha + d & Q = -7.274 \;\; \text{MeV}, \\
\rightarrow\; &\alpha + Be^8 + d & Q = -7.37 \;\; \text{MeV}, \\
\rightarrow\; &\alpha + Be^9 + p & Q = -7.93 \;\; \text{MeV}, \\
\rightarrow\; &\alpha + B^9 + n & Q = -9.78 \;\; \text{MeV}.
\end{aligned}
$$
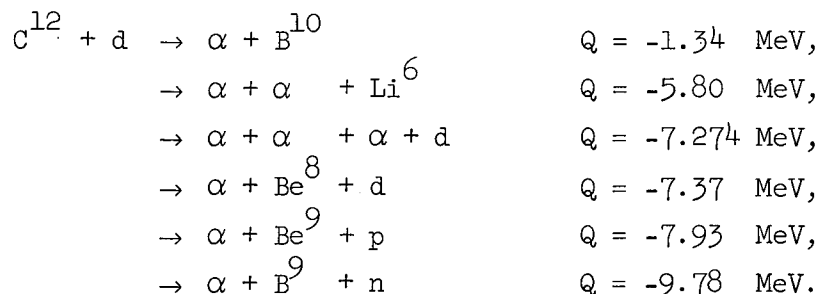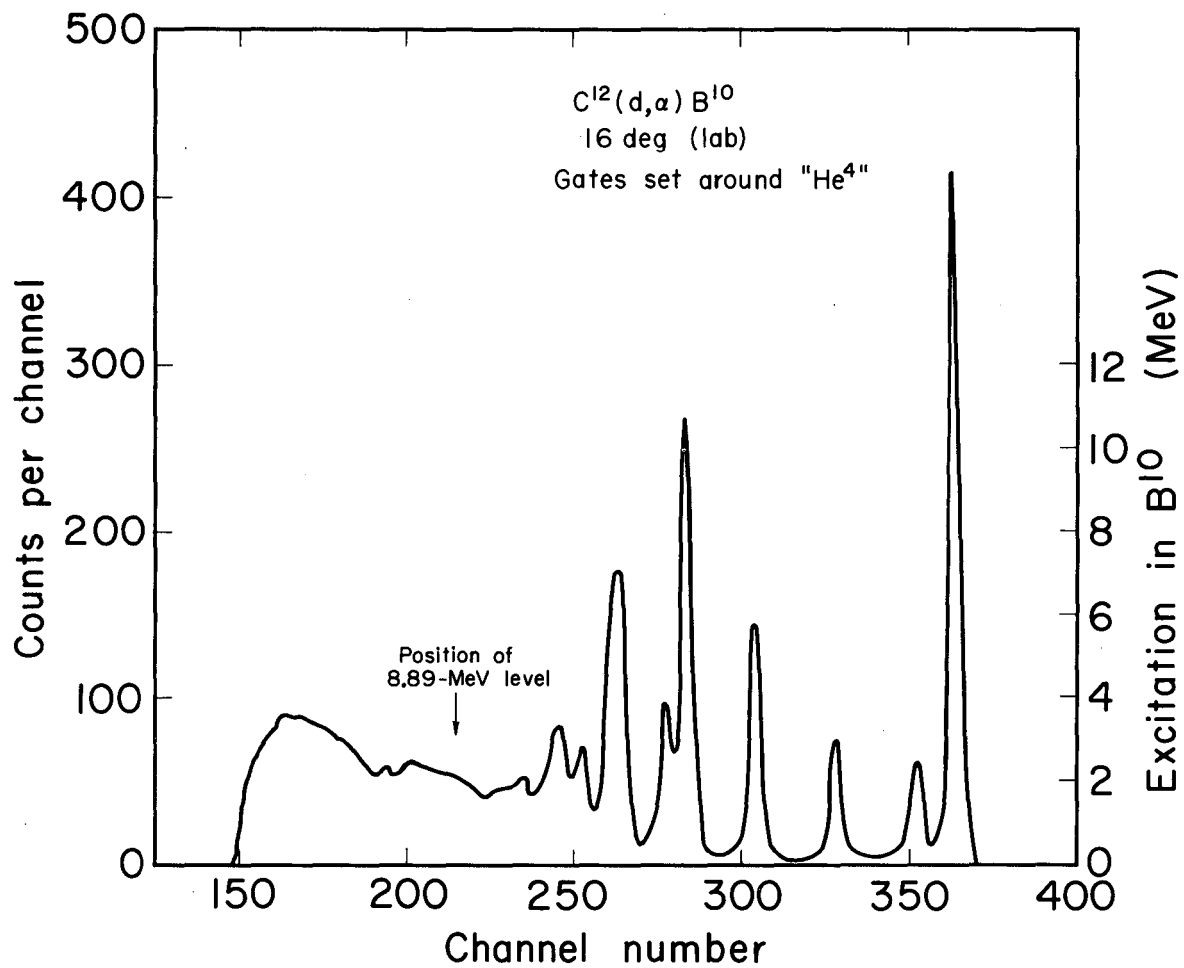
Fig. 15. Alpha particle energy spectrum from the $C^{12}(d,\alpha)B^{10}$ reaction.
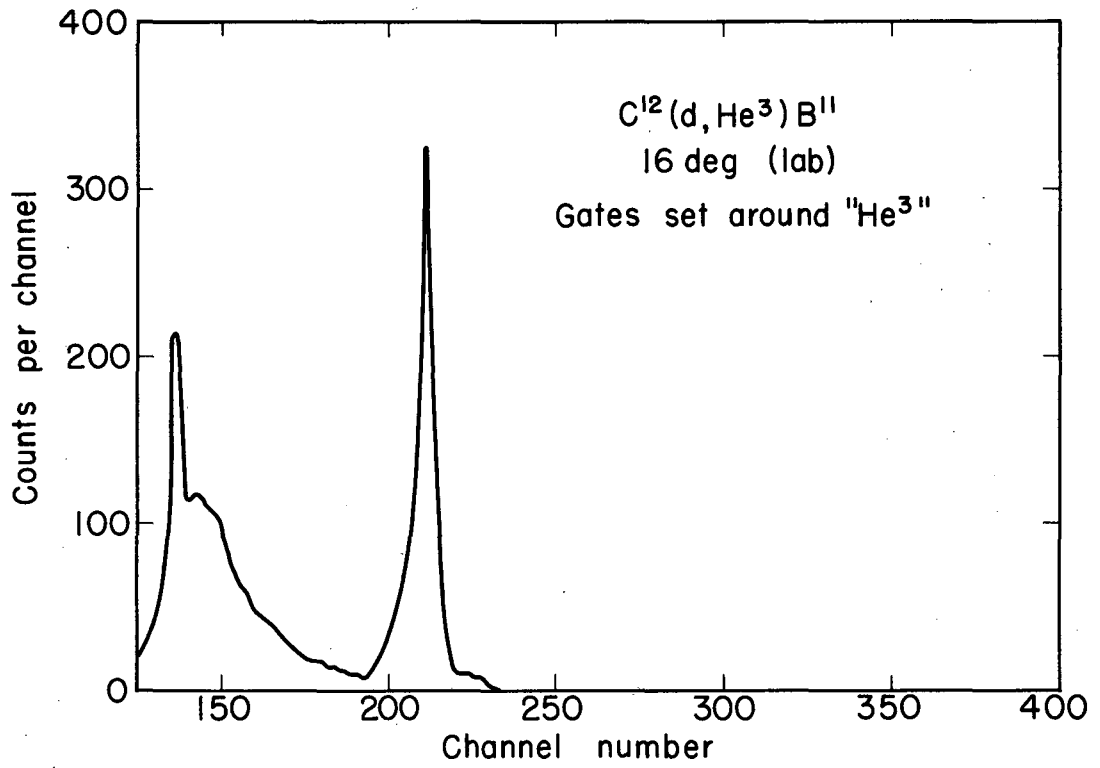
Fig. 16. He^3-ion energy spectrum from the $C^{12}(d,He^3)B^{11}$ reaction.

Thus the continuum begins at an alpha energy corresponding to the upper limit from the $C^{12} + d \rightarrow 2\alpha + Li^6$ reaction.

Although the large alpha particle continuum would obscure a level made with relatively small cross section at 8.89-MeV excitation, none of the energy spectra obtained when the $He^3$ ions were gated out (such as shown in Fig. 15) show any indication of a peak rising above the continuum in the 8.89-MeV excitation region.

To remove the alpha particle continuum an anticoincidence counter that would intersect a very large solid angle is needed. Although such an experiment is feasible it would be quite difficult and no attempt was made to do it.

Precise analysis of the energy spectra above an excitation of about 6 MeV is severely hampered by the continuum, and no angular distributions were obtained for levels above the 6.04-MeV level. The angular distributions of the alpha particles corresponding to formation of the B^{10} ground state, 0.717-, 2.15-, 3.59-, 4.77-, 5.18-, and 6.04-MeV levels are presented in Figs. 17, 18, and 19. The error bars shown are typical and represent counting statistics only; the angular accuracy in all cases is about ± 0.3 deg. The uncertainty of the absolute values of the differential cross sections was estimated to be less than 20%, which arose from the measurement of the target thickness and from the beam-current measurements.

The analysis of the last three of the above levels made use of the computer program that fit the experimental energy spectra. Part of the necessary input data is the number of levels and their approximate position. The levels used corresponded to excitations of 0, 0.717, 2.15, 3.59, 4.77, 5.11, 5.58, 5.92, 6.04, and 6.16 MeV. The cross sections for making the 5.58- and 5.92-MeV levels were negligible. The computer invariably placed the "5.11"-MeV level at about 5.18-MeV excitation, which is closer to the T=1 level at 5.16 MeV. The analysis was completed prior to learning[56] of the identification of the doublet states at about 5.16-MeV excitation in B^{10} wherein a T=0 level is placed at 5.18 MeV. Consequently
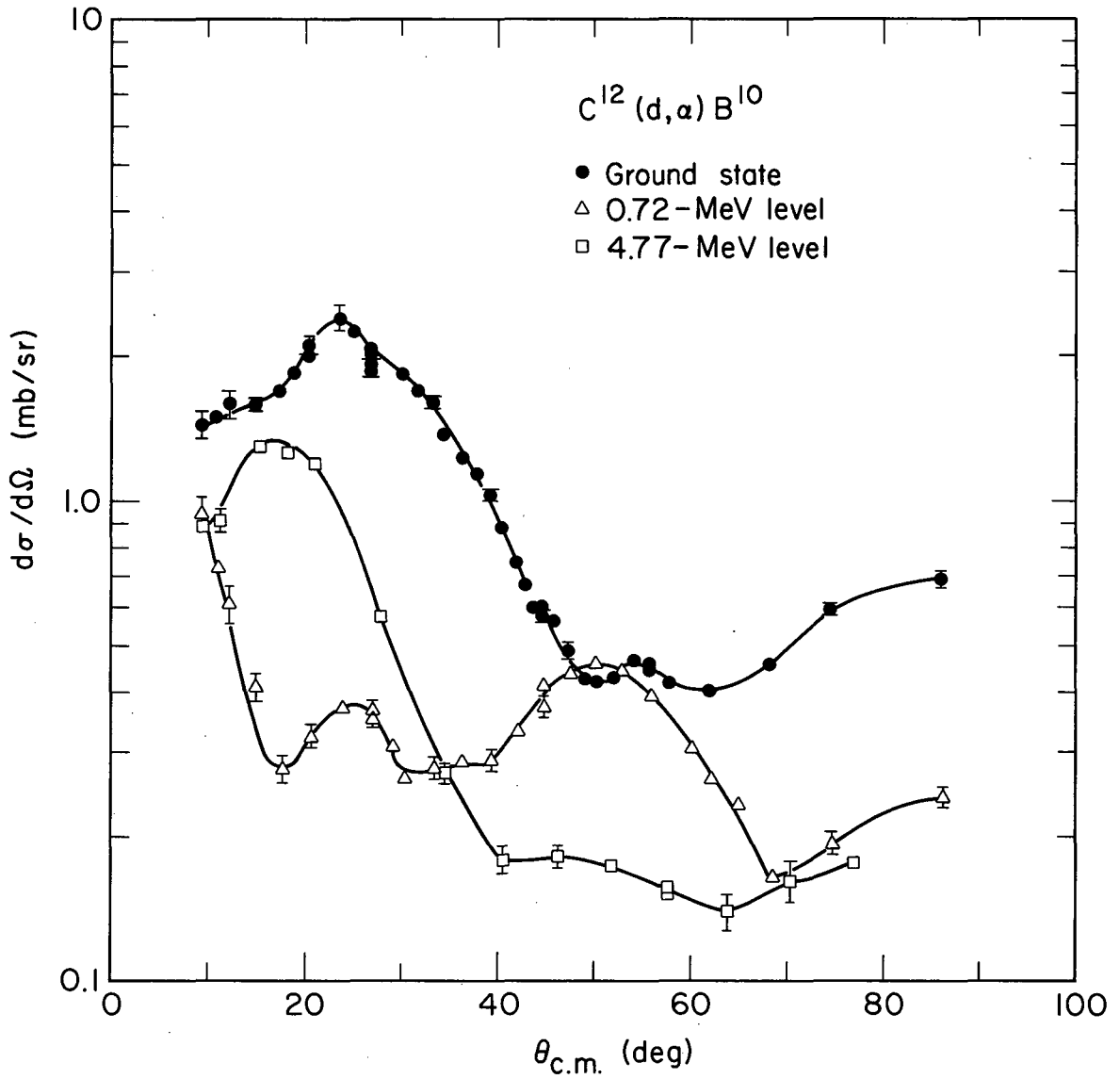
Fig. 17. Angular distributions of alpha particles from formation of the ground state, 0.72-, and 4.77-MeV levels of B^{10}.
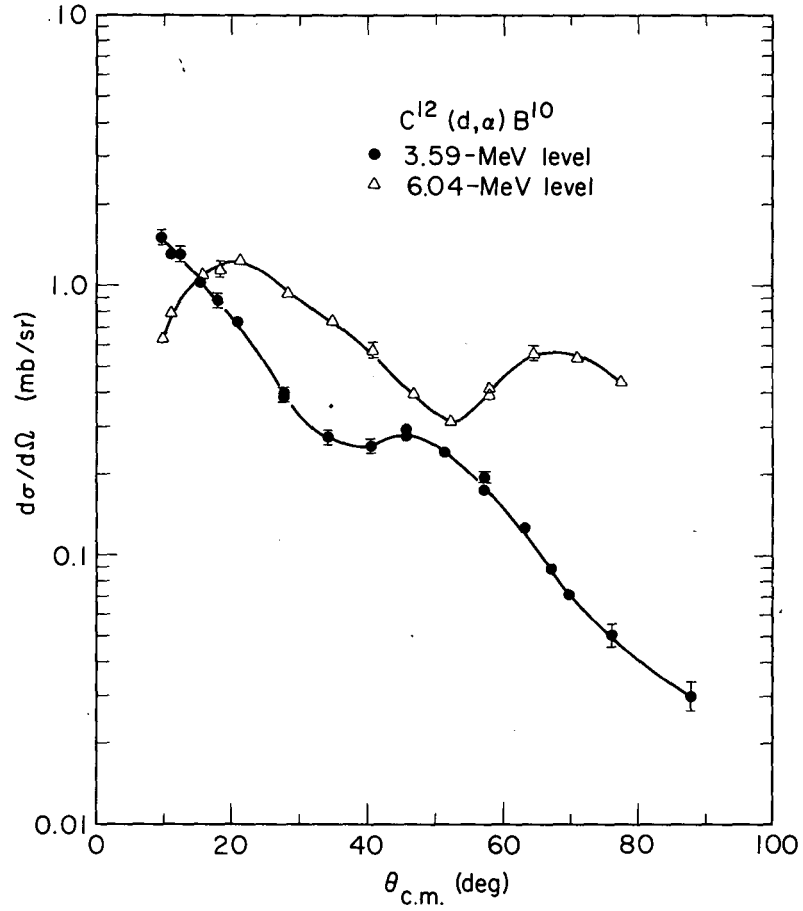
Fig. 18. Angular distributions of alpha particles from formation of the 3.59- and 6.04-MeV levels of B^{10}.
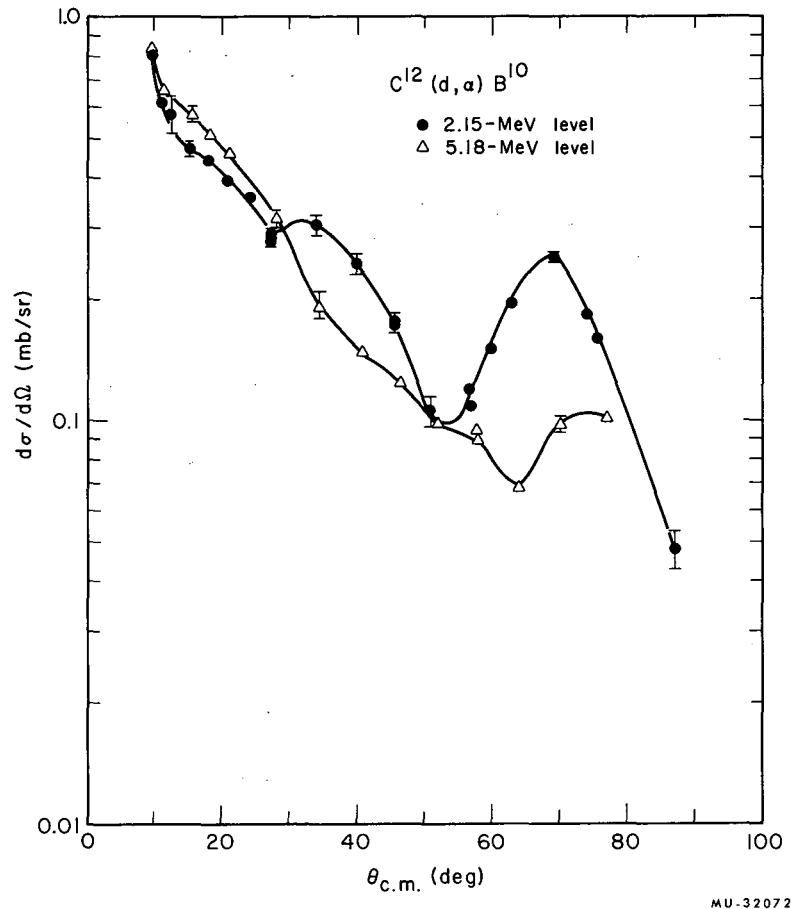
Fig. 19. Angular distributions of alpha particles from formation of the 2.15- and 5.18-MeV levels of B^{10}.

the angular distribution of the 5.18-MeV level was obtained assuming the level at 5.11 MeV was completely absent. The program does not allow for the continuum, which may be large enough to distort the spectra around the 6.04- and 6.16-MeV levels to such an extent that the computer analysis cannot be used to resolve the two levels. The analysis indicated that only the 6.04-MeV level was appreciably populated, and indeed, the latest energy-level scheme for B^{10} has omitted the 6.16-MeV level.[44] Consequently the angular distribution of the 6.04-MeV level was obtained assuming the level at 6.16 MeV was completely absent. Table III lists the integrated cross sections for the eight B^{10} levels analyzed.

Table III. Integrated cross sections for B^{10}.

Level (MeV)	Cross section (mb)	Range of integration (in deg, c.m.)
0	4.85 ± 0.3	0 - 86
0.717	1.68 ± 0.2	9.4 - 86.4
2.15	1.16 ± 0.2	9.5 - 87
3.59	1.34 ± 0.2	9.6 - 87.7
4.77	1.5 ± 0.3	9.7 - 76.7
5.18	1.0 ± 0.4	9.8 - 77
6.04	2.2 ± 0.5	9.9 - 77.5

An analysis of the observed selectivity in the formation of excited states of B^{10} is complicated because mass number ten is the middle of the 1p shell and therefore shell-model calculations on it are difficult. Few exact shell-model configuration assignments have been advanced although intermediate coupling calculations of Kurath[57] in the p shell predict the positions of the first five levels of B^{10} almost quantitatively. Furthermore, the intermediate-coupling calculations by Kurath indicate that the C^{12} ground state is not pure $(p_{3/2})^8$.

A pickup mechanism can account for formation of the B^{10} levels that have configurations $(p_{3/2})^{6-x}(p_{1/2})^x$ where x is 0, 1, or 2 since the nucleon configurations in the C^{12} ground state (Kurath's calculations) are 48.7% $(p_{3/2})^8$ + 40.2% $(p_{3/2})^6(p_{1/2})^2$ + 7.2% $(p_{3/2})^5(p_{1/2})^3$ + 3.9% $(p_{3/2})^4(p_{1/2})^4$. However, calculations by True and Warburton[58] indicate that the 5.18- and 7.56-MeV levels arise from the group of levels $1s^4 1p^4 (2s,1d)$; that is, they belong to the group of states formed by raising two nucleons from the 1p shell into the 2s and 1d shells. Since the 5.18-MeV level is observed, one must invoke a mechanism in which an alpha particle is knocked out of the C^{12} target and the nucleons of the incident deuteron captured in the s and d shells unless the C^{12} ground state has a large admixture of $1s^4 1p^6 (2s,1d)$.* Of course it is possible that different levels are made by different reaction mechanisms, but one would not expect differing mechanisms to be equally likely, in general, and consequently levels made by different mechanisms would not be populated to the same extent. However, this is a question that requires more study and is presented here only as speculation.

Since the 4.77-MeV level is made with a large cross section in this and previous (d,α) investigations,[53,54] the doubtful isotopic-spin assignment[44] of T=0 is certainly correct. The levels at 6.04, 6.67, and 7.05 MeV also have T=0 since they are formed with a relatively large cross section in our work.

---

*This point and similar arguments presented for the $N^{14}(d,\alpha)C^{12}$ and $O^{16}(d,\alpha)N^{14}$ transitions observed, Subsecs. III.E and III.F.2, are based on a j-j coupling picture. However, many features of the level structure of the 1p-shell nuclei have been described by coupling intermediate between L-S and j-j; Li^6 is near the L-S limit, with the relative strength of the spin-orbit forces increasing as the shell fills, resulting in predominantly j-j coupling near the shell closure.[57,59,60]

At no angle was an alpha particle group observed that corresponded to formation of the T=1 level at an excitation of 1.74 MeV in B^{10}. The absence of this group is expected from angular momentum and parity conservation, and from isotopic spin conservation as discussed earlier for 0+, T=0 → 0+, T=1 (d,α) transitions. Determination of an accurate upper limit for the cross section for this transition is difficult because of the following reasons: (a) The observed base line for the energy spectra does not reach zero between well-separated peaks [probably because of the C^{13} "impurity" (1.11%) in the natural carbon target]; (b) a few alpha particles from the C^{12}(d,α)B^{10*} (2.15-MeV) transition overlap into the alpha particle energy region corresponding to the 1.74-MeV level with the experimental resolution obtained. However, an upper limit for the cross section for the C^{12}(d,α)B^{10*} (1.74-MeV) transition can be set at about 1% of the ground state cross section.

D. $\underline{B^{10}(\alpha,d)C^{12}}$

This reaction has been studied previously at bombarding energies around 3.5 MeV[61] and at 42 MeV.[62] Our work covered the angular range between 28 and 61 deg (lab). Figure 20 shows a typical deuteron energy spectrum at a laboratory scattering angle of 35 deg. The measurements were not extended to smaller angles because the counter system available at the time was not thick enough to stop the more energetic deuterons unless an excessively thick Al absorber was placed between the target and counter telescope.

The angular distributions of the deuterons from this reaction corresponding to formation of the C^{12} ground state, 4.43-, 7.66-, and 9.64-MeV levels are shown in Fig. 21. The relative cross sections for the formation of these levels are discussed in Subsec. III. E.
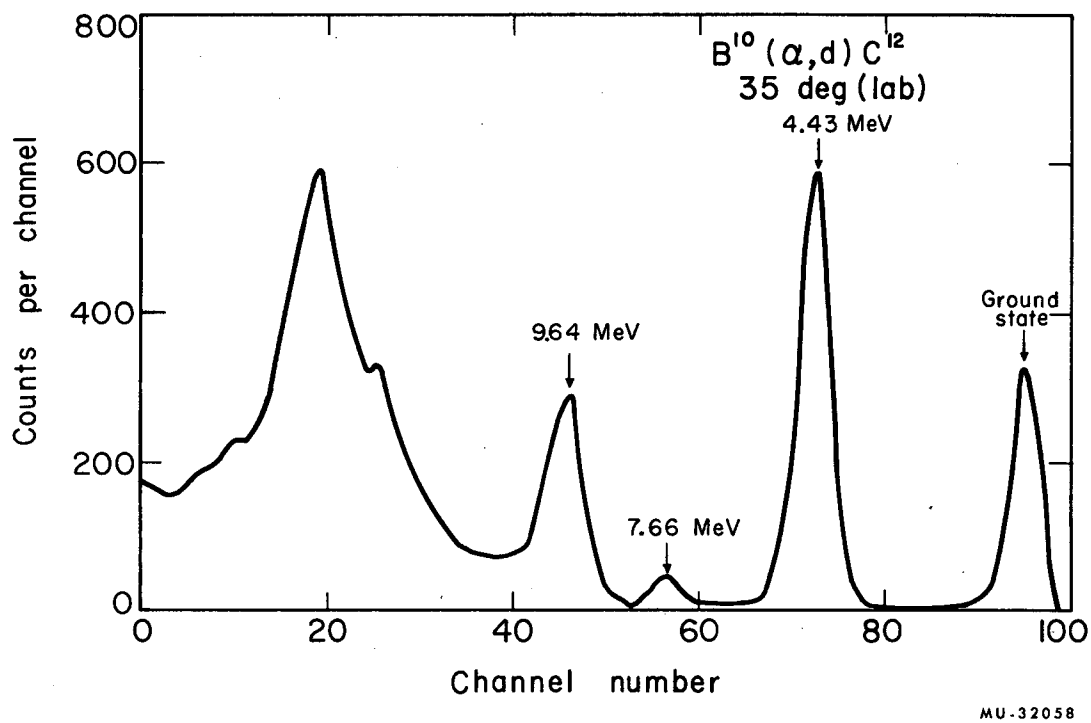
Fig. 20. Deuteron energy spectrum from the $B^{10}(\alpha,d)C^{12}$ reaction.
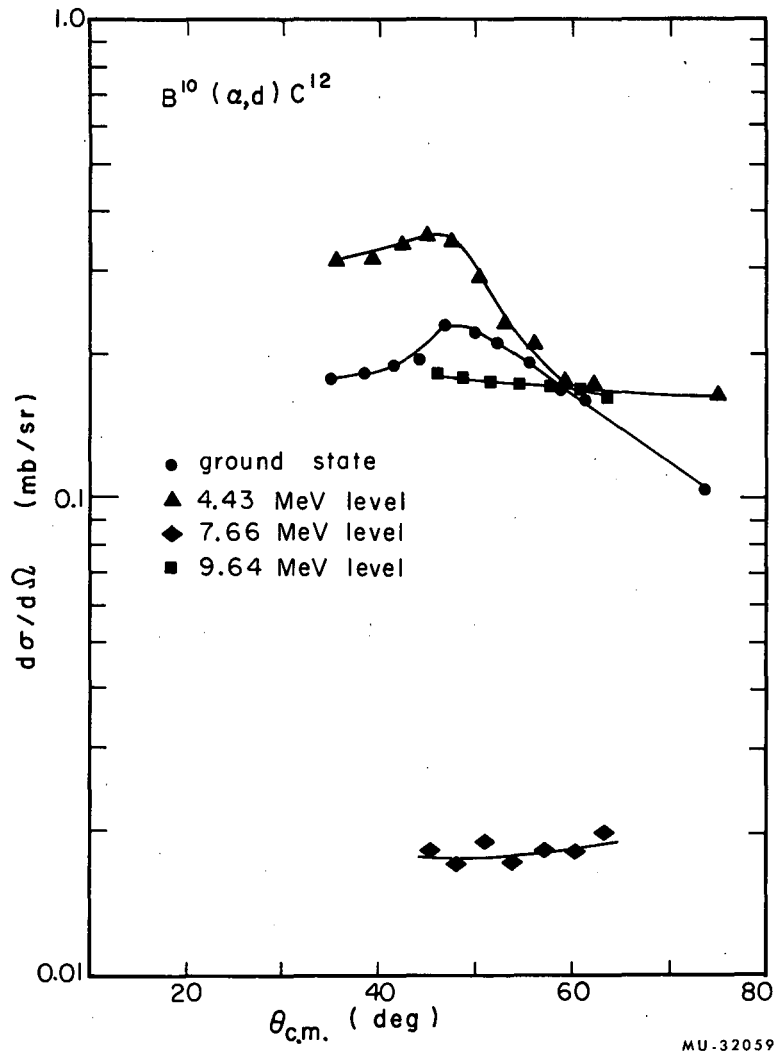
Fig. 21. Angular distributions of deuterons from formation of the ground state, 4.43-, 7.66-, and 9.64-MeV levels of C^{12}.

E. $\underline{N^{14}(d,\alpha)C^{12}}$

Previous investigations of this reaction have been carried out at bombarding energies up to 21 MeV.[32,44] The large positive Q value (13.57 MeV) allows one to use a single counter and still observe fairly high excitation in C^{12}. Except for three energy spectra obtained with the counter telescope plus multiplier system, our investigation of this reaction was accomplished with a single counter. Alpha particle energy spectra have been obtained over the angular range from 10 to 130 deg (lab). The observable excitation ($\theta_{lab} < 50$ deg) reached about 13 MeV when the single counter was used. But, as shown in Fig. 22, this range was extended to about 22 MeV for the spectra obtained using the multiplier. However, peaks corresponding to He^3 ions from the $N^{14}(d,He^3)C^{13}$ reaction enter the spectra at C^{12} excitations greater than 15 MeV. No attempt was made to resolve He^3 from He^4 with the multiplier since the study of this reaction was essentially completed before the thin dE/dx counters were developed. The primary purpose for the three runs with the multiplier was to determine whether the use of such a system would introduce any experimental difficulty that would have to be remedied before it could be used on other (d,α) reactions. The differential cross sections measured with the multiplier system were in excellent agreement with those measured with the single counter. A comparison of the levels of C^{12} observed with those previously reported is presented in Table IV.

As Fig. 22 illustrates, an alpha particle continuum begins at a position in the energy spectra corresponding to an excitation in C^{12} of about 7.5 MeV. The various reactions which could produce alpha particles via several-body breakup are:

$$N^{14} + d \rightarrow \alpha + C^{12} \qquad Q = 13.5712 \text{ MeV},$$
$$\rightarrow \alpha + \alpha + \alpha + \alpha \qquad Q = 6.2952 \text{ MeV},$$
$$\rightarrow \alpha + \alpha + Be^8 \qquad Q = 6.2012 \text{ MeV},$$
$$\rightarrow \alpha + B^{11} + p \qquad Q = -2.3848 \text{ MeV},$$
$$\rightarrow \alpha + C^{11} + n \qquad Q = -5.1498 \text{ MeV}.$$
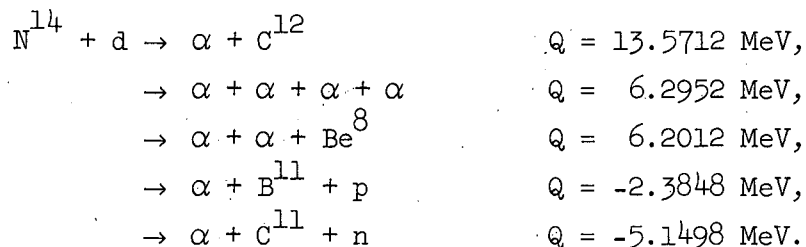
Table IV.   Comparison of C^{12} levels observed in this experiment with those previously reported.[a]

Levels identified (MeV)	Previously reported levels		
	Energy (MeV)	J^π	T
0	0	0+	0
4.43 ± 0.02	4.433	2+	0
7.66 ± 0.03	7.656	0+	0
9.64 ± 0.03	9.64	3-	0
	10.1	(0+)	0
	10.84	(1-)	
	11.83	(1-)	
12.71 ± 0.05	12.71	(1+)	0
	13.34		

[a]
References 32 and 44.
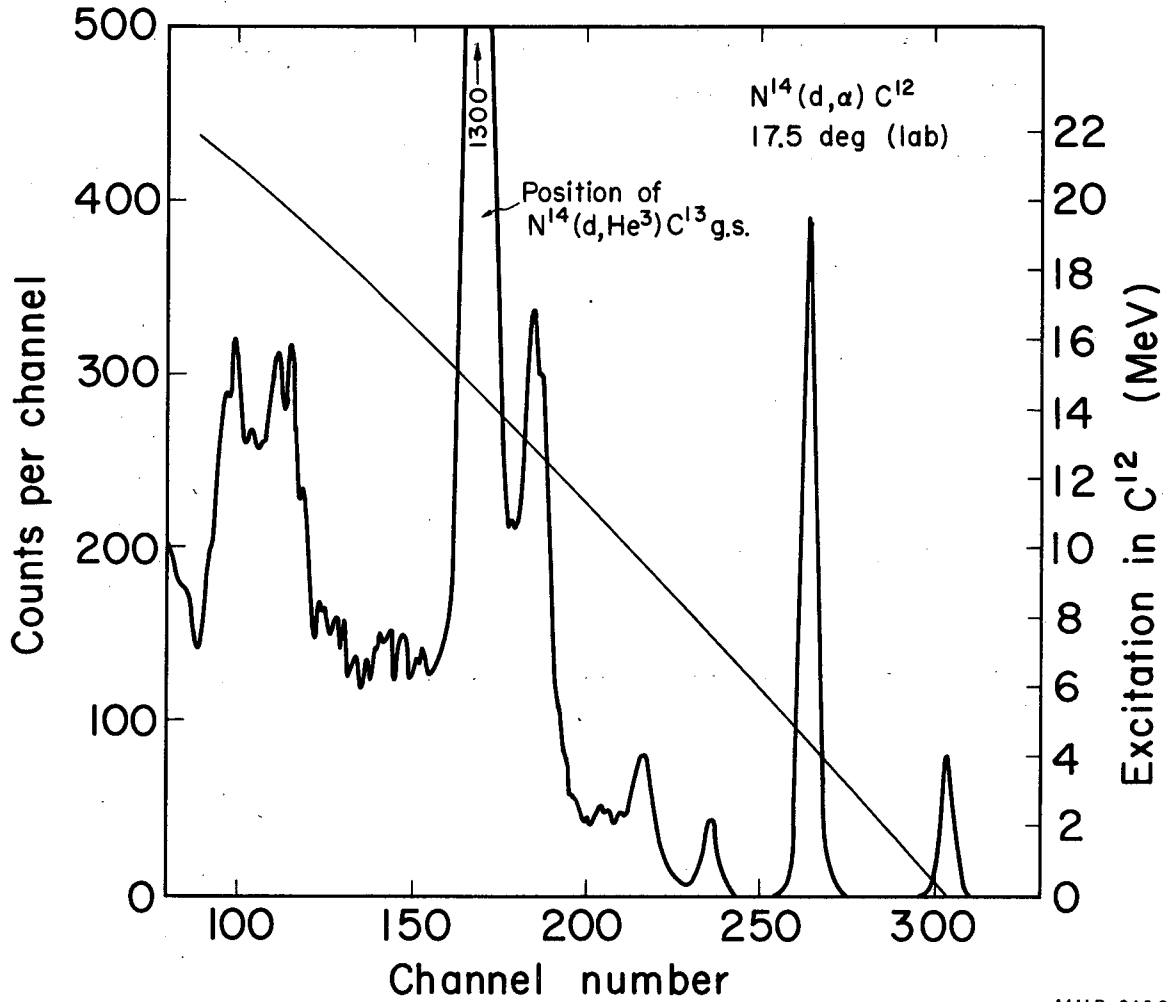
Fig. 22. Alpha particle energy spectrum from the $N^{14}(d,\alpha)C^{12}$ reaction.

Thus the continuum begins at an alpha energy corresponding to the upper limit from the N^{14} + d → 4α reaction.

The $N^{14}(d,\alpha)C^{12}$ reaction offers a similar opportunity for testing the isotopic-spin selection rule as does the $C^{12}(d,\alpha)B^{10}$ reaction, but it too is faced with the problems of He^3 interference and an alpha particle continuum.*

The angular distributions of the alpha particles corresponding to formation of the C^{12} ground state, 4.43-, 7.66-, and 9.64-MeV levels are presented in Fig. 23. The error bars shown are typical and represent counting statistics only. The circles used to represent the 4.43-MeV level usually encompassed the statistical uncertainty. The uncertainty of the absolute values of the differential cross sections to the ground state and 4.43-MeV level was estimated to be less than 10%. However, the alpha particle continuum prevents such a precise analysis of the 7.66- and 9.64-MeV levels because the arbitrary subtraction of the continuum introduces a relatively large source of error. The integrated cross sections for the ground state and 4.43-MeV transitions were 0.52 mb (13.0 to 137.6 deg c.m.) and 3.50 mb (13.1 to 138.1 deg c.m.), respectively. No angular distribution is presented for the 12.71-MeV level because it was not observed over a wide range of angles, and because the alpha continuum and the nearby He^3 ions make it very difficult to determine accurate values. However, the differential cross section to the 12.71-MeV level appears to be comparable to the 4.43-MeV level.

---

*In fact, the $N^{14}(d,\alpha)C^{12*}$ (15.11 MeV) 1+, T=0 → 1+, T=1 transition has been reported to have a relatively large cross section.[63] However, the He^3 peak arising from the $N^{14}(d,He^3)C^{13}$ reaction in this study would obscure the observation of the alpha particles corresponding to a C^{12} excitation of 15.11 MeV unless He^3 were separated from He^4, and apparently this was not done.
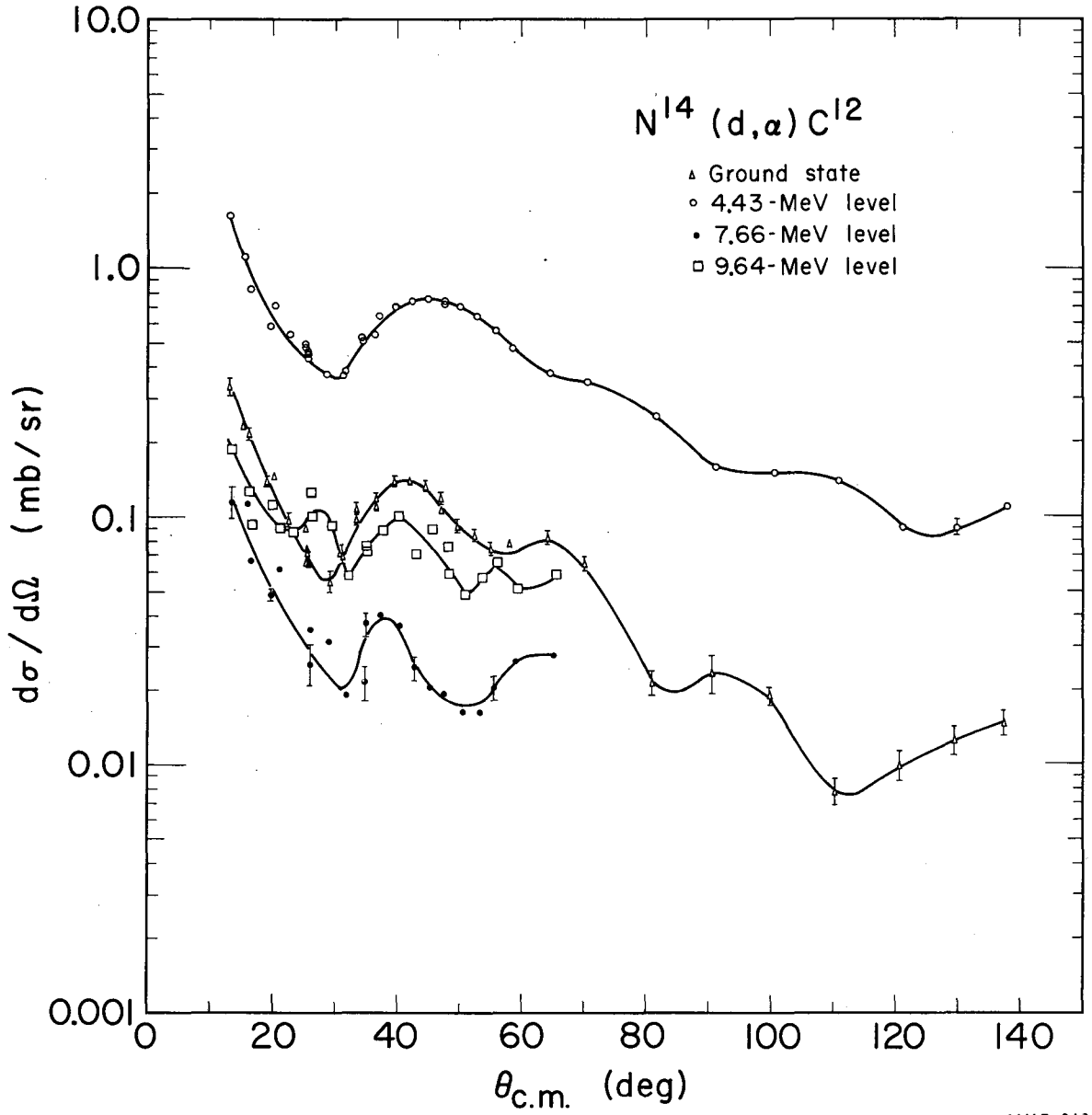
Fig. 23. Angular distributions of alpha particles from formation of the ground state, 4.43-, 7.66-, and 9.64-MeV levels of C^{12}.

It is noteworthy that the two highly populated levels (4.43- and 12.71-MeV) are both mainly $(p_{3/2})^7 (p_{1/2})^1$ configurations whereas the two 0+ levels (ground state and 7.66-MeV) are mixtures of the $(p_{3/2})^8$ and $(p_{3/2})^6 (p_{1/2})^2$ configurations.[64] No statistical factor is included when comparing the cross sections of different levels made by a given pickup reaction since

$$\frac{d\sigma}{d\Omega} \propto \frac{2I_f + 1}{2I_i + 1},$$

where I_i and I_f are the spins of the incident and outgoing particles, respectively.[65] This is in contrast with a stripping reaction where

$$\frac{d\sigma}{d\Omega} \propto \frac{2J_f + 1}{2J_i + 1},$$

where J_i and J_f are the spins of the target and residual nuclei, respectively, and the $2J_f + 1$ term must be allowed for when comparing the cross sections of different levels. Since the nucleon configuration of the N^{14} ground state is reported[64] to be $(p_{3/2})^8 (p_{1/2})^2$ with a strong admixture of $(p_{3/2})^7 (p_{1/2})^3$, a pickup mechanism would not favor formation of a $(p_{3/2})^7 (p_{1/2})^1$ configuration unless the admixture is very small and it is easier to pick up $p_{3/2} p_{1/2}$ than either $(p_{3/2})^2$ or $(p_{1/2})^2$. As discussed in Subsec III. F.2, picking up $p_{3/2} p_{1/2}$ from O^{16} is definitely favored over picking up $(p_{1/2})^2$. The observed selectivity would also arise if the converse were true; i.e., pickup of either $(p_{3/2})^2$ or $(p_{1/2})^2$ is highly favored relative to $p_{3/2} p_{1/2}$ pickup and the admixture is very large. However, this approach requires invoking rather extreme values; e.g., if one assumes that picking up $p_{3/2} p_{1/2}$ is inhibited by a factor of ten compared with picking up $(p_{3/2})^2$ or $(p_{1/2})^2$, the "admixture" needed to reproduce the experimental ratio is

100%. Since neither of these values are reasonable this explanation is eliminated. If a knockout mechanism is invoked there is still no apparent reason why transitions to levels having $(p_{3/2})^7 (p_{1/2})^1$ configurations should be highly enhanced.

Formation of the 3-level at 9.64 MeV would require raising one p nucleon into a $d_{5/2}$ shell in addition to the removal of two nucleons. However, this level is observed, and in considerably larger yield than the 7.66-MeV level. Unless the N^{14} ground state contains an appreciable $d_{5/2}$ admixture this level must be formed primarily by a knockout mechanism. (Nagarajan[66] has mentioned that the N^{14} ground state may contain a 10% admixture of $d_{5/2}$.)

Table V shows the approximate relative cross sections for several C^{12} levels made via the $B^{10}(\alpha,d)C^{12}$, $C^{12}(\alpha,\alpha')C^{12}$, and $N^{14}(d,\alpha)C^{12}$ reactions (inelastic-scattering data with 48-MeV alphas taken from Vaughn[67]), and their dominant configurations. For the (α,d) reaction the cross section to each C^{12} level is divided by $(2J + 1)$, relative to the ground state cross section divided by $(2J_{g.s.} + 1)$. This removes the statistical factor mentioned earlier in regard to stripping reactions.

The $B^{10}(\alpha,d)C^{12}$ reaction exhibits a very strong preference for the ground state transition compared with the $N^{14}(d,\alpha)C^{12}$ reaction. Furthermore, this is the only (d,α) reaction studied that strongly favors the population of excited states relative to the ground state transition. Possible reasons for such behavior are discussed extensively in Subsec. $\overline{IV}$. A.

F. $\underline{O^{16}(d,\alpha)N^{14}}$

1. General Discussion

Previous investigations of this reaction have been carried out at bombarding energies up to 19 MeV.[32,44] However, most of these studies were made using solid targets, commonly Mylar $(C_8H_4O_2)$ or silicon dioxide.

Table V. Shell-model configurations and relative cross sections for the formation of C^{12} levels.

Level			Dominant configuration[a]	Relative cross sections		
MeV	J^π	T		(α, d)	(α, α')	(d, α)
0	0+,	0	$(p_{3/2})^8$ and $(p_{3/2})^6 (p_{1/2})^2$	1	--	1
4.433	2+,	0	$(p_{3/2})^7 (p_{1/2})^1$	0.3	1	7
7.656	0+,	0	$(p_{3/2})^8$ and $(p_{3/2})^6 (p_{1/2})^2$	0.1	0.025	0.3
9.64	3-,	0	$(p_{3/2})^7 (d_{5/2})^1$	0.2	0.5	0.8

[a]Reference 64.

Consequently the observable excitation in N^{14} was restricted to 4 MeV
at the most, owing to the carbon or silicon "contamination" because the
Q values for (d,α) reactions on O^{16}, C^{12}, and Si^{28} are 3.11, -1.34,
and 1.43 MeV, respectively.

In our work alpha particle energy spectra corresponding to
excitation in N^{14} up to about 13 MeV have been obtained. The angular
range studied covered from 9.6 to 90 deg (lab). Figures 24 and 25 show
alpha particle energy spectra at laboratory scattering angles of 22 and
61 deg, respectively. A comparison of the levels of N^{14} observed with
those previously reported is presented in Table VI.

Although most of the work was done using the multiplier system,
the majority of the energy spectra were obtained with the multiplier
signal gated so as to allow peaks from both He^3 and He^4 in the energy
spectra. Figure 26 shows an energy spectrum with the gates set to
eliminate He^3 ions. The alpha particle continuum appears to be relatively
less important than for the other (d,α) reactions studied. The various
reactions that could produce alpha particles via several-body breakup
are:

$$O^{16} + d \rightarrow \quad \alpha + N^{14} \qquad\qquad Q = 3.1152 \text{ MeV,}$$
$$\rightarrow \quad \alpha + C^{13} + p \qquad\qquad Q = -4.4338 \text{ MeV,}$$
$$\rightarrow \quad \alpha + C^{12} + d \qquad\qquad Q = -7.1568 \text{ MeV,}$$
$$\rightarrow \quad \alpha + N^{13} + n \qquad\qquad Q = -7.4378 \text{ MeV,}$$
$$\rightarrow \quad \alpha + \alpha \quad + B^{10} \qquad\qquad Q = -8.4978 \text{ MeV.}$$
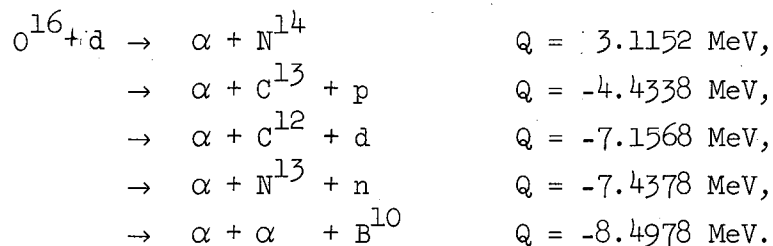
Thus the continuum can begin at a position in the energy spectra corre-
sponding to an excitation in N^{14} of 7.6 MeV. However, it is difficult
to determine where the continuum begins experimentally.

The large broad peak that appears at an excitation between 11
and 12 MeV in Fig. 24 must be an alpha peak because all other possibilities
can be eliminated. The first excited level in N^{15} lies 5.28 MeV above
the ground state; thus the observed peak cannot arise from a $O^{16}(d, He^3)N^{15*}$
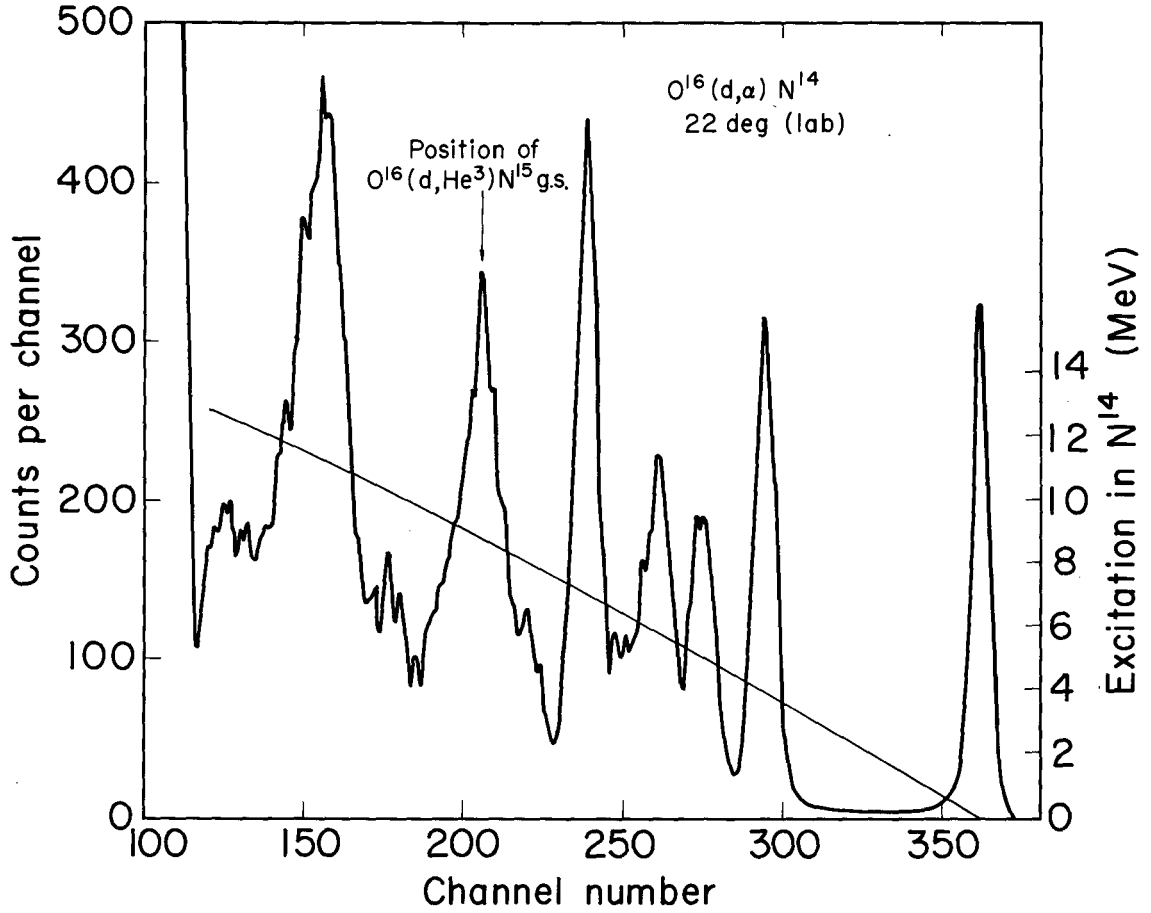
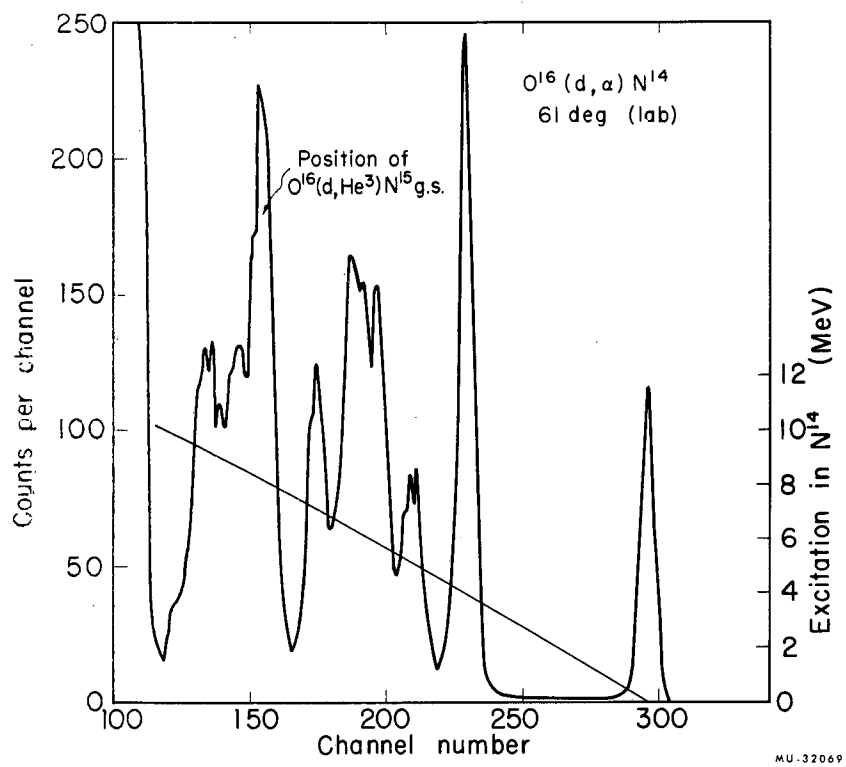Fig. 24. Alpha particle energy spectrum from the $O^{16}(d,\alpha)N^{14}$ reaction.

Fig. 25. Alpha particle energy spectrum from the $O^{16}(d,\alpha)N^{14}$ reaction.

Table VI. Comparison of N^{14} levels observed in this experiment with those previously reported.[a]

Levels identified (MeV)	Previously reported levels		
	Energy (MeV)	J^{π}	T
0	0	1+	0
	2.311	0+	1
3.95 ± 0.02	3.945	1+	0
b	4.91[c]	(0)-	0
	5.10[c]	2-	0
b	5.69[c]	1-	0
	5.83[c]	3-	0
	6.05		
b	6.21	1+	0
	6.44[d]	3+	0
	6.70		
7.03 ± 0.03	7.03[c]	2+	0
	7.40		
	7.60		
8.0 ± 0.07	7.97	2-	0
	8.06	1-	1
	8.47		(0)
	8.63	0+	1
f	8.71	0-	1
	8.91	3-	1
	8.99	1+	(0)
	9.00[e]	5+	0
	9.17	2+	1
9.4 ± 0.10	9.41	1-	
	9.51	2-	1
g	9.71	1+	
h	10.09	(1+)	0
h	10.22	1-	
	10.43	2+	1
g	10.55	1-	
	11.08	1+	0
	11.23	3-	1
	11.29	2-	0
	11.39	(1+)	0
i	11.51	3+	
	11.66		
	11.74	1+	
	11.80	(2+)	
	11.97	(2-)	
	12.05		

[a]References 32 and 44.

[b]Both levels observed but not experimentally resolved from each other.

[c]The parity assignments for these levels were taken from reference 27.

[d]A positive parity for this level has been experimentally measured by E. K. Warburton (private communication to William W. True, University of California, Davis, California).

[e]Reference 27.

[f]The He^3 peak arising from the $O^{16}(d,He^3)N^{15}$ ground state transition falls in this region, obscuring any alpha peak. However, several spectra were obtained using the multiplier system to eliminate the He^3 peak, and no alpha peak was observed above the alpha continuum (Fig. 26), except probably one at 8.45 MeV.

[g]Not made significantly above continuum.

[h]Probably made but with small cross section.

[i]A large broad alpha peak appears at this excitation region. However, it is not possible to resolve any of the separate levels.
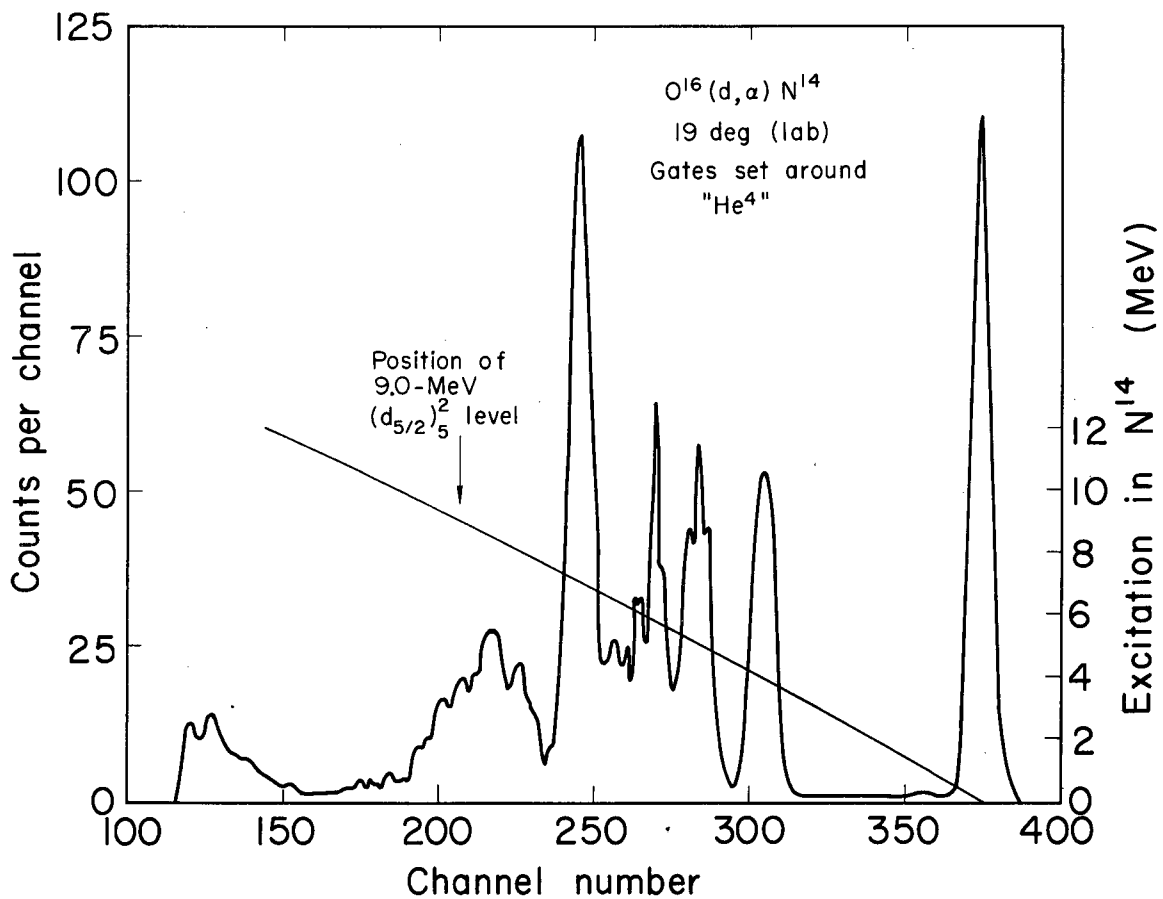
Fig. 26. Alpha particle energy spectrum from the $O^{16}(d,\alpha)N^{14}$ reaction.

transition. The possibility that the peak corresponded to Li^6 ions from the $O^{16}(d,Li^6)C^{12}$ transition was also eliminated because the Li^6 ions would not be energetic enough to reach the E counter and consequently the pulse-height analyzer would not receive a trigger pulse from the multiplier. A large peak at about this excitation is also observed in the alpha particle energy spectra for the reaction $N^{14}(\alpha,\alpha')N^{14*}$ (see Fig. 30 and reference 27).

The observation of the levels at 8.47, 9.41 (possibly 9.71), and 10.22 MeV in this reaction indicates that these levels have T=0. Further evidence for the T=0 nature of the first two of these levels comes from a recent study of the $C^{12}(\alpha,d)N^{14}$ reaction in which these levels were populated relatively strongly.[68] The 9.71-MeV level was definitely observed also but with a considerably lower cross section.

The angular distributions of the alpha particles corresponding to formation of the N^{14} ground state, 3.95-, 4.91- and 5.10-, 5.69- and 5.83-, 6.21- and 6.44-, and 7.03-MeV levels are shown in Fig. 27 and 28. The three "doublets" were treated as a single peak since the experimental resolution was not sufficient to allow these levels to be analyzed separately. Typical error bars, which represent counting statistics only, are shown. The uncertainty of the absolute values of the differential cross sections was estimated to be less than 10%. Table VII presents the integrated cross sections for the N^{14} levels analyzed.

2. Comparison of N^{14} Levels Formed by Different Reactions

Extensive theoretical studies of the N^{14} nucleus have been made. Warburton and Pinkston,[69] by a careful analysis of γ-decay and nuclear reaction data, have given shell-model assignments for a large number of levels in N^{14}. Talmi and Unna have taken a different approach, adjusting several parameters which describe an effective two-body force between the particles so that the best agreement with the experimental levels is obtained.[70] True has performed a shell-model calculation of the energies of the various possible configurations.[71] Consequently,
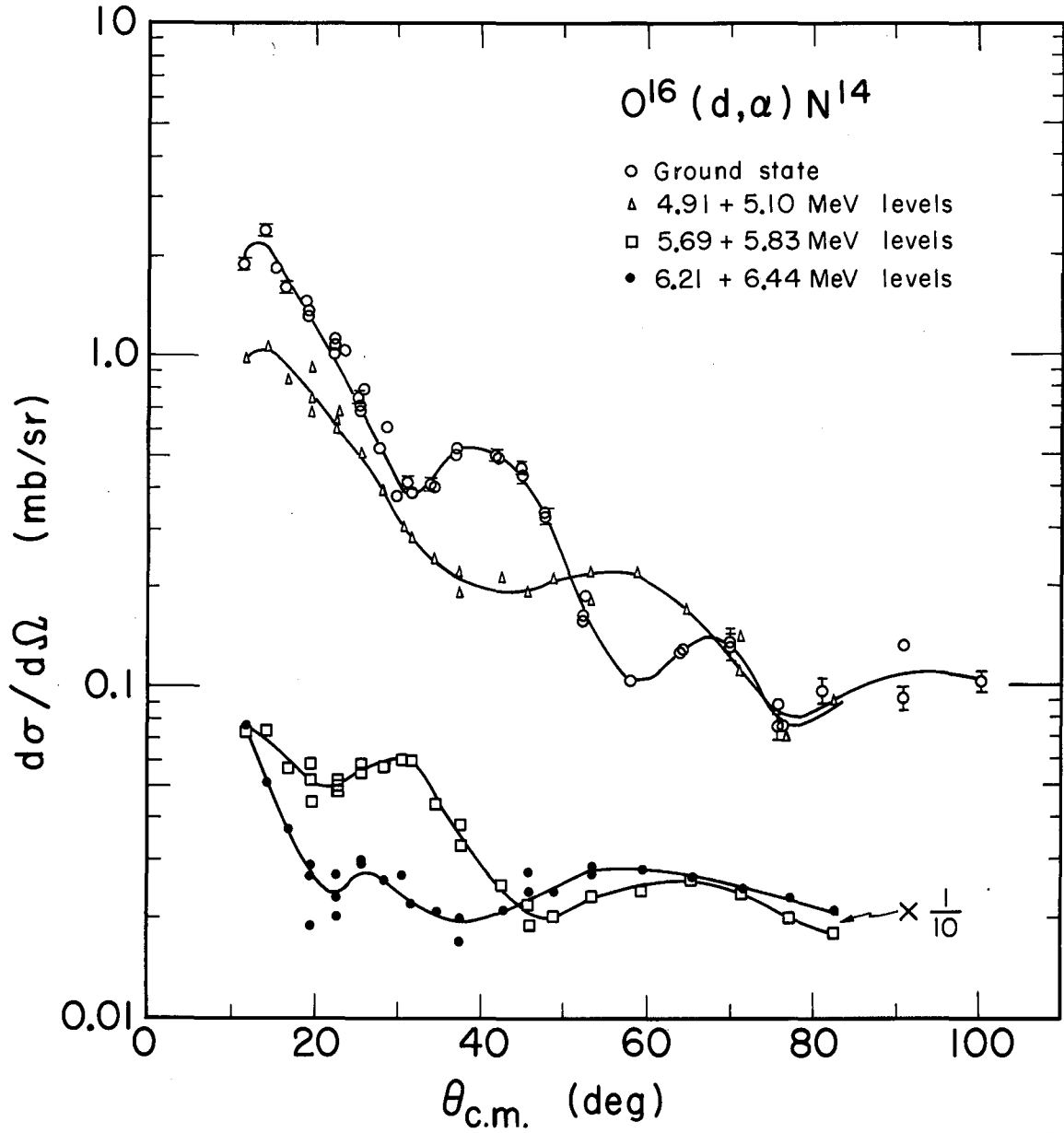
Fig. 27. Angular distributions of alpha particles from formation of the ground state, 4.91- and 5.10-, 5.69- and 5.83-, and 6.21- and 6.44-MeV levels of N[14].
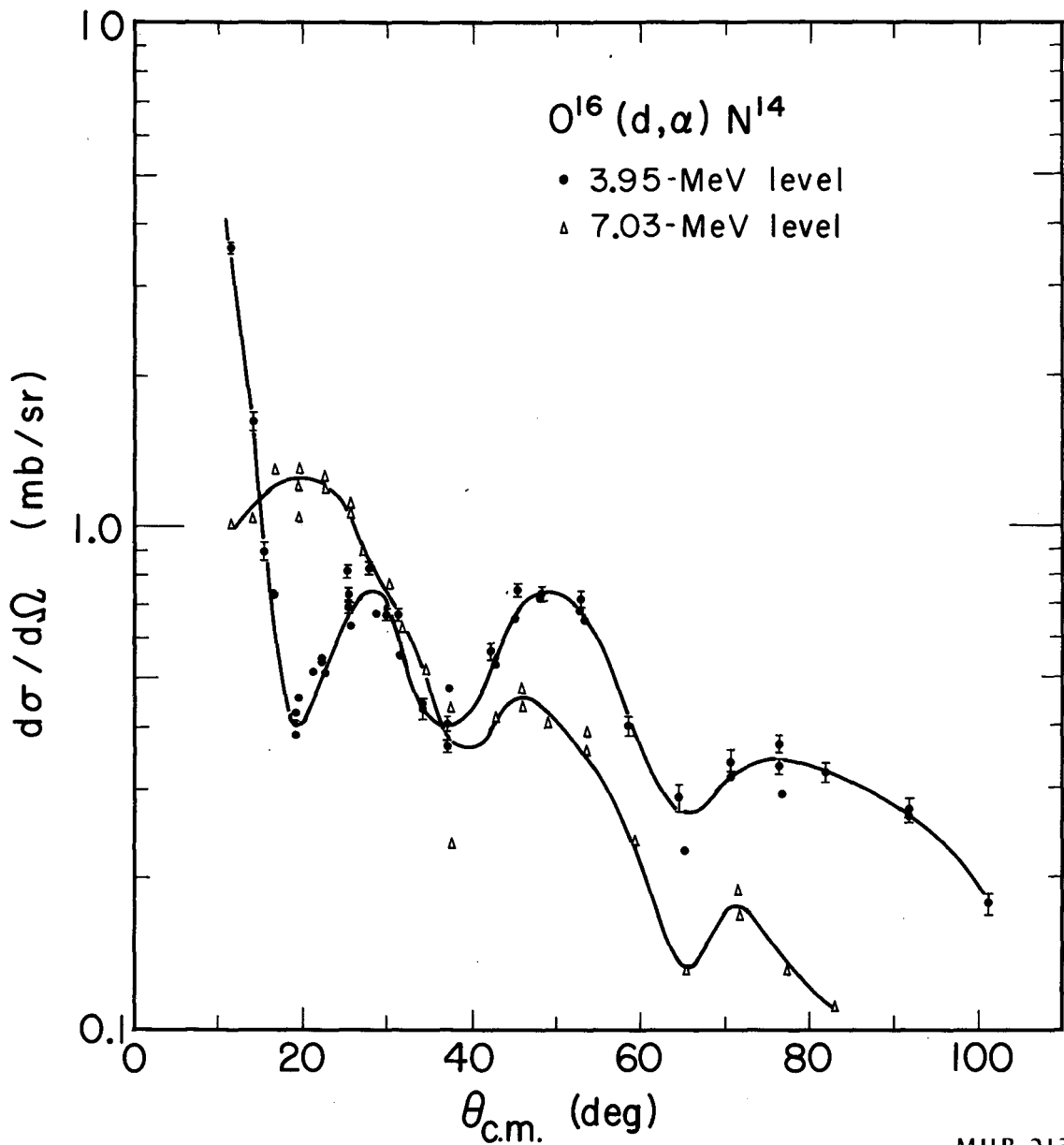
Fig. 28. Angular distributions of alpha particles from formation of the 3.95- and 7.03-MeV levels of N[14].

Table VII. Integrated cross sections for N^{14}.

Level (MeV)	Cross section (mb)	Range of integration (in deg, c.m.)		
0	1.97	11.3	-	100.2
3.95	3.16	11.5	-	101.2
4.91 5.10	1.29	11.5	-	82.2
5.69 5.83	1.68	11.6	-	82.5
6.21 6.44	1.28	11.6	-	82.6
7.03	2.11	11.6	-	82.9

the observed selectivity in the formation of the N^{14} levels via different reactions is especially interesting. For example, N^{14} levels formed strongly in the reaction $O^{16}(d,\alpha)N^{14}$ should be those whose configurations are such that they can be produced by simple removal of two nucleons from O^{16} if the reaction proceeds by a double pickup. One would not expect to form N^{14} levels in which one or more nucleons are in the $2s_{1/2}$ or $1d_{5/2}$ shells, since the amplitudes for such configurations are probably not large in O^{16}. The $C^{12}(\alpha,d)N^{14}$ reaction should populate the N^{14} levels whose configurations are an unchanged C^{12} core plus two nucleons. The $N^{14}(\alpha,\alpha')N^{14}$ reaction should show which N^{14} levels can be made from the ground state by excitation of a single nucleon.

Figures 29 and 30 show typical energy spectra obtained for the (α,d)[68] and (α,α')[72] reactions using bombarding energies of 50 and 65 MeV, respectively. Table VIII presents the approximate relative cross sections for a number of N^{14} levels and their dominant configuration. For the (α,d) reaction the cross section of each N^{14} level is divided by $(2J + 1)$, relative to the ground state divided by $(2J_{g.s.} + 1)$. Only a qualitative description of the cross section for the (α,α') reaction and some of the highly excited levels made by the (α,d) and (d,α) reactions are given.

In general the (α,d) results are in excellent agreement with the shell-model assignments of references 69, 70, and 71. The 3.95- and 7.03-MeV hole states, which cannot be formed by the addition of two nucleons to C^{12} in a $(s_{1/2})^4 (p_{3/2})^8$ configuration, are formed with rather small cross section. These levels could, however, be formed through the $(p_{3/2})^6 (p_{1/2})^2$ minor component of the C^{12} ground state. The $p_{1/2} d_{3/2}$ level at 7.97 MeV was not populated to the extent expected if the assigned configuration is correct. One could speculate that this configuration should be assigned to the heretofore unexplained level at 8.47 MeV, which is populated several times as much as the 7.97-MeV level.

The (α,α') reaction was observed to strongly populate all T=0 levels that can be made by excitation of a single nucleon, except for the 7.97-MeV level. Although the 8.47-MeV level was not strongly
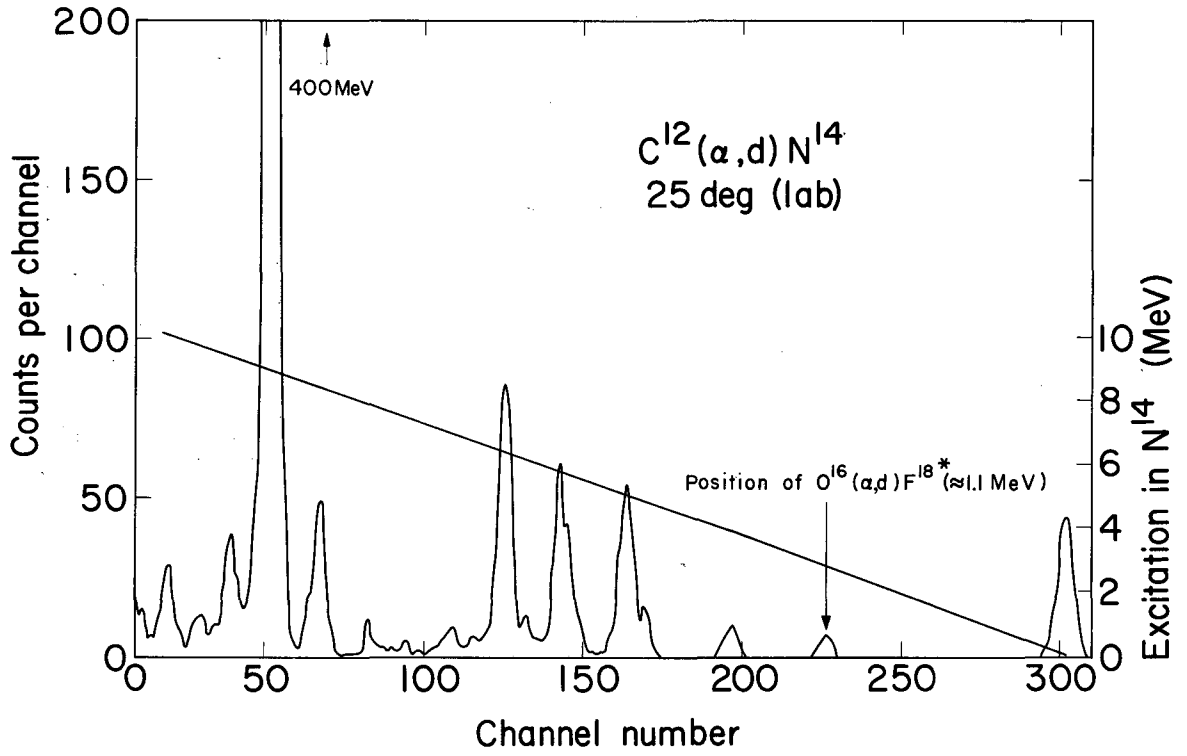
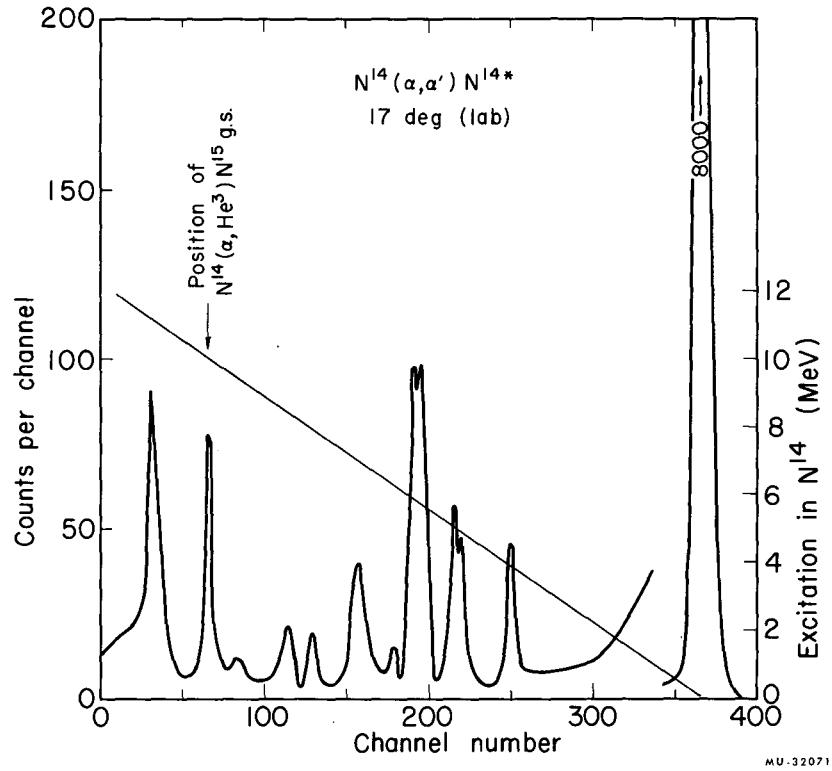Fig. 29. Deuteron energy spectrum from the $C^{12}(\alpha,d)N^{14}$ reaction.

Fig. 30. Alpha particle energy spectrum from the $N^{14}(\alpha,\alpha')N^{14*}$ reaction.

Table VIII. Shell-model configurations and relative cross sections for formation of N^{14} levels.

Level			Dominant	Relative cross sections		
MeV	J^π	T	configuration[a]	(α,d)[b]	(α,α')	(d,α)
0	1+	0	$(p_{1/2})^2$	1	—	1
2.31	0+	1	$(p_{1/2})^2$	d	d	d
3.95	1+	0	$(p_{3/2})^{-1}(p_{1/2})^{-1}$	0.2	Strong	1.60
4.91	0-	0	$p_{1/2}\,s_{1/2}$	1^c	Strong	0.72
5.10	2-	0	$p_{1/2}\,d_{5/2}$			
5.69	1-	0	$p_{1/2}\,s_{1/2}$	0.4^c	Strong	0.94
5.83	3-	0	$p_{1/2}\,d_{5/2}$			
6.05			?	d	d	d
6.21	1+	0	$(s_{1/2})^2$	0.7^c	Very weak	0.72
6.44	3+	0	$s_{1/2}\,d_{5/2}$			
7.03	2+	0	$(p_{3/2})^{-1}(p_{1/2})^{-1}$	Weak	Strong	1.19
7.40			?	d	d	d
7.60			?	d	d	d
7.97	2-	0	$p_{1/2}\,d_{3/2}$	Weak	Weak	Weak
8.06	1-	1	$p_{1/2}\,s_{1/2}$	d	d	d
8.47		0	?	Fairly strong	Weak	Fairly strong[e]
8.63	0+	1	$(s_{1/2})^2$	d	d	d
8.71	0-	1	$p_{1/2}\,s_{1/2}$	d	d	d
8.91	3-	1	$p_{1/2}\,d_{5/2}$	d	d	d
8.99	1+	(0)	?	1.5^c	d	d
9.00	5+	0	$(d_{5/2})^2$			
9.17	2+	1	$(s,d)+(p_{3/2})^{-1}(p_{1/2})^{-1}$	d	d	d
9.41	1-		$p_{1/2}\,d_{3/2}$ (?)	Fairly strong	Weak	Fairly strong
9.51	2-	1	$p_{1/2}\,d_{5/2}$	d	f	d
9.71	1+		$(d_{5/2})^2$	Weak	f	Very Weak
10.09	1+	0	$s_{1/2}\,d_{5/2}$[g]	Fairly strong	d	Weak
10.22	1-		?	h	d	Weak
10.42	2+	1	$s_{1/2}\,d_{5/2}$	h	d	d

[a]References 69, 70, 71.

[b]Numerical values from data obtained at $E_\alpha = 48$ MeV. Comments pertaining to levels above 7 MeV refer to data obtained at $E_\alpha = 50$ MeV.

[c]Assuming equal population of each magnetic substate of the unresolved pair of levels.

[d]Not observed.

[e]Obscured somewhat by He^3 peak.

[f]Obscured by He^3 peak arising from the $N^{14}(\alpha,He^3)N^{15}$ ground state transition.

[g]The assigned configuration is wrong if the spin of this level is 1+ as recently reported, instead of 2+ as previously thought.[73]

[h]Observable excitation did not extend to this level.

populated the cross section to this level was several times as great as
that to the 7.97-MeV level; this lends weight to the results obtained
from the (α,d) reaction. Transitions requiring double excitations
occurred with a considerably reduced cross section. For example, the
6.21- and 6.44-MeV levels — which required the double excitations
$(p_{1/2})^2 \rightarrow (s_{1/2})^2$ and $(p_{1/2})^2 \rightarrow (s_{1/2} \, d_{5/2})$, respectively — were
formed in only about one-tenth or less of the yield of levels marked
"strong" in Table VIII.

The (d,α) results are more difficult to understand. The double
closed-shell configuration of O^{16} could, by removal of two nucleons,
produce the levels in N^{14} at 0, 3.95, and 7.03 MeV. However, formation
of the levels at 4.91, 5.10, 5.69, and 5.83 MeV would require raising
one p nucleon into a s or d shell in addition to the removal of two
nucleons, and formation of the levels at 6.21 and 6.44 MeV would require
raising two p nucleons into the s and/or d shell. These six levels
were observed, although in slightly reduced yield. All these levels
could arise from an admixture of $[p^{-2}(s_{1/2})^2 + p^{-2}s_{1/2}d_{5/2} + p^{-2}(d_{5/2})^2]$
in the O^{16} ground state.[74] This O^{16} component should not produce the
$(d_{5/2})^2$ level at 9.0 MeV, since this level is believed[27] to have a spin
of 5. A $d_{5/2}$ pair coupled in this way could not be a component of the
spin-zero O^{16} ground state under j-j coupling rules. An admixture of
$\left[p^{-4}(d_{5/2})^4\right]$ would be needed to account for the population of the 9.0-
MeV level in the simple pickup-mechanism picture. As Fig. 26 indicates,
the cross section for formation of the 9.0-MeV level is small although
interference from the He^3 peak prevents setting an extremely low upper
limit.

The N^{14} levels with one or two s or d nucleons could be formed
by knockout of an alpha particle from the $(p_{3/2})^8 (p_{1/2})^4$ configuration
and capture of one or both nucleons of the incident deuteron in the s
or d shells. Although a knockout mechanism might be expected to form
the 9.0 MeV level also, the momentum transfer requirements for this transi-

tion are not met (assuming an interaction radius of 5 fermis) in the angular range that was carefully studied. Unless the (sd) admixture in O^{16} is quite large the knockout mechanism must be considered a likely explanation. The transitions that involve picking up $p_{3/2}\, p_{1/2}$ (formation of the 3.95- and 7.03-MeV levels) have larger cross sections than does the transition to the ground state that requires picking up $(p_{1/2})^2$. The fact that there are more $p_{3/2}$ nucleons available to be picked up probably contributes to the preference of $p_{3/2}\, p_{1/2}$ pickup. This result is in agreement with the tentative conclusion reached in Subsec. III. E.

3. The Forbidden Transition to the First Excited State

The $O^{16}(d,\alpha)N^{14*}$ (2.31 MeV) 0+, T=0 → 0+, T=1 direct-reaction transition is forbidden on the basis of angular momentum and parity conservation in addition to isotopic-spin conservation, as discussed in Subsec. III. D. At no angle was an alpha particle group observed that corresponded to formation of the T=1 level. The low backgrounds and excellent resolution obtained in this investigation enables one to set an upper limit for the ratio of the cross section for the forbidden transition to the cross section for the ground state transition of 0.7 ± 0.6%. This result and previously reported values for the ratio of these cross sections at other energies by different experimenters are presented in Fig. 31.

The effect of the isotopic-spin impurity depends upon the mechanism of the reaction. If the $O^{16}(d,\alpha)N^{14}$ reaction proceeds via a compound-nucleus mechanism, $\Delta T=1$ transitions could occur through the isotopic-spin impurities of the initial or final states or though impurities of states of the compound nucleus. It has been shown[55,78,79] that the isotopic-spin impurities of ground or low-lying levels of these nuclei should be small, $\approx 2\text{-}4 \times 10^{-3}$, for these states[78] of N^{14} and O^{16}. As the excitation energy of the compound nucleus increases with increasing bombarding energy, large isotopic-spin impurities may appear because of the closer proximity of levels of the same J^{π} and different T. However,
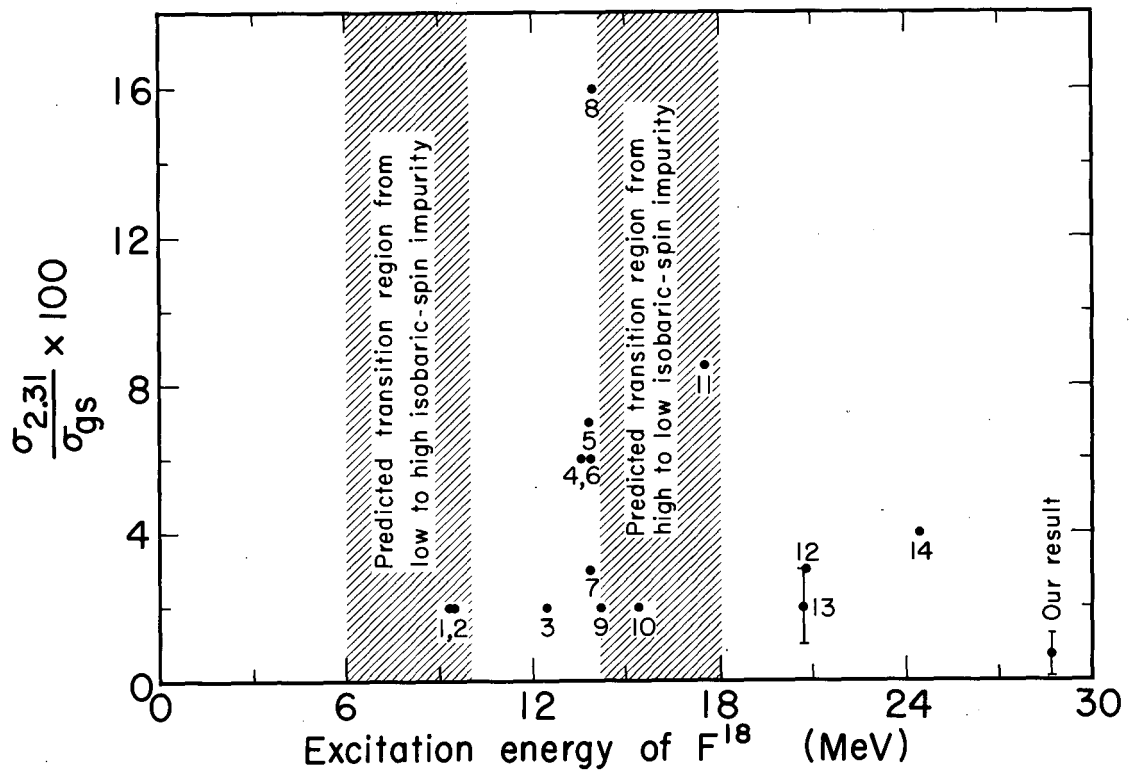
MU-31314

Fig. 31. Experimental ratios of the $O^{16}(d,\alpha)N^{14*}$ (2.31-MeV) cross
section to the $O^{16}(d,\alpha)N^{14}$ (ground state) cross section as a
function of compound-nucleus excitation energy. Points (1,2)
(reference 75), (3,9) from reference 32 (Br 56f), and 4,6-8,10)
from reference 32 (Da 58b) represent upper limits from observa-
tions at only one angle. Points 5, from 32 (Br 56f), and 14,
from reference 32 (Fr 53e), represent upper limits determined
from measurements from 15 to 130 deg and 20 to 155 deg, respec-
tively. Point 11 (reference 76) was estimated by us from data
given at 45, 80, and 90 deg. Point 12 (reference 53) represents
the highest value for this ratio between ≈ 15 and ≈ 100 deg. Point
13 (reference 77) represents the range of the ratio from 20 to
80 deg.

Lane and Thomas[55] and Wilkinson[79] have shown that at sufficiently high
excitation a region should be attained in which there is a low "effective"
i-spin impurity. This low impurity of the compound system arises from
the simultaneous excitation of many overlapping levels in a total state
of initially well-defined isotopic spin, which then breaks up before
the Coulomb forces have had time to cause appreciable mixing. Wilkinson's
limits for the regions of low i-spin impurity are represented in Fig. 31
by shading.

To compare the experimental results on i-spin forbidden trans-
itions with the prediction of the magnitude of i-spin admixtures in the
intermediate compound nucleus, one should subtract out the direct-
interaction contribution to both the ground and 2.31-MeV states. A
detailed calculation of this contribution would be valuable but has
not been done; hence the data plotted in Fig. 31 ignore this correction,
which will be discussed below. The results are seen to agree quali-
tatively with the theoretical prediction. Large cross sections to the
2.31-MeV level are observed only in the transition region between the
two limits.

It is important to estimate the relative direct-interaction
contribution to the ground (1+, T=0) and 2.31-MeV (0+, T=1) states.
Direct-reaction transitions to the 2.31-MeV level could occur only
through (a) a breakdown of the parity selection rule for two-nucleon
transfer reactions, $\pi_f = \pi_i(-1)^L$ from contributions of other than S
states of relative orbital angular momentum in the picked up pair of
nucleons, or (b) a spin flip of one of the transferred nucleons, either
or both operating in conjunction with the isotopic-spin impurities of
the initial or final state. One would therefore expect that the pre-
dominant part of any observed transitions to the 2.31-MeV level would
proceed through a compound-nucleus mechanism, so that the only important
direct-interaction correction would be to the ground state cross section.
For intermediate-energy incident deuterons, the fraction of the cross
section arising from a direct-interaction mechanism would be expected,

in general, to increase with increasing bombarding energy; this would lead to a decrease similar to that observed in the ratio plotted in Fig. 31. Fischer and Fischer[80,81] have made a very rough calculation of the theoretical compound-nucleus cross section for the $O^{16}(d,\alpha)N^{14}$ ground state transition and have found it to be only 9% of the observed cross section for 19-MeV deuterons. Thus some large corrections to the above ratios would probably be required.

Another factor that should be included in this analysis is that 0+, T=0 → 0+, T=1(d,α) compound-nucleus transitions are also significantly reduced by restrictions imposed by angular momentum and parity conservation.[82] With a target nucleus of zero spin and even parity, deuterons of angular momentum 1 will form compound states of spin j=1, 1 ± 1 and parity $(-)^1$. Alpha emission to a 0+ state is only possible, however, from states of spin J, parity $(-1)^J$. Hence it appears that only about one-third of the states formed in the compound nucleus will be able to decay by alpha emission to the 0+ state. Thus part of the forbiddenness attributed to i-spin conservation in reality arises from this.

Thus both effects mentioned in the preceding two paragraphs would tend to increase the value of the ratio indicating the effect of i-spin conservation in forbidding the $O^{16}(d,\alpha)N^{14*}$ (2.31-MeV) transition. Theoretical calculations of (a) the effect of angular momentum and parity conservation in restricting compound-nucleus transitions to the 2.31-MeV state and (b) the expected compound-nucleus cross section to the ground state, over the range of bombarding energies, would be quite valuable for adjusting the experimental data to show accurately the behavior of the isotopic-spin impurity of a light compound nucleus.

G. (d,He^3) Reactions

The angular distributions of the He^3 ions arising from the $C^{12}(d,He^3)B^{11}$ ground state and $O^{16}(d,He^3)N^{15}$ ground state transitions are shown in Figs. 32 and 33, respectively. Since the $N^{14}(d,He^3)C^{13}$
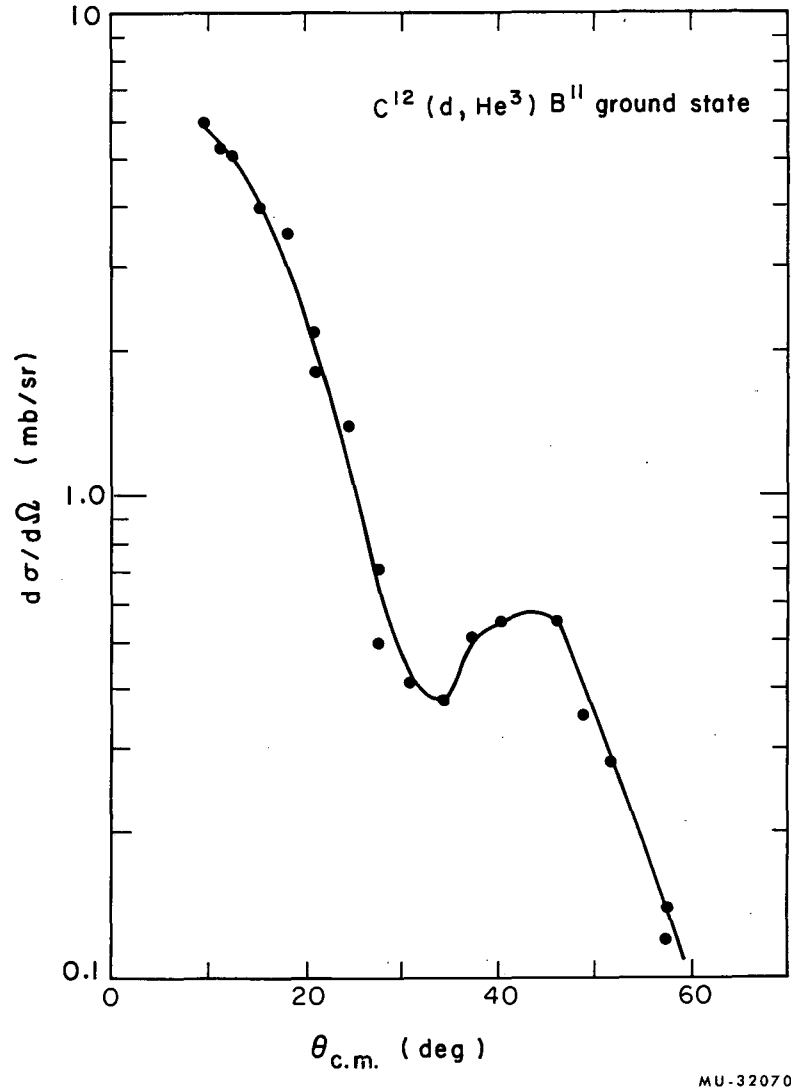
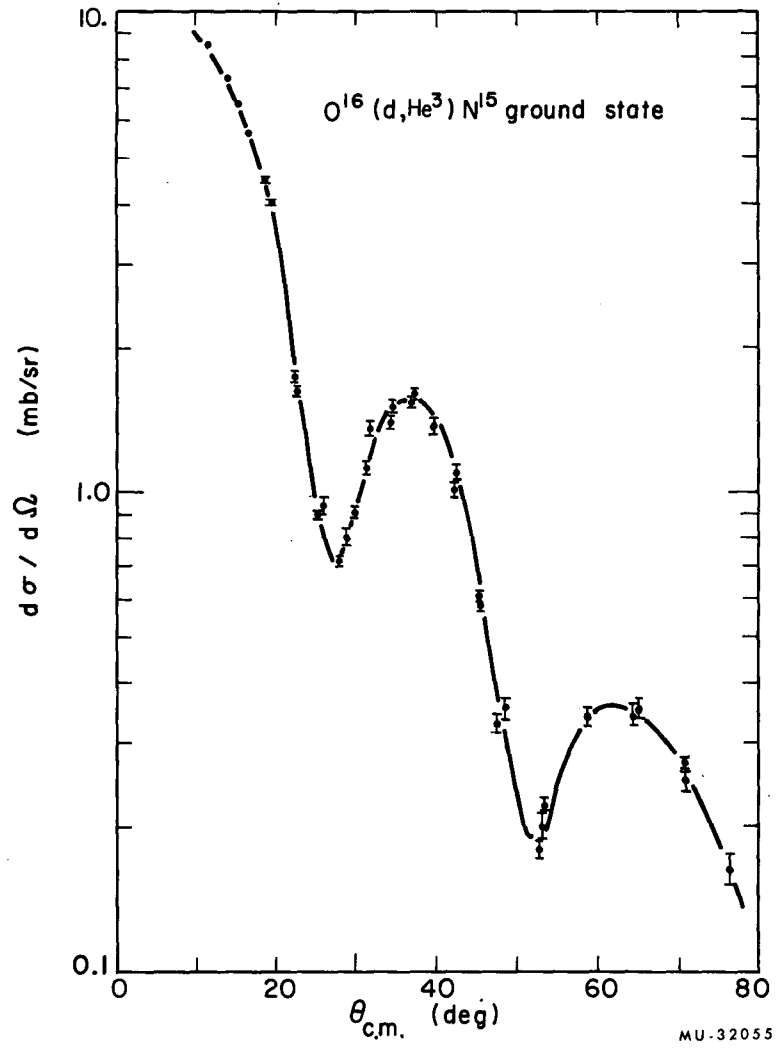Fig. 32. Angular distribution of He^3 ions from the C^{12}(d,He^3)B^{11} ground state transition.

Fig. 33. Angular distribution of He^3 ions from the $O^{16}(d,He^3)N^{15}$ ground state transition.

reaction was only observed at three angles, no angular distribution is presented. However, it should be noted that the absolute values of the differential cross section for this reaction at the angles observed are approximately the same as the other two (d,He^3) reactions. This is in marked contrast to the relative (d,α) cross sections for these three targets. Since the He^3 peaks were not separated from the alpha particle continuum or nearby alpha peaks, the analysis involved a somewhat arbitrary subtraction of the "pure He^3 peak" from the energy spectra. Consequently another source of error is introduced, although the error bars shown are again due to counting statistics only.

These specific reactions have not been studied previously, probably because of the experimental difficulties involved in separating the He^3 ions from the alpha particles. In fact, only three (d,He^3) experiments from which angular distributions were obtained have been reported in the light elements ($Z = 2$ to 10): $Li^6(d,He^3)He^5$ (reference 34), $Li^7(d,He^3)He^6$ (reference 49), and $F^{19}(d,He^3)O^{18}$ (reference 83). However, the (d,He^3) reaction which involves the pickup of a single proton should compliment the other proton pickup reactions, (n,d) and (t,α). It also has the experimental advantage of working with a deuteron beam instead of either a neutron or triton beam. The observation of the (d,He^3) transitions in our work was a "bonus," but no further analysis of these reactions has been undertaken.

IV. GENERAL DISCUSSION AND CONCLUSIONS

### A. Reaction Mechanism: Pickup vs Knockout

The two direct reaction mechanisms for (d,α) reactions considered in this section are represented in Fig. 34 in a highly schematic manner for an observer in the center-of-mass system. In the "pickup" reaction one considers an incoming deuteron to become attached to an additional "deuteron-like cluster" near the surface of the target, forming an alpha particle which travels on, leaving the final nucleus behind. The "knock-out" reaction occurs when a deuteron knocks an alpha particle out of the surface of the target and is itself captured to form the final nucleus. In the latter case, the target nucleus is considered to be a "core" + alpha particle, while the final nucleus is represented by the "core" + deuteron.

If the reaction takes place primarily at the surface the outgoing alpha particle originates in a well-defined zone, and wave-mechanical interference gives an angular distribution that oscillates in intensity as the angle between the incident and outgoing particle varies. Butler et al.[84] showed that this angular distribution is given approximately by

$$d\sigma/d\Omega \ \propto \ F(\theta) \ j_1^{\ 2}(QR), \qquad (1)$$

where Q is the momentum transferred to the core and R is the distance from the center of the nucleus at which the reaction is assumed to take place. Since Q increases with increasing angle of observation, the oscillating spherical Bessel function j_1, gives peaks and valleys in the angular distribution.

The momentum transfer to the core for pickup is $\vec{Q} = \dfrac{M_f}{M_i} \vec{k}_d - \vec{k}_\alpha$, which differs only slightly from that for knockout:[85]
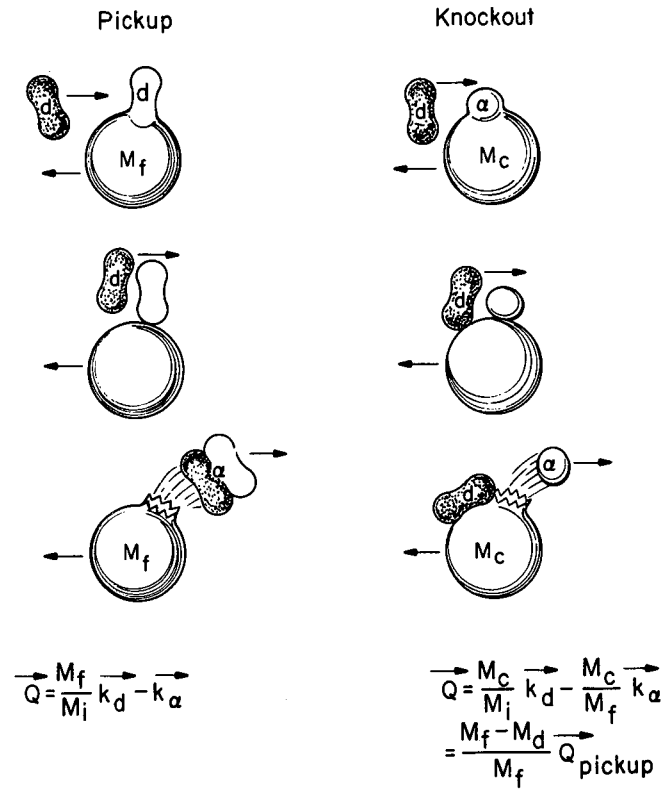
Fig. 34. Schematic representation of the (d,α) reaction mechanisms.

$$\vec{Q} = \frac{M_c}{M_i} \vec{k}_d - \frac{M_c}{M_f} \vec{k}_\alpha = \frac{M_f - M_d}{M_f} \vec{Q}_{pickup} \; ,$$

where k_d and k_α are the wave numbers of the deuteron and alpha particles in the center-of-mass system. Consequently, by adjusting R slightly (about 1F for the (d,α) reactions studied) one obtains the same angular distribution for pickup and knockout except for the slowly varying form factor $F(\theta)$. Thus it is not possible to distinguish reaction mechanisms by fitting angular distributions (see references 86 and 87 for specific examples).

From the spectral shapes of many inverse-reaction pairs ——(p,d) and (d,p); (p,t) and (t,p); (p,α) and (α,p) —— Cohen and Rubin[8] conclude that all these reactions proceed through either stripping or pickup rather than through a knockout mechanism. They, and Ball et al.,[88] cite the decrease of cross section from (p,d) to (p,t) to (p,α) reactions as further evidence of a pickup mechanism. However, Mead and Cohen[9] conclude that it is difficult to explain the results of their survey of (d,α) reactions in heavy elements by either a pickup or knockout model, although they tend to favor pickup.

Evidence strongly indicates that the (α,d) reaction in the light elements proceeds by a stripping mechanism.[3,25,27,62,86] Since the (d,α) reaction is the time-reversed (α,d) reaction for the respective ground state transitions, and pickup is the inverse of stripping, this constitutes another strong argument in favor of the pickup mechanism for (d,α) reactions.

The mass-number dependence of the integrated cross section for the ground state transitions, presented in Fig. 35 for the (d,α) reactions studied, could be construed as evidence in favor of a knockout mechanism. Unfortunately the data do not extend to 180 deg but the comparison is based on the same angular range (10 to 90 deg, center-of-mass) for the reactions. The large uncertainty in the Be^9 point arises from the comparatively small angular range over which the $Be^9(d,\alpha)Li^7$ reaction
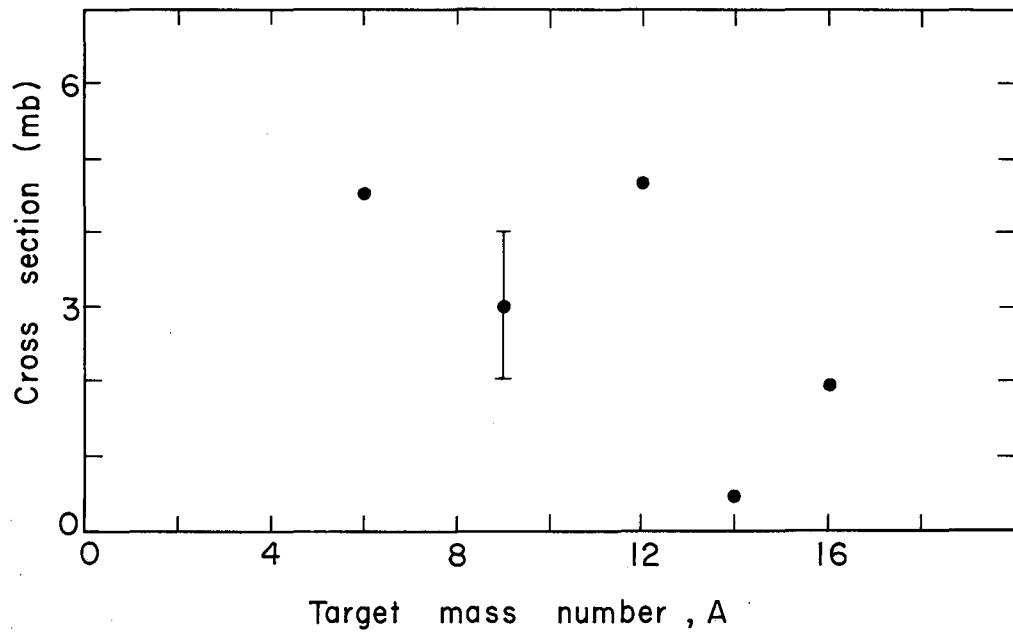
Fig. 35. Integrated cross sections of the ground state transitions
as a function of the mass number A of the target.

was studied. The $Li^6(d,\alpha)He^4$ cross section was divided by a factor of two to take account of the fact that two alpha particles are produced in each reaction event.

Yanabu[77] and Takamatsu[89] have also found a remarkable difference between 4n and non-4n target nuclei. Using 14.7-MeV deuterons and extrapolating their measurements so as to include the total solid angle cross sections, they found that C^{12}, O^{16}, Ne^{20}, Mg^{24}, and S^{32} targets had cross sections for ground state (d,α) transitions which fell on a line considerably above the line on which the cross sections for N^{14}, F^{19}, Al^{27}, and P^{31} targets fell.

Since direct-interaction theories contain an energy dependence the greatly differing Q values of the reactions introduce a factor which should be considered when comparing their cross sections. A qualitative explanation of the results shown in Fig. 35 which does not invoke a knock-out mechanism can be presented. Assume that the ground state transitions for the (d,α) reactions on C^{12}, N^{14}, and O^{16} all proceed by the pickup of two p nucleons. If the reaction takes place primarily at the surface, incoming partial waves L_d and outgoing waves L_α will contribute strongly to the reaction only at $L_d \approx k_d R$ and $L_\alpha \approx k_\alpha R$. Since the angular momentum transferred to the core is $\vec{L} = \frac{M_f}{M_i} \vec{L}_d - \vec{L}_\alpha$, and two p nucleons can couple to a maximum of L=2, reactions with $\left| \frac{M_f}{M_i} \vec{L}_d - \vec{L}_\alpha \right| > 2$ should be inhibited. The greater the difference $\left[\frac{M_f}{M_i} \vec{L}_d - \vec{L}_\alpha -2 \right]$, the stronger will be the inhibition. As shown in Table IX the momentum mismatch is considerably greater for $N^{14}(d,\alpha)C^{12}$ than for $C^{12}(d,\alpha)B^{10}$, with $O^{16}(d,\alpha)N^{14}$ in between, in agreement with their relative cross sections. In fact, the momentum mismatch is always greater for (d,α) reactions on non-4n target nuclei since these reactions have large positive Q values relative to (d,α) reactions on 4n target nuclei. The momentum mismatch also increases as A increases, if nucleons of the same shell configuration are being picked up, because of the larger interaction radius. This would tend to account for the downward slope observed for both the 4n and non-4n targets.

Table IX. Comparison of momentum mismatch for various two-nucleon pickup reactions.

Reaction	Bombarding energy (MeV)	Q value (MeV)	R (F)	$L_{\theta\,=\,20\ deg}$	$L_{\theta\,=\,60\ deg}$
$O^{16}(d,\alpha)N^{14}$	24	3.11	6.00[a]	5.37	10.00
$N^{14}(d,\alpha)C^{12}$	24	13.57	5.25[a]	6.42	10.12
$C^{12}(d,\alpha)B^{10}$	24	-1.34	4.80[a]	3.40	6.85
$N^{14}(\alpha,Li^{6})C^{12}$	42	-8.80	5.25	3.88	10.60
$C^{12}(\alpha,Li^{6})B^{10}$	42	-23.72	4.80	3.72	7.50
$N^{14}(p,He^{3})C^{12}$	50	-4.77	5.25	5.85	10.00
$C^{12}(p,He^{3})B^{10}$	50	-19.68	4.80	3.44	7.28

[a]Interaction radius determined from fitting angular distribution, Subsec. IV. C.3.

If the cross-section differences observed are caused by a momentum mismatch a similar difference should be observed in other two-nucleon pickup reactions such as (p,He^3) and (α,Li^6). No (p,He^3) reactions have been reported and very little work has been done with the (α,Li^6) reaction. Zafiratos[62] investigated the $N^{14}(\alpha,Li^6)C^{12}$ and $C^{12}(\alpha,Li^6)B^{10}$ reactions, using 42-MeV alpha particles, and found the cross sections of the respective ground state transitions approximately the same. But as shown in Table IX the relative difference of the momentum mismatch for these two reactions at this bombarding energy is considerably less than for the corresponding (d,α) reactions. Therefore the momentum-mismatch inhibition should not be as great. An extensive investigation of a series of targets —— using both the (p,He^3) and (α,Li^6) reactions in conjunction with the (d,α) reaction —— might be valuable for determining the importance of momentum-mismatch inhibition. Such a study might also provide better insight into the reaction mechanism than is possible with the present information.

When comparing the cross sections of different reactions the spectroscopic factor should be considered. Since direct interactions are characterized by the fact that only a few nucleons are actively involved in the reaction, overlap integrals involving the passive nucleons must always enter the expression for the cross section. Such an overlap measures the degree to which the passive nucleons occupy the same configuration in the initial and final states. The sum of these overlap integrals is called the spectroscopic factor.[1,90] However, the validity of the present quantitative calculation of these factors for two-nucleon transfer reactions in the light elements is questionable.[66] Nevertheless, spectroscopic factors were calculated by following the method of Yoshida[91] for the (d,α) ground state transitions on O^{16}, N^{14}, and C^{12}. Assuming pure j-j coupling and configurations of $(p_{1/2})^4$, $(p_{1/2})^2$ and $(p_{3/2})^8$ for O^{16}, N^{14}, and C^{12}, respectively, the spectroscopic factor for the $N^{14}(d,\alpha)C^{12}$ reaction is about half the value obtained for the other two transitions.

Thus, both momentum-mismatch and the spectroscopic factor tend to lower the cross section of the $N^{14}(d,\alpha)C^{12}$ ground state transition relative to the $O^{16}(d,\alpha)N^{14}$ and $C^{12}(d,\alpha)B^{10}$ ground state transitions. These factors are probably sufficiently large to account for the results illustrated in Fig. 35.

Although a pickup mechanism appears to be more likely, as discussed above, the observed trend could also be explained on the basis of a knockout mechanism as discussed in the following. For illustrative purposes the $C^{12}(d,\alpha)B^{10}$ and $N^{14}(d,\alpha)C^{12}$ ground state transitions will be compared. Consider C^{12} as being composed of three alpha particles,[92] and N^{14} as being a deuteron + "C^{12} (or 3 alphas) core". From a simple picture one would think that the incident deuteron could pickup the more loosely bound deuteron from N^{14} more easily than the tightly bound deuteron from C^{12}. However, the experimental cross section for the ground state transition for the (d,α) reaction on C^{12} is over ten times greater than for N^{14}. But if we assume the reactions are taking place by a knockout mechanism the (d,α) reaction on C^{12} would be favored, since the possibility of the incident deuteron knocking an alpha cluster from the target nucleus, and itself sticking, without exciting the remaining "core" would probably be greater than such an occurrence in N^{14} since in the latter reaction the "outer deuteron" would often be excited. Consequently the $N^{14}(d,\alpha)C^{12}$ reaction would favor exciting levels other than the ground state, and as noted in Subsec. III. E. this reaction strongly favored formation of excited levels relative to the ground state. In contrast the cross section for the ground state transition of the $C^{12}(d,\alpha)B^{10}$ reaction is over twice as large as the cross section to any excited level. Furthermore, although the $O^{16}(d,\alpha)N^{14}$ ground state transition cross section is slightly smaller than the cross section to two excited levels it is larger than any other observed level.

Another possible point in favor of a knockout mechanism is the relative cross section of (d,α) to (d,He^3) ground state transitions. Since it is easier to pick up one particle than two, the (d,He^3) cross

section should be considerably larger than the (d,α) cross section in analogy to the (p,d) to (p,t), to (p,α) cross sections.[8,88] The statistical ratio

$$\frac{2I_f + 1}{2I_i + 1}$$

also favors the (d,He^3) reaction by a factor of two. However, for the C^{12} target the (d,He^3) cross section is larger than the (d,α) cross section only at angles less than 20 deg. For the O^{16} target the (d,He^3) and (d,α) cross sections are approximately equal if the statistical factor of two is included. But for the N^{14} target the (d,He^3) cross section is much larger than the (d,α) cross section, in accord with a pickup mechanism.

The relatively large cross sections for the formation of levels that could not be made through a pickup mechanism — unless one assumed that the target nuclei had large (sd) admixtures — has already been pointed out in Sec. III. This constitutes another argument in favor of a knockout mechanism, although once again the situation is not clear.

For the sake of completeness a third mechanism, heavy-particle stripping (or exchange stripping), should be mentioned.[93] Heavy-particle stripping envisages the projectile as interacting with the "core" of the target nucleus, thereby "stripping" the core from the target nucleus and releasing the alpha particle. The alpha particle continues in the original direction of the motion of the target nucleus in the center-of mass system, which is the backward direction. Thus heavy-particle stripping will enhance the cross section in the backward direction, since

$$\vec{Q} = \vec{k}_d + \frac{M_d}{M_f} \vec{k}_\alpha,$$

which has a large magnitude in the forward direction and decreases in the backward direction. Many (d,α) angular distributions, obtained with

low bombarding energies, show an increased cross section in the back-
ward direction; this has led a number of people to include a contribution
from the heavy-particle stripping mechanism to the calculated cross sec-
tion to improve the fits to the experimental data (e.g., see references
77 and 87). However, distorted-wave calculations for low-energy (d,p)
reactions can produce a strong backward peak whereas no such effect is
seen in the plane-wave theoretical calculation.[5,94] Thus, the need of
invoking heavy-particle stripping is open to question and the present work
ignores this mechanism.

B. Pseudo Detailed Balance

Time-reversal invariance implies a detailed balance between
nuclear reactions, although the inverse statement is not always true.[95,96]
If the detailed balance is to be made for the reactions

$$A + 2 + d \rightleftarrows A + \alpha ,$$
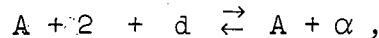
the bombarding energies must be adjusted so that the momentum of the
outgoing alpha particle (incoming deuteron) from the (d,α) reaction is
the same as the momentum of the incoming alpha particle (outgoing deuteron)
for the (α,d) reaction (all values in center-of-mass system of course).
Another way of stating the energy requirement is that the excitation of
the compound state must be the same via both reactions. The differential
cross sections for the two reactions should then satisfy the equation[97]

$$\left(\frac{d\sigma}{d\Omega}\right)_{d,\alpha} = \frac{(2J_\alpha + 1)(2J_A + 1)}{(2J_d + 1)(2J_{A+2} + 1)} \left(\frac{p_\alpha^2}{p_d^2}\right) \left(\frac{d\sigma}{d\Omega}\right)_{\alpha,d} , \quad (2)$$

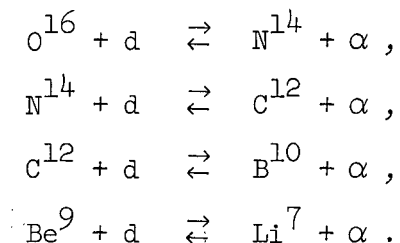where p_α and p_d are the momenta of the alpha particle and deuteron,
respectively.

However, Legg[98] has noted that if a simple plane-wave theory of
a two-nucleon transfer reaction is applicable [see Eq. (1)] the energy

dependence of the differential cross section enters only through the momentum transfer. For a given momentum transfer the differential cross sections are related by

$$\left(\frac{d\sigma}{d\Omega}\right)_{d,\alpha} = \frac{(2J_\alpha + 1)(2J_A + 1)}{(2J_d + 1)(2J_{A+2} + 1)} \left(\frac{p_\alpha}{p_d}\right)_{d,\alpha} \left(\frac{p_\alpha}{p_d}\right)_{\alpha,d} \left(\frac{d\sigma}{d\Omega}\right)_{\alpha,d} . \quad (3)$$

Thus a pseudo detailed balance can be made by varying the angles at which the differential cross sections are to be compared so that the momentum transfer of the two reactions are equal.

The degree to which the pseudo detailed balance fails is a measure of the failure of the simple plane-wave theory. As the difference between a proper pair of bombarding energies for a detailed balance and the pair of bombarding energies actually used increases, the degree to which the pseudo detailed balance fails would probably also increase. With these considerations in mind the following pseudo detailed balances were studied:

$$O^{16} + d \rightleftarrows N^{14} + \alpha ,$$

$$N^{14} + d \rightleftarrows C^{12} + \alpha ,$$

$$C^{12} + d \rightleftarrows B^{10} + \alpha ,$$

$$Be^9 + d \rightleftarrows Li^7 + \alpha .$$

The $O^{16}(d,\alpha)N^{14}$ angular distribution obtained with 23.8-MeV deuterons was compared with $N^{14}(\alpha,d)O^{16}$ angular distributions obtained with 46.5- (reference 86) and 42-MeV (reference 62) alpha particles. As shown below these relative energies are far from being appropriate for a detailed balance:

Reaction	Excitation of compound state
O^{16} + 23.8-MeV d	28.64 MeV
N^{14} + 46.5-MeV α	40.53 MeV
N^{14} + 42-MeV α	37.1 MeV .

Figure 36 shows the extent to which the pseudo detailed balance holds. For this comparison, and for the comparisons illustrated later, the momentum transfer was calculated on the basis of pickup and stripping kinematics for the (d,α) and (α,d) reactions, respectively. The magnitudes of the (α,d) angular distributions were multiplied by the factors needed to satisfy Eq. (3).

The $N^{14}(d,\alpha)C^{12}$ angular distribution obtained with 23.8-MeV deuterons was compared with the $C^{12}(\alpha,d)N^{14}$ angular distribution obtained with 48-MeV alpha particles.[3] These relative enegies are almost appropriate for a detailed balance as shown below:

Reaction	Excitation of compound state
N^{14} + 23.8-MeV d	41.70 MeV
C^{12} + 48-MeV α	43.15 MeV .

Thus the momentum transfers for the two reactions are almost equal when compared at the same angle. Consequently Fig. 37 compares the differential cross sections directly without adjusting to get exact momentum-transfer equality. The shift needed to obtain exact equality is about 1.5 deg in the direction of better agreement [compare $(d\sigma/d\Omega)_{\alpha,d}$ at 15 deg with $(d\sigma/d\Omega)_{d,\alpha}$ at 16.5 deg].

The $C^{12}(d,\alpha)B^{10}$ angular distribution obtained with 24.1-MeV deuterons was compared with the $B^{10}(\alpha,d)C^{12}$ angular distribution obtained with 42-MeV alpha particles.[62] Once again the relative energies are far from being appropriate for a detailed balance:
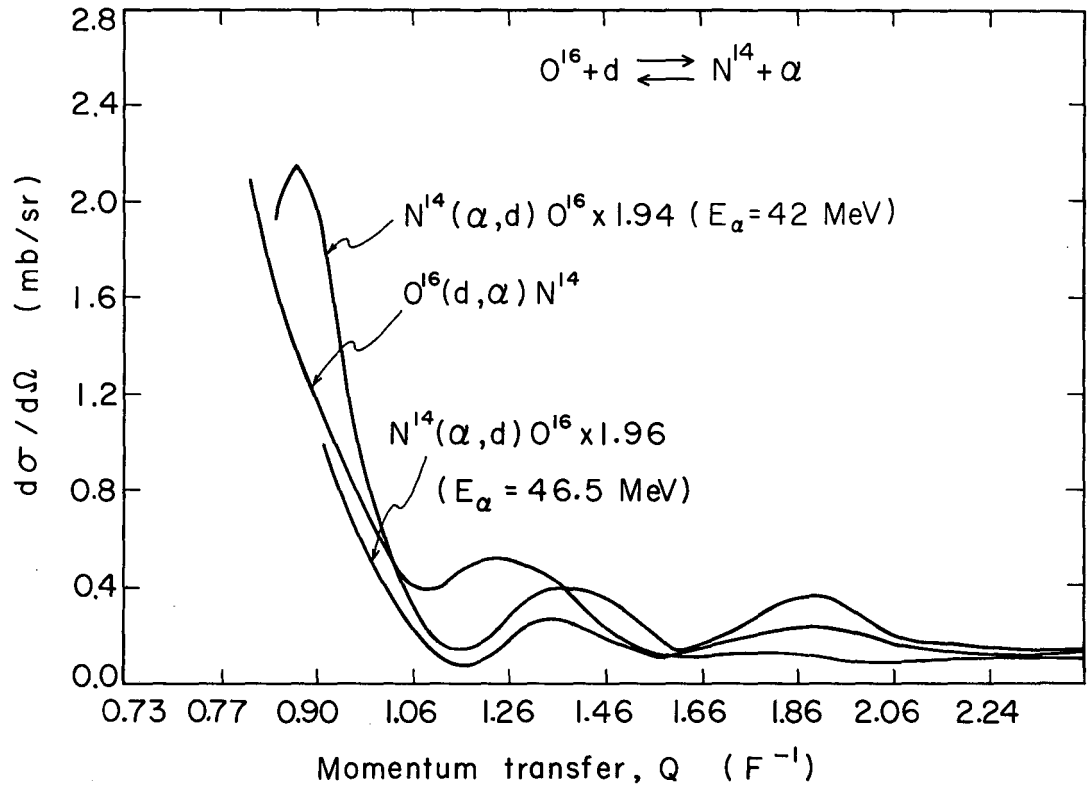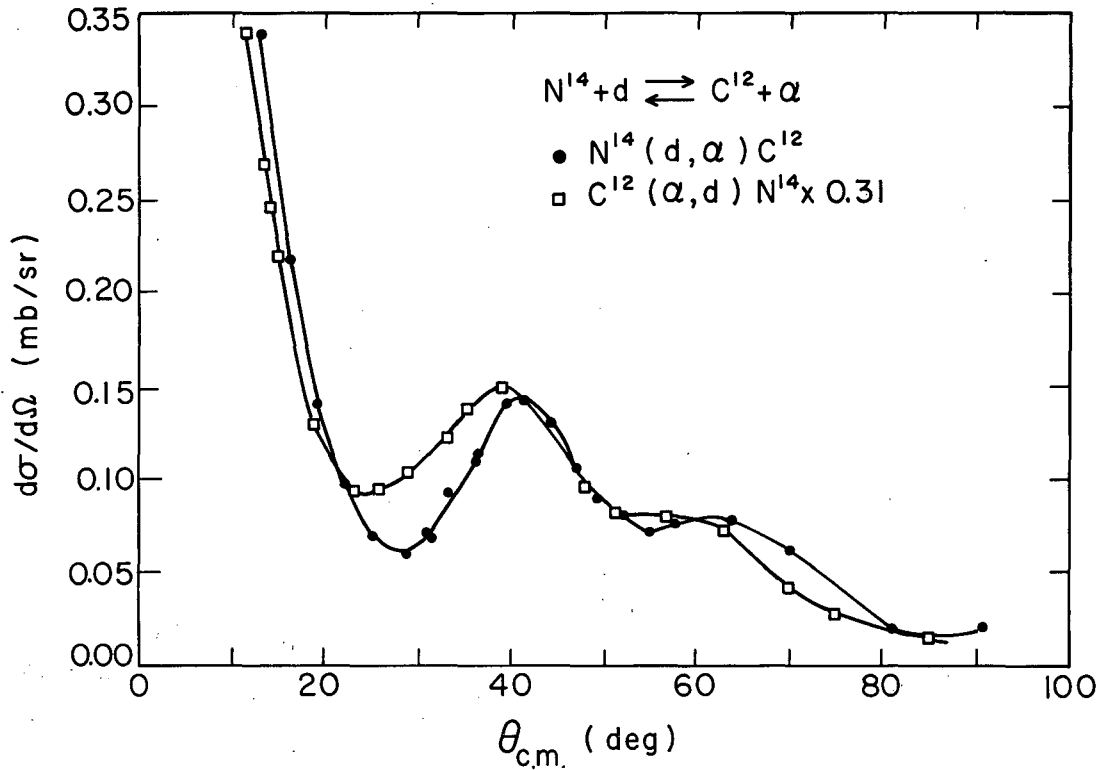
Fig. 36. Pseudo detailed balance for the $O^{16} + d \rightleftarrows N^{14} + \alpha$ system.

Fig. 37. Pseudo detailed balance for the N^{14} + d $\rightleftarrows$ C^{12} + α system.

Reaction	Excitation of compound state
C^{12} + 24.1-MeV d	30.97 MeV
B^{10} + 42-MeV α	41.61 MeV .

Figure 38 shows the extent to which the pseudo detailed balance holds.

The limited $Be^9(d,\alpha)Li^7$ angular distribution obtained with 24.1-MeV deuterons was compared with the $Li^7(\alpha,d)Be^9$ angular distribution obtained with 48-MeV alpha particles.[25] These relative energies are fairly well matched although not to the degree of the $N^{14} + d \rightleftarrows C^{12} + \alpha$ set:

Reaction	Excitation of compound state
Be^9 + 24.1-MeV d	35.51 MeV
Li^7 + 48-MeV α	39.16 MeV .

As Fig. 39 illustrates, the pseudo detailed balance appears to hold quite well but the comparison could be made only over a small angular range.

The $N^{14} + d \rightleftarrows C^{12} + \alpha$ pseudo detailed balance definitely exhibited the best agreement, as might be expected since it came nearest to satisfying the relative energy requirements for a detailed balance. However, all the comparisons showed fairly good agreement, especially at small angles, which indicates that the absolute values of the (d,α) cross sections measured are probably quite accurate.

C. Distorted-Wave Calculations

1. General Discussion

The general form of the differential cross section for two-nucleon transfer reactions is derived and discussed extensively by Glendenning.[65] For the two nucleon pickup reaction the cross section can be summarized by
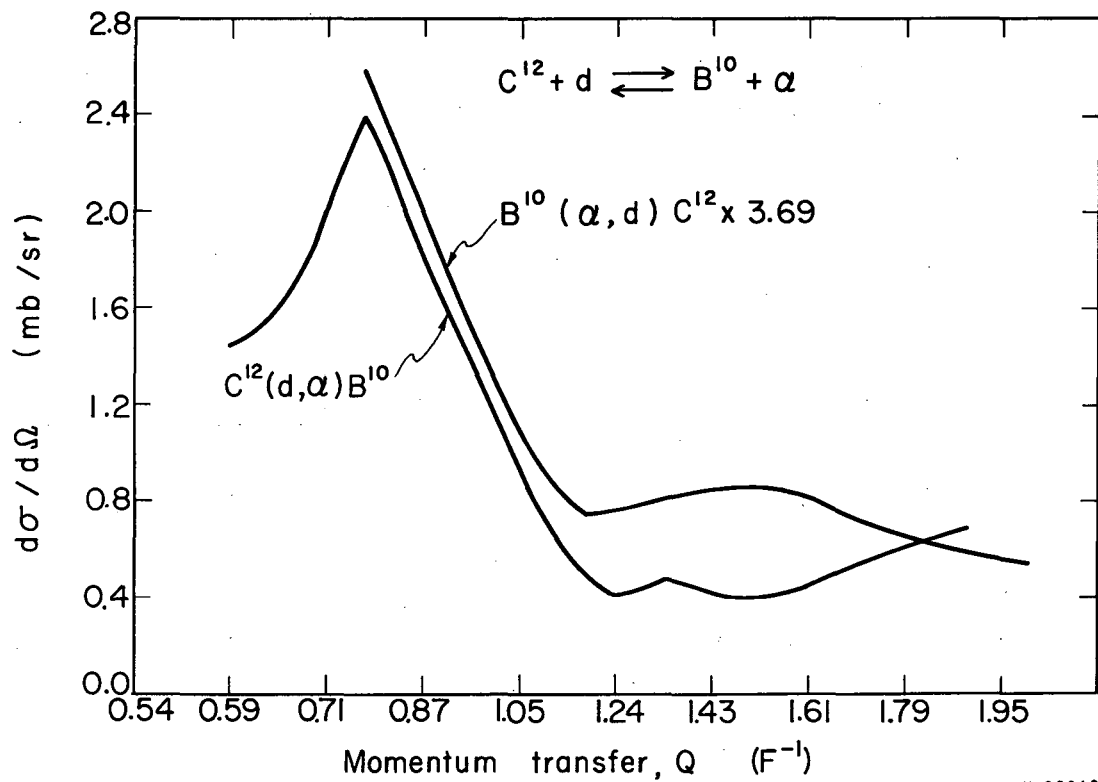
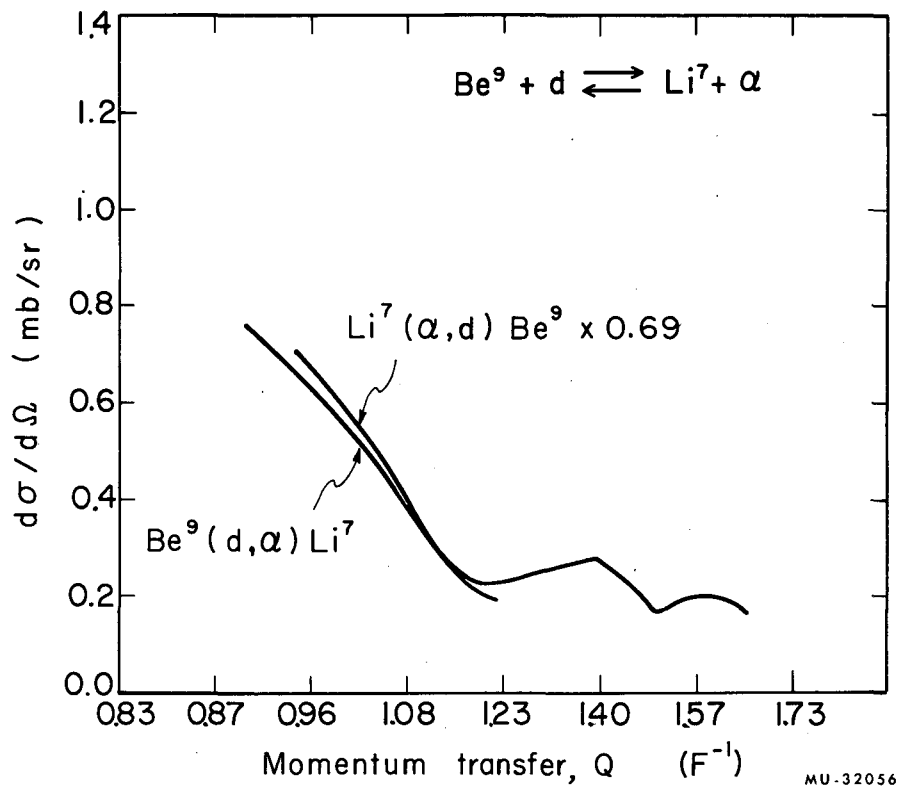Fig. 38. Pseudo detailed balance for the $C^{12} + d \rightleftarrows B^{10} + \alpha$ system.

Fig. 39. Pseudo detailed balance for the $Be^9 + d \rightleftarrows Li^7 + \alpha$ system.

$$\frac{d\sigma}{d\Omega} = \frac{2I_f + 1}{2I_i + 1} \ \frac{m_i^* \ m_f^*}{(2\pi \ \hbar^2)^2} \ \frac{k_f}{k_i} \ (fC)^2 \sum_{LSJM} \frac{b_S^2}{2S+1} \ \left| \sum_{\gamma} \beta_{\gamma LSJ} \ B_{\gamma L}^M \right|^2 \ , \qquad (4)$$

where

I_i and I_f are the spins of the incident and outgoing particles, respectively,

m_i^* and m_f^* are the reduced masses,

k_i and k_f are the wave numbers for relative motion in the initial and final states,

fC is a statistical factor needed to account for the equivalence principle,

$b_S^2/2S+1$ is a factor arising from the spin selection rule,

$\beta_{\gamma LSJ}$ is the nuclear structure coefficient which represents the degree of overlap between the configurations of the initial and final states,

and

$B_{\gamma L}^M$ is the transfer amplitude for the pickup of two nucleons with quantum numbers (LM).

The sum on γ introduces a coherent effect; e.g., this sum might refer to configuration mixing in the wave function. The cross section for stripping reactions is similar except that the factor $(2I_f+1)/(2I_i+1)$ is replaced by $(2J_f+1)/(2J_i+1)$, where J_i and J_f are the spins of the target and residual nuclei, respectively.

The quantity $B_{\gamma L}^M$, which contains the dependence on the scattering angle, depends very sensitively on the value of L. To this fact transfer reactions owe their value as a source of spectroscopic information. There are two current methods employed for the evaluation of the transfer amplitudes, known commonly as the plane-wave and distorted-wave calculations. In the latter, the scattering of the incident and outgoing particles by the nucleus is taken into account. This is a necessary step if one hopes to obtain a detailed agreement between theory and experiment since the

scattering and partial absorption of the incident particle, before the actual reaction event, and the emitted particle after, can have an important effect on the differential cross section. In performing a distorted-wave calculation, one usually adopts the optical potential as a representation of the interaction in the entrance and exit channels. These potentials are determined by an analysis of elastic scattering, polarization, and σ_R, the total reaction cross section, when these data are available at the required energies. Thus no new parameters are introduced, in principle. The next subsection presents the optical-model analysis that was carried out; the last subsection illustrates the distorted-wave fits to several (d,α) angular distributions.

2. Optical-Model Analysis

The following discussion is based in part on the joint work of Dr. Bruce Wilkins and the author. Reference 99 contains a more extensive description of some aspects of this study than will be presented here.

An optical-model program written by Dr. N. K. Glendenning for the IBM 7090 computer was used for the optical-model analysis. A comprehensive mathematical description of the optical-model computer program appears in the literature,[100] and consequently will not be repeated here.

The optical potential used in this analysis was of the form

$$V = V_c - \left\{ \frac{V_R}{1+\exp\left(\frac{r-R}{a}\right)} + \frac{iW(1-\alpha)}{1+\exp\left(\frac{r-R_W}{b}\right)} + iW\alpha \exp\left[-\left(\frac{r-R_W}{1.45b}\right)^2\right] \right\} \tag{5}$$

where

V_R is the strength of the real potential and W is the strength of the imaginary potential, which allows for the possibility of the incident particle being removed from the beam by absorption into a compound state; a and b are the surface diffusenesses of the real and imaginary potentials, respectively;

the radius parameters R and R_W are given by

$$R = r_0 A^{1/3} + r_1 \text{ and } R_W = r_W A^{1/3} + r_1 , \qquad (6)$$

where r_0 and r_W are the radius constants for the real and imaginary potentials, r_1 is the radius of the incident particle, and A is the atomic weight of the target nucleus. The inclusion of r_W and b allows one to calculate cases for which $r_W \neq r_0$ and $a \neq b$. Most of the calculations, however, were made with $r_W = r_0$.

the quantity α, by ranging from 0 to 1, allows the imaginary potential to assume any proportion of volume to surface absorption,

V_c is the Coulomb potential for which one assumes an incident point charge and an extended constant-charge density nucleus:

$$V_c = (Z_1 Z_2 e^2 / 2 r_0 A^{1/3}) \, [3 - (r/r_0 A^{1/3})^2] \text{ for } r \leq r_0 A^{1/3} ,$$

$$\qquad (7)$$

$$= Z_1 Z_2 e^2 / r \qquad\qquad \text{for } r > r_0 A^{1/3} ,$$

the number 1.45 in the denominator of the Gaussian form factor of Eq. (5) is the normalization constant that provides the proper relationship between the width of the Gaussian form factor and the diffuseness of the volume form factor when $0 < \alpha < 1$.

No spin-orbit force was included in the optical potential. However, this force in general affects only slightly the prediction[101] of elastic scattering and σ_R. And of course this force is not pertinent for the spinless alpha particle.

The usual method of analysis is to assume a set of parameters, calculate the phase shifts and cross sections numerically, and compare with the experimental values. One or more of the parameters are then altered and the calculation repeated. The need of a fast computer is obvious, as is the need of an automatic parameter search routine. In a

many-parameter problem such as this, a directional-derivative approach for a search routine usually converges quickly to a good fit. It is important, however, that the search routine not be misled by the parameter interdependencies. For this reason the parameters b and r_0, which show strong parameter interdependencies for protons (the search routine was originally developed for proton analysis), were chosen as grid parameters. Directional derivatives are used on the remaining parameters. For a search routine it is necessary to establish a goodness-of-fit criterion. The elastic-scattering diffraction pattern for high-energy deuterons and alpha particles scattered off nuclei is so complex that the standard definition of a least-squared fit, x^2 (as used for proton analysis), was found inadequate. It was necessary to define an empirical x^2 that gave priority to those characteristics of the diffraction pattern considered most important, the position of maxima and minima. The following equation was used:

$$x^2 = \sum_{i=M}^{N} \left(\frac{\{[\sigma_i(\theta) + \sigma_{i+1}(\theta)]_{pred} - [\sigma_i(\theta) + \sigma_{i+1}(\theta)]_{exp}\}^2}{(\% \text{ error})^2 [\sigma_i(\theta) + \sigma_{i+1}(\theta)]_{pred} [\sigma_i(\theta) + \sigma_{i+1}(\theta)]_{exp}} \right. \quad (25)$$

$$\left. + \left\{ \frac{[\sigma_i(\theta) - \sigma_{i+1}(\theta)]_{pred} - [\sigma_i(\theta) - \sigma_{i+1}(\theta)]_{exp}}{(n)(\% \text{ error}) \{[\sigma_i(\theta) + \sigma_{i+1}(\theta)]_{pred} [\sigma_i(\theta) + \sigma_{i+1}(\theta)]_{exp}\}^{1/2}} \right\}^n \right) ,$$

$$(8)$$

where n = 1 when

$$\frac{[\sigma_i(\theta) - \sigma_{i+1}(\theta)]_{pred}}{[\sigma_i(\theta) - \sigma_{i+1}(\theta)]_{exp}} \geq 0 ,$$

and where n = 2 when

$$\frac{[\sigma_i(\theta) - \sigma_{i+1}(\theta)]_{pred}}{[\sigma_i(\theta) - \sigma_{i+1}(\theta)]_{exp}} < 0 \; ;$$

M to N represents the range of experimental data.

The search routine that we developed, called GULLEY, uses what shall be called a "b valley" approach. It takes as its starting point a set of parameters that must be near a minimum in x^2 space for a specified value of b and r_0. A short grid routine called ELASTIC 6 determines the value of the parameters for this starting point. From the starting point GULLEY increments the parameter b and arrives at some point A. It then determines the derivative of x^2 with respect to the parameters V, W, and a. With this knowledge it guesses a new point B, in parameter space, and reevaluates the derivatives. From the two sets of derivatives and the x^2 values at points A and B, a new guess C is made. The program then assumes x^2 space to be parabolic in shape between these points in each of the three dimensions V, W, and a, and calculates a point D which lies somewhere between the values of the parameters at these two points. If the value of x^2 at D is not the lowest value of the set A, B, C, and D, a new guess C' is made. A point D' is reached in a manner analogous to that for point D. This procedure continues until the D point has the lowest value of x^2. In practice this is almost always the first D guess. The program then increments b and from its knowledge of how the parameters V, W, and a changed from the starting point to point D, a new A point is chosen and the whole A, B, C, and D procedure is repeated for this new value of b. In this manner, GULLEY works its way along the "b valley," adjusting the parameters V, W, and a to keep x^2 at a minimum. The grid parameter r_0 is then incremented and a new GULLEY run. Attempts to incorporate r_0 into the dynamic set of parameters V, W, and a were unsuccessful because of the strong V-R ambiguity(for protons).
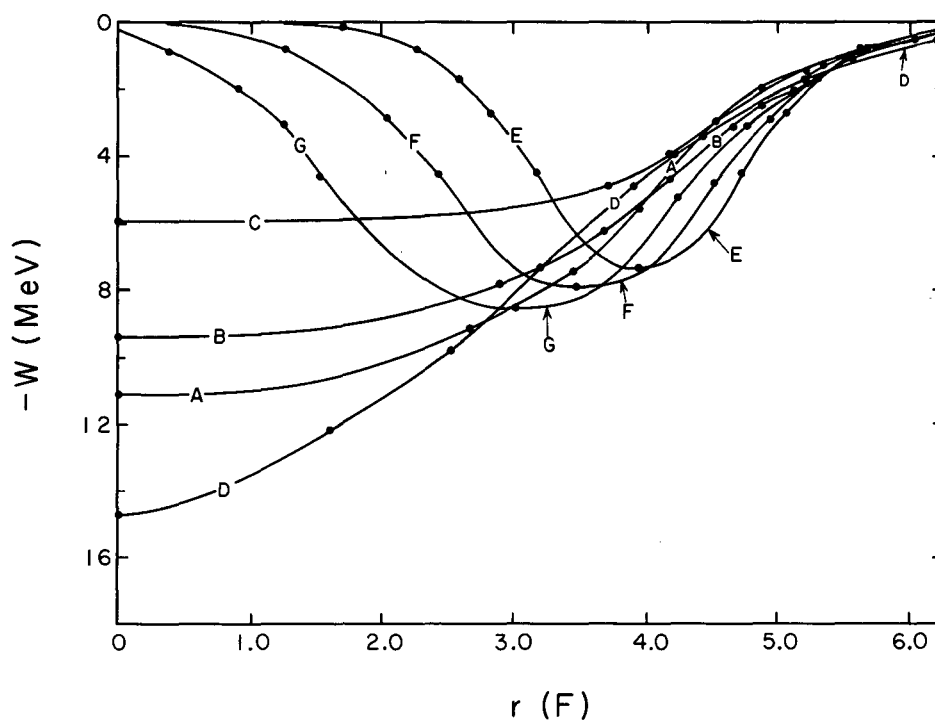
Fig. 41. Comparison of several imaginary potentials that give good fits to σ_{el} (θ) for 48-MeV alpha particles on C^{12}. The letters in the graph refer to parameter sets listed in Table $\overline{X}$.

Table X. Sets of parameters that give good fits to $\sigma_{SE}(\theta)$ for 48-MeV alpha particles on C^{12}; $r_1 = 1.20$ F.

Curve	Form factor	r_O (F)	r_W (F)	b (F)	a (F)	-V (MeV)	-W (MeV)	χ^2	σ_R (mb)
A	Volume	1.20	1.20	0.70	0.45	37.9	11.1	200	887
B	Volume	1.30	1.30	0.70	0.34	33.0	9.4	177	899
C	Volume	1.45	1.45	0.50	0.32	20.7	5.9	470	764
D	Volume	1.30	0.88	1.00	0.36	32.2	14.7	166	1001
E	Surface	1.20	1.20	0.80	0.37	41.5	7.3	274	770
F	Surface	1.20	1.00	1.00	0.385	40.8	7.9	220	795
G	Surface	1.20	0.80	1.20	0.40	40.1	8.5	180	822

of Table X, appears in Fig. 42. An experimental value of 901 ± 16 mb obtained[99] for 40-MeV alphas on C^{12} compares favorably with the theoretical value of 899 mb.

As seen in Fig. 41, it is meaningless to speak of the alpha-particle interaction in terms of a Gaussian shape or Woods-Saxon shape for the imaginary potential. It is necessary only to adjust the para-meters of the potential until it matches a certain shape at the very edge of the nucleus. Figure 43 shows the imaginary potential at large values of r and illustrates that a direct relationship exists between the strength of the imaginary potential and the predicted σ_R in the region of about 5.5 to 7.0 F. (All the curves in this figure are about equally good fits to $\sigma_{el}(\theta)$.) From this it can be inferred that the alpha particle does not penetrate with any appreciable probability within about 5.2 F and still have any chance to escape as an elastic event; otherwise, the optical model — using potentials E, F, and G — would be expected to predict a large σ_R.

Figure 44 shows a plot of the various "best fit" real potentials in this surface region. Proper adjustment of the parameters V, r_0, and a, which lead to the same shape potential beyond 5 F, gives almost equally good fits. This explains how the nonuniqueness of parameters arises from the use of a nuclear potential form factor by which one attempts to de-scribe the interaction in a region that the alpha particle does not sample.

A similar situation appears to hold for deuteron scattering although an optical-model analysis as extensive as just discussed for alphas on C^{12} was not carried out. From this information the hypothesis can be made that the optical-model parameters used to generate the dis-torted waves for a calculation of (d,α) angular distributions need not be known precisely. Once a set of parameters that approximately matches a certain shape at the very edge of the nucleus is found the job is finished. And since some of the parameters do not have a large effect on the shape of the potential at the surface, unless varied to an un-reasonable degree, with experience one can usually "guestimate" a "usable"
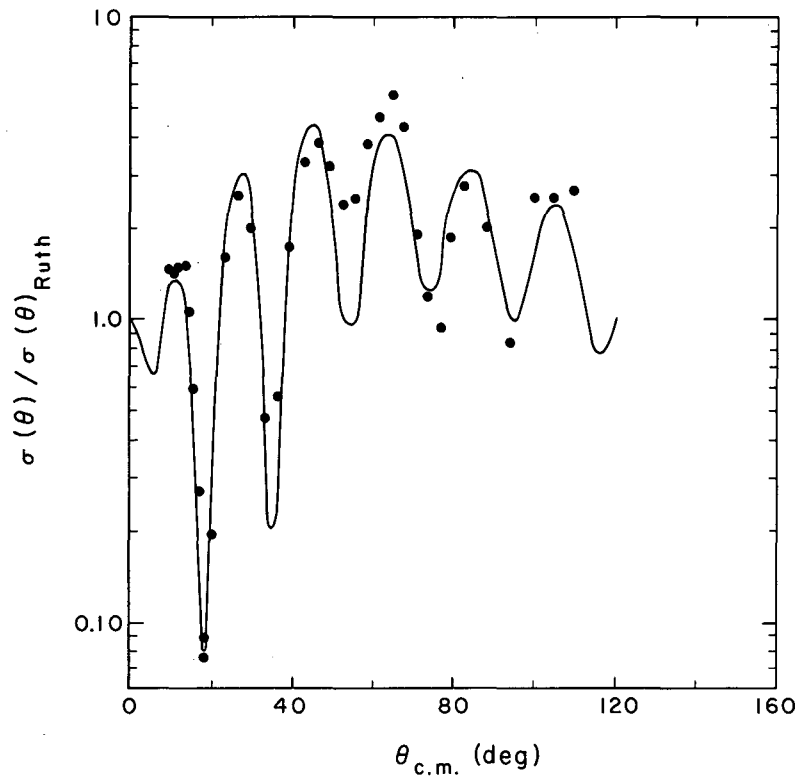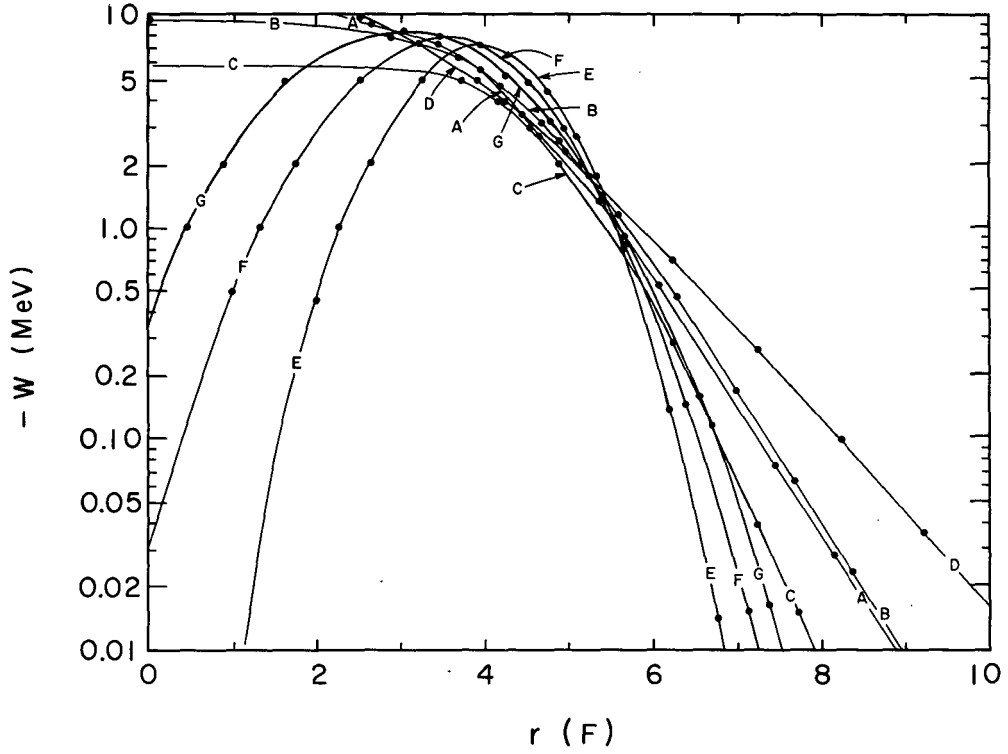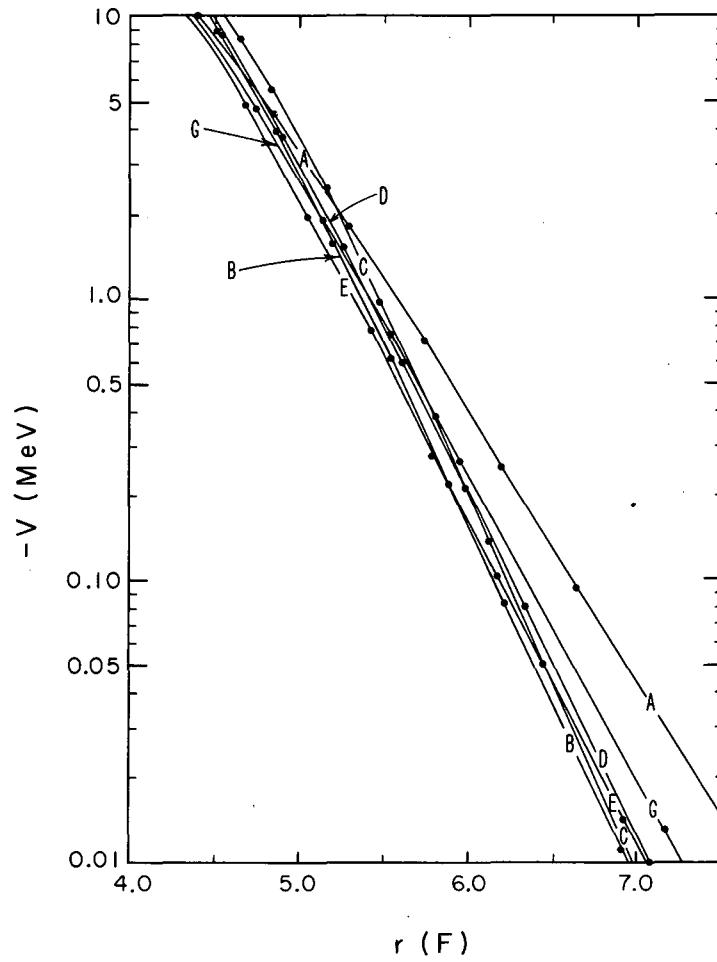
Fig. 42. A plot of σ/σ_{Ruth} for 48-MeV alpha particles scattered[67] from C^{12}. The solid line is the predicted value of σ/σ_{Ruth} obtained using the optical-model parameters listed at B in Table $\overline{X}$.

Fig. 43. Comparison of the imaginary potentials listed in Table $\overline{X}$ at large values of r. The letters refer to the parameter sets listed in Table $\overline{X}$.
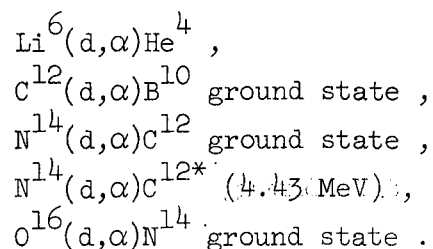
Fig. 44. Comparison of the real potentials listed in Table X̄ at large
values of r. The letters refer to the parameter sets listed in
Table X̄.

set of parameters. Agreement with this hypothesis is illustrated in the next subsection where the calculation of (d,α) angular distributions is shown to be very insensitive to some of the optical-model parameters. These calculations also demonstrate the sensitivity to r_0, which of course has a marked effect on the shape of the potential at the edge of the nucleus.

Although the "guestimate" approach seems to give acceptable results a proper analysis should always be carried out when the data are available. Fits were made to the angular distributions of the following (d,α) transitions:

$$Li^6(d,\alpha)He^4 \ ,$$
$$C^{12}(d,\alpha)B^{10} \ \text{ground state} \ ,$$
$$N^{14}(d,\alpha)C^{12} \ \text{ground state} \ ,$$
$$N^{14}(d,\alpha)C^{12*} \ (4.43 \ \text{MeV}) \ ,$$
$$O^{16}(d,\alpha)N^{14} \ \text{ground state} \ .$$

Only a summary of the optical-model analysis on the respective targets will be presented here. The parameters used are listed in Table XI, and comparisons of experimental and predicted values of σ/σ_{Ruth} are shown in Figs. 45 through 53. (The $He^4(\alpha,\alpha)He^4$ comparison is for $d\sigma/d\Omega$ rather than σ/σ_{Ruth}). Deuteron scattering data on natural lithium were used since no data on Li^6 were available in the literature. Likewise no alpha scattering data on B^{10} near the proper energy were available. Instead, $\sigma_{el}(\theta)$ for alphas of the appropriate energy on C^{12} were used. Many of the "fits" obtained could undoubtedly be improved if a more extensive analysis were undertaken. It was felt, however, that such an analysis was not warranted at the present time because of the prohibitive amount of computer time that would be required, with little to gain as far as the calculation of (d,α) angular distributions was concerned.

Table XI. Optical-model parameters used for fits illustrated.[a]

Reaction	Bombarding energy (MeV)	r_0	-V (MeV)	-W (MeV)	a (F)	b (F)	r_1 (F)	σ_R (mb)
Li + d	28	1.20	47.0	20.0	0.70	0.65	0.75	803
C^{12} + d	28	1.20	59.26	12.92	0.617	0.60	0.75	865
N^{14} + d	20.9	1.20	54.18	11.73	0.612	0.65	0.75	970
N^{14} + d	27	1.20	54.62	10.0	0.716	0.70	0.75	926
O^{16} + d	26.3	1.20	55.90	12.64	0.655	0.55	0.75	955
He^4 + α	46.12	1.14	50.0	1.0	0.30	0.50	1.00	89
C^{12} + α	21.2	1.30	60.0	6.0	0.40	0.65	1.20	892
C^{12} + α	38.1	1.30	32.64	9.00	0.474	0.60	1.20	893
N^{14} + α	25.7	1.30	35.23	7.12	0.435	0.60	1.20	923

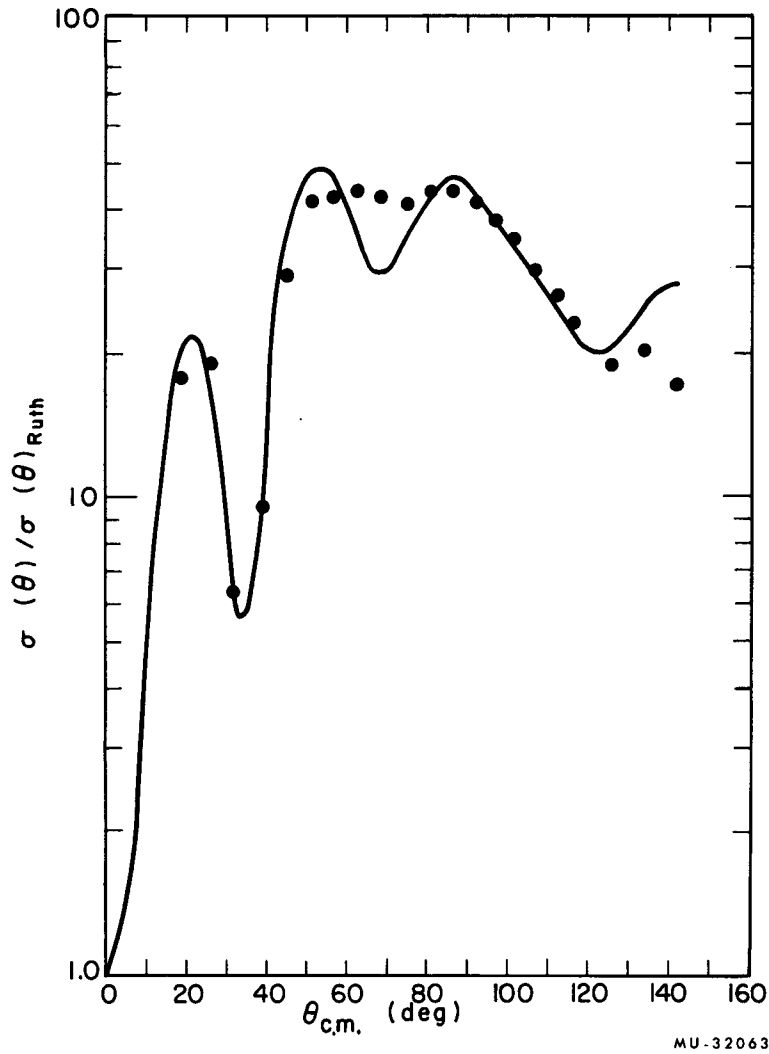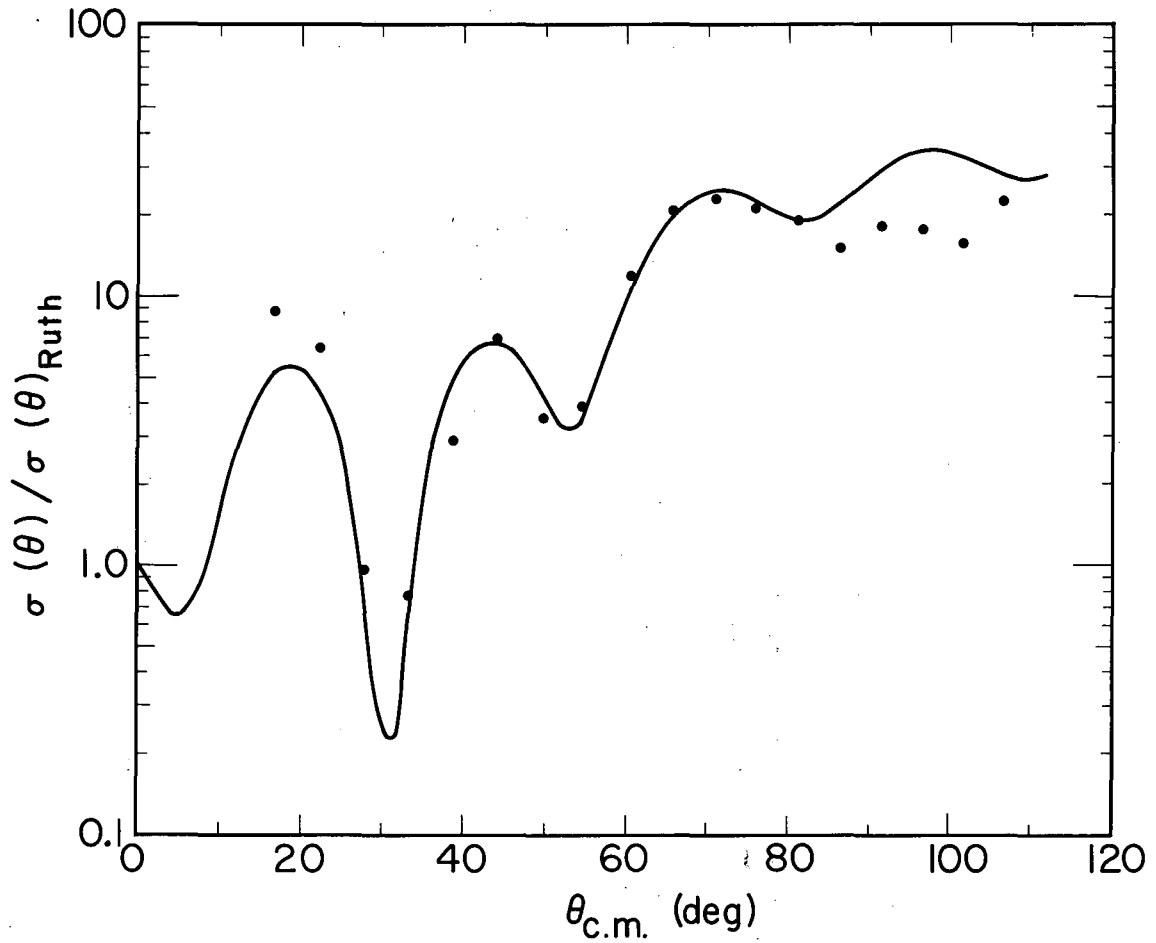[a]Volume absorption is used for all sets; $r_W = r_0$.

MU-32063

Fig. 45. A plot of σ/σ_{Ruth} for 28-MeV deuterons scattered[102] from natural Li. The solid line is the predicted value of σ/σ_{Ruth} obtained using the optical-model parameters listed in Table XI.
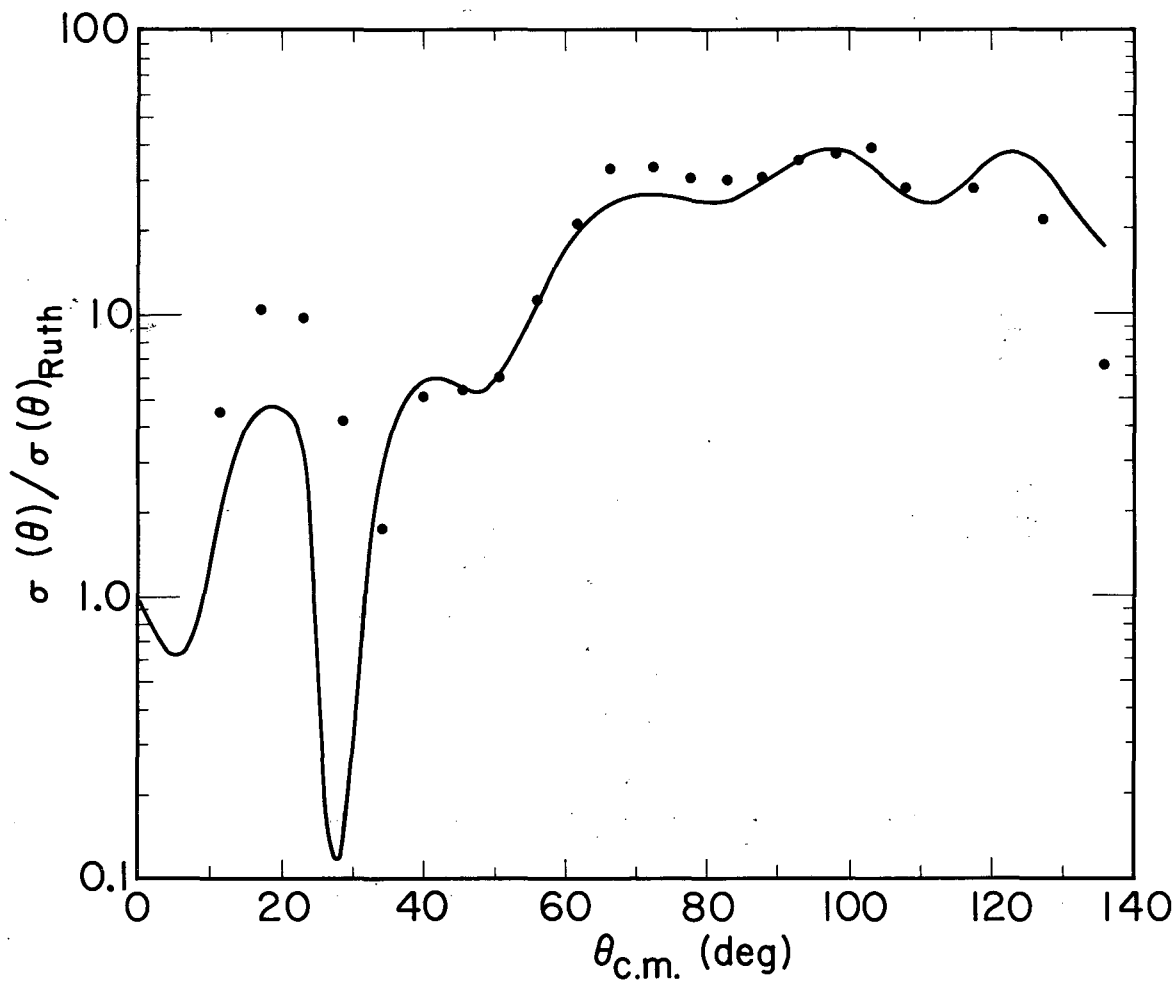
Fig. 46. A plot of σ/σ_{Ruth} for 28-MeV deuterons scattered[102] from C^{12}. The solid line is the predicted value of σ/σ_{Ruth} obtained using the optical-model parameters in Table $\overline{XI}$.
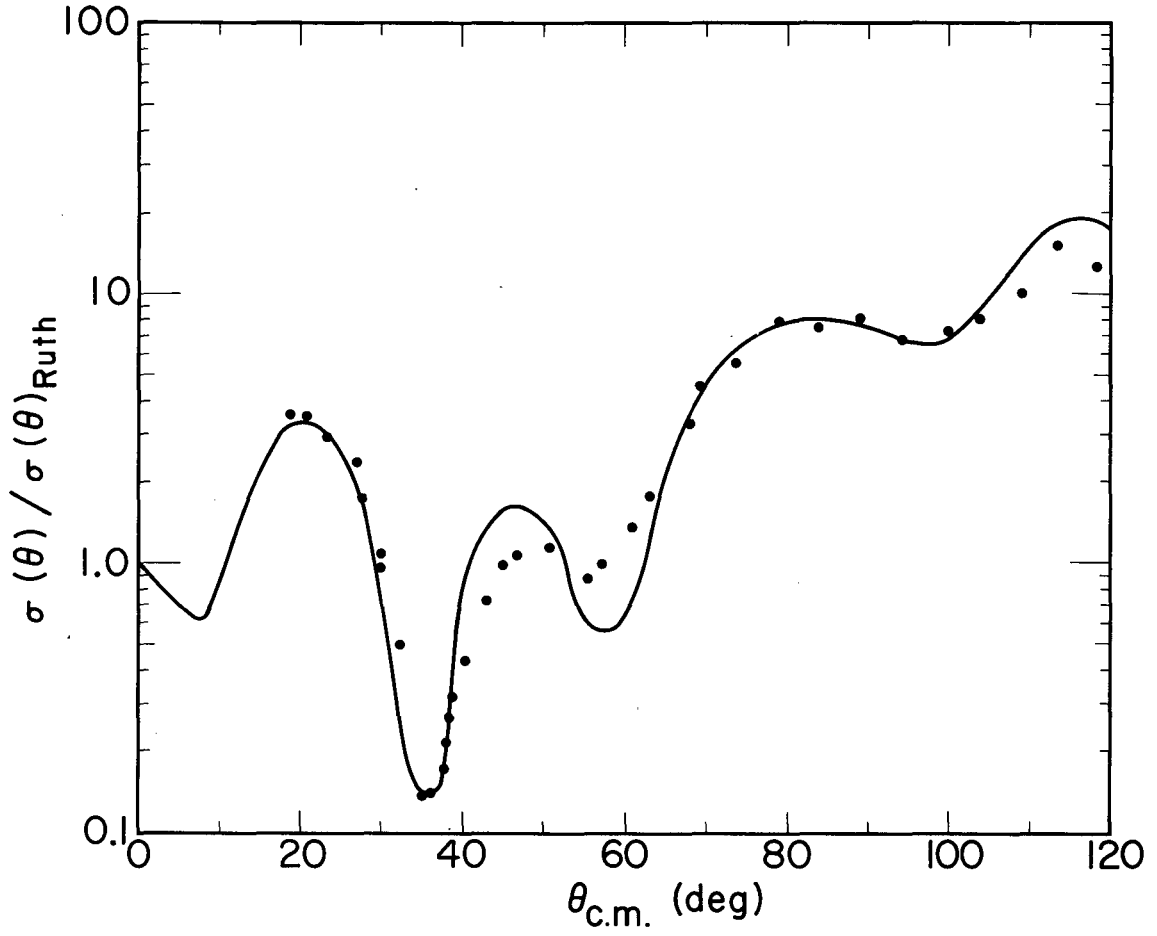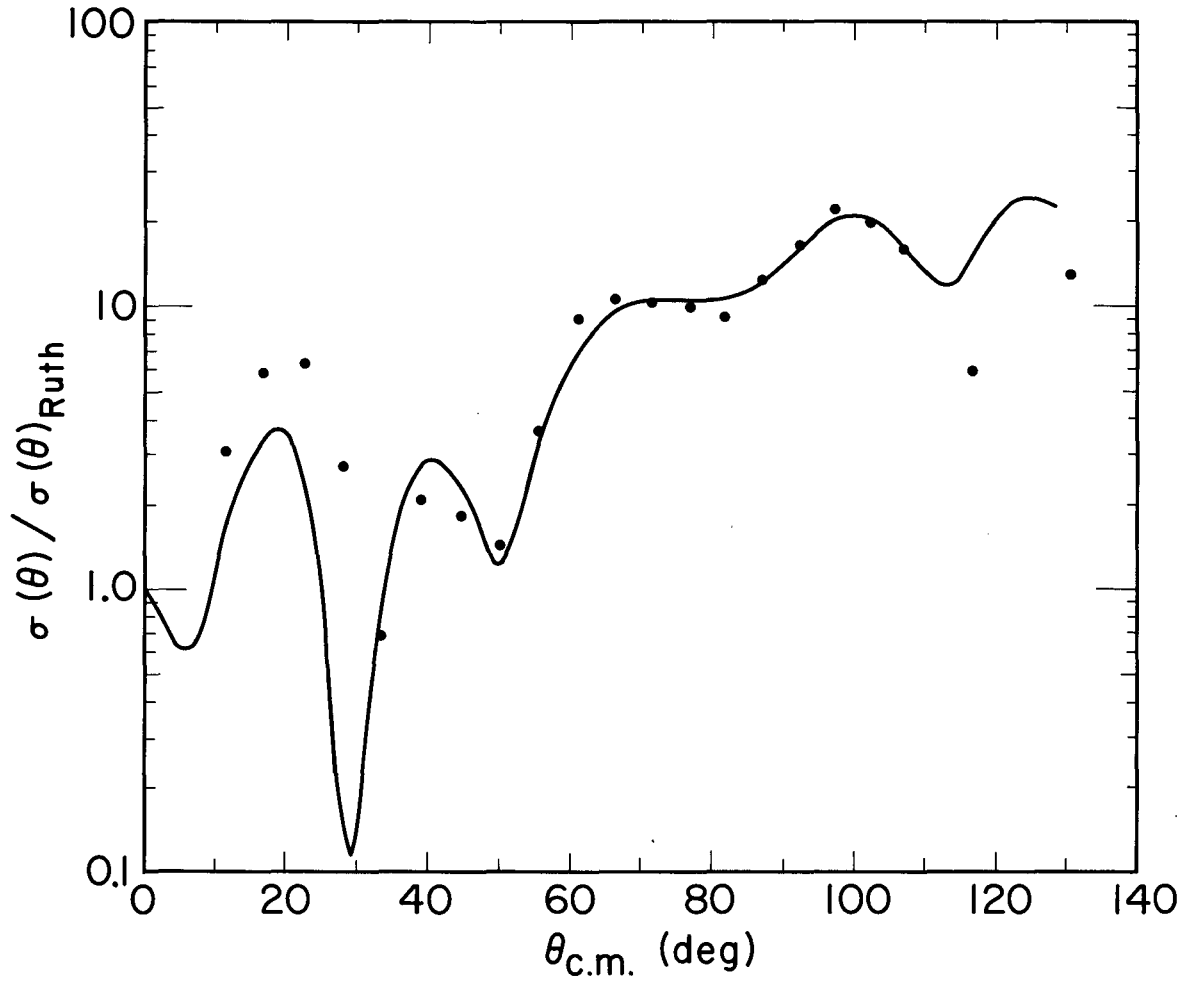
MUB-2137

Fig. 47. A plot of σ/σ_{Ruth} for 20.9-MeV deuterons scattered[80] from N^{14}. The solid line is the predicted value of σ/σ_{Ruth} obtained using the optical-model parameters listed in Table XI .

MUB-2138

Fig. 48. A plot of σ/σ_{Ruth} for 27-MeV deuterons scattered[103] from N[14]. The solid line is the predicted value of σ/σ_{Ruth} obtained using the optical-model parameters listed in Table XI.

MUB-2139

Fig. 49. A plot of σ/σ_{Ruth} for 26.3-MeV deuterons scattered[104] from O^{16}. The solid line is the predicted value of σ/σ_{Ruth} obtained using the optical-model parameters listed in Table XI.

MUB-2140

Fig. 50. Differential cross section for elastic scattering of 46.12-MeV alpha particles[42] from He[4]. The solid line is the predicted value obtained using the optical-model parameters listed in Table XI.

MU-32074

MUB-2141

Fig. 51. A plot of σ/σ_{Ruth} for 21.2-MeV alpha particles scattered[105] from C^{12}. The solid line is the predicted value of σ/σ_{Ruth} obtained using the optical-model parameters listed in Table $\overline{XI}$.
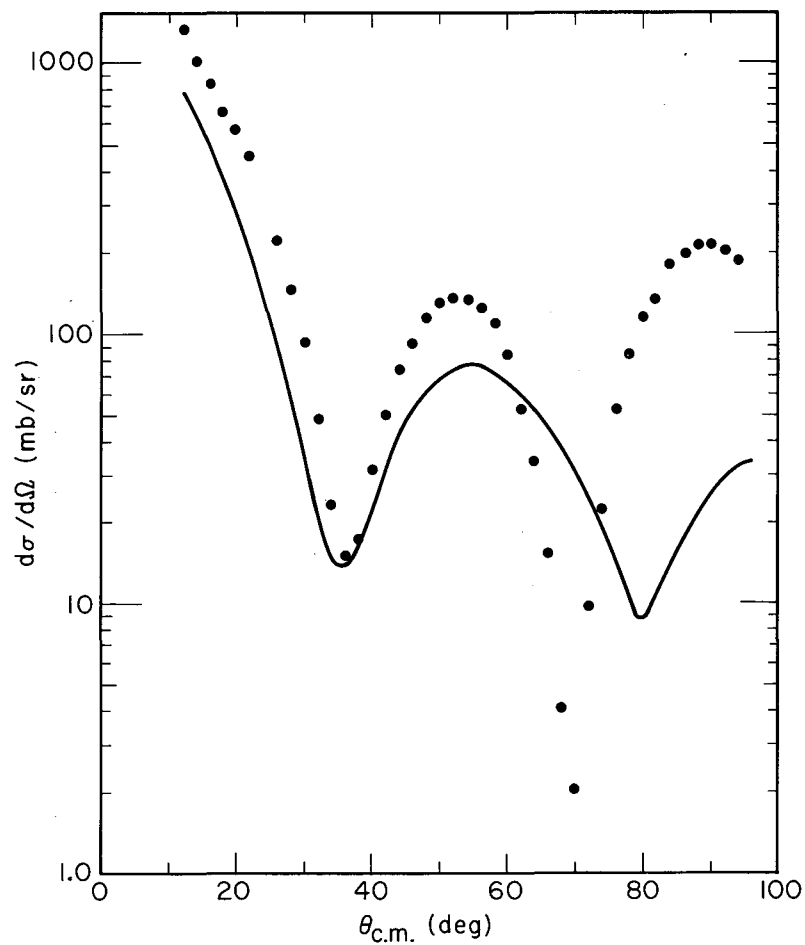
Fig. 52. A plot of σ/σ_{Ruth} for 38.1-MeV alpha particles scattered[106] from C^{12}. The solid line is the predicted value of σ/σ_{Ruth} obtained using the optical-model parameters listed in Table $\overline{XI}$.
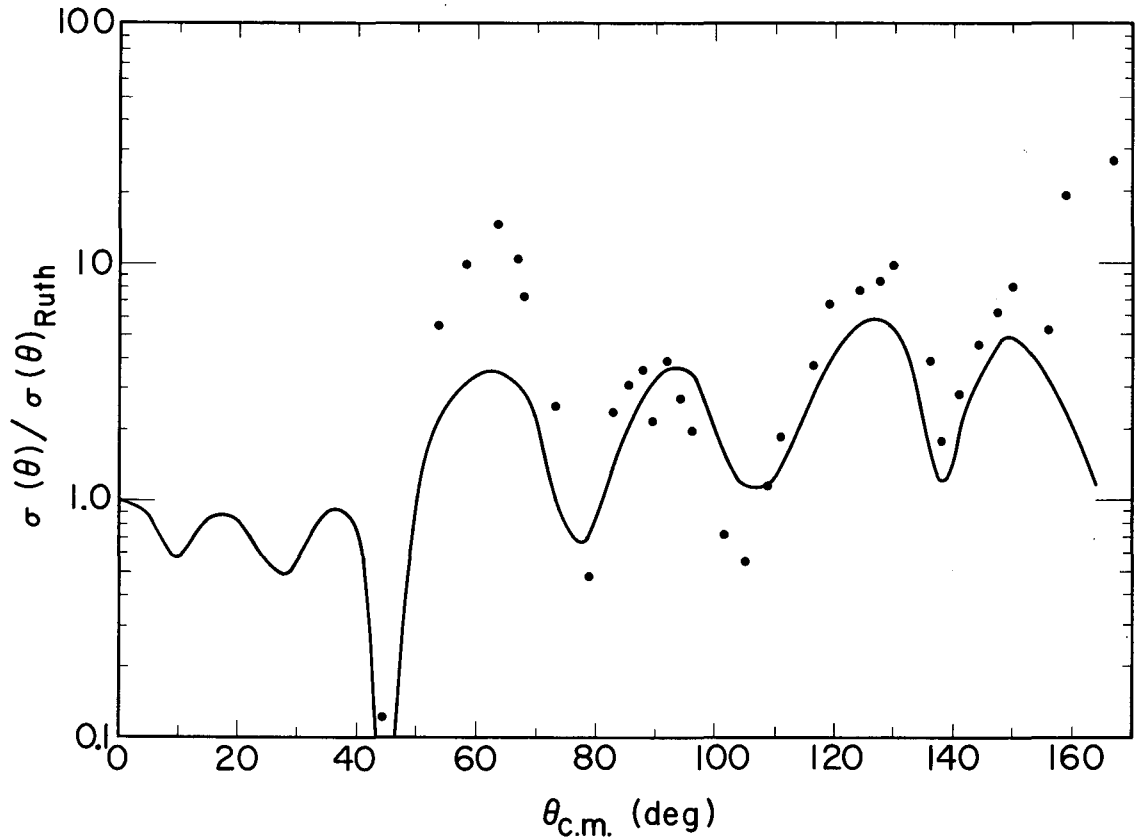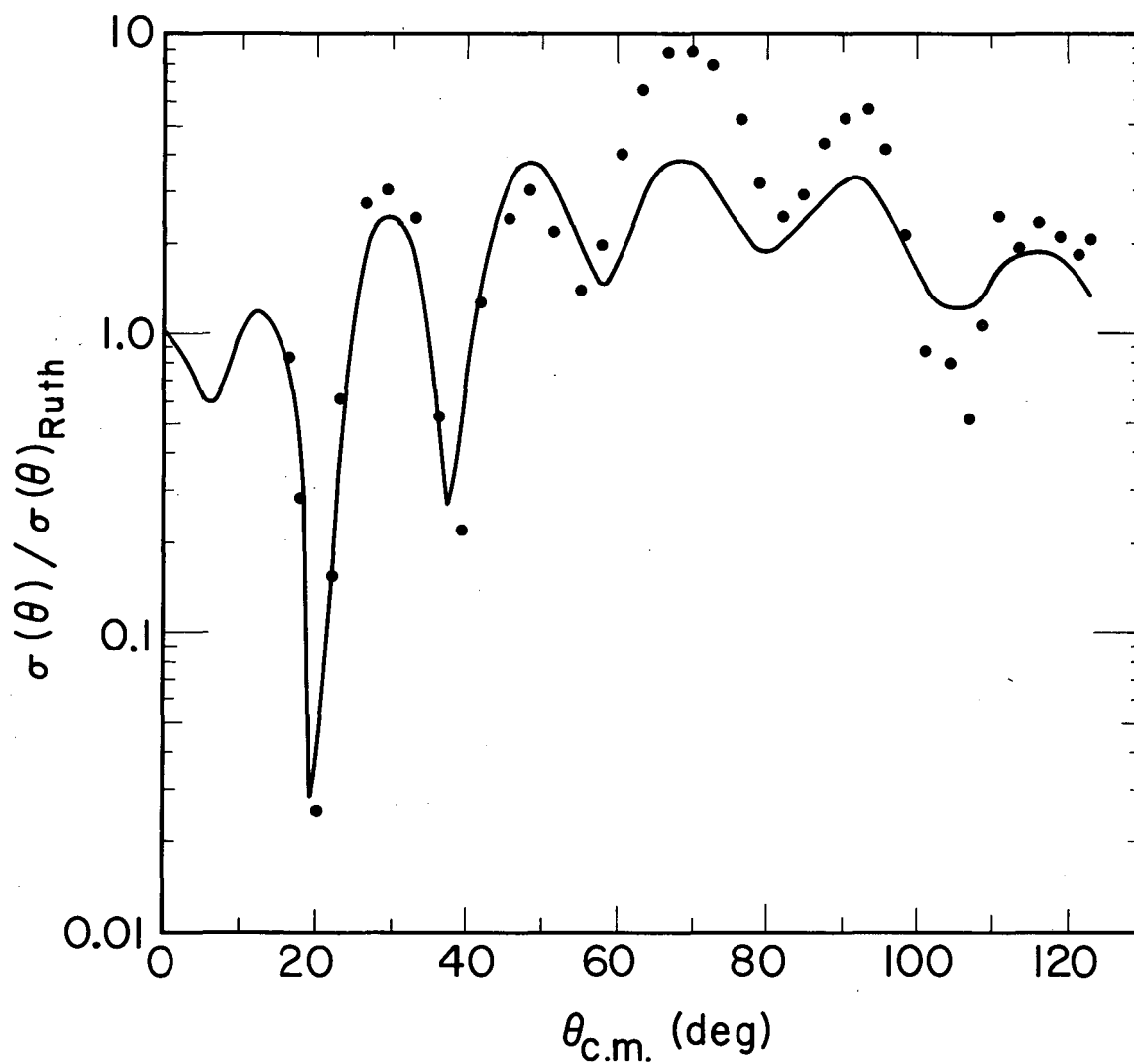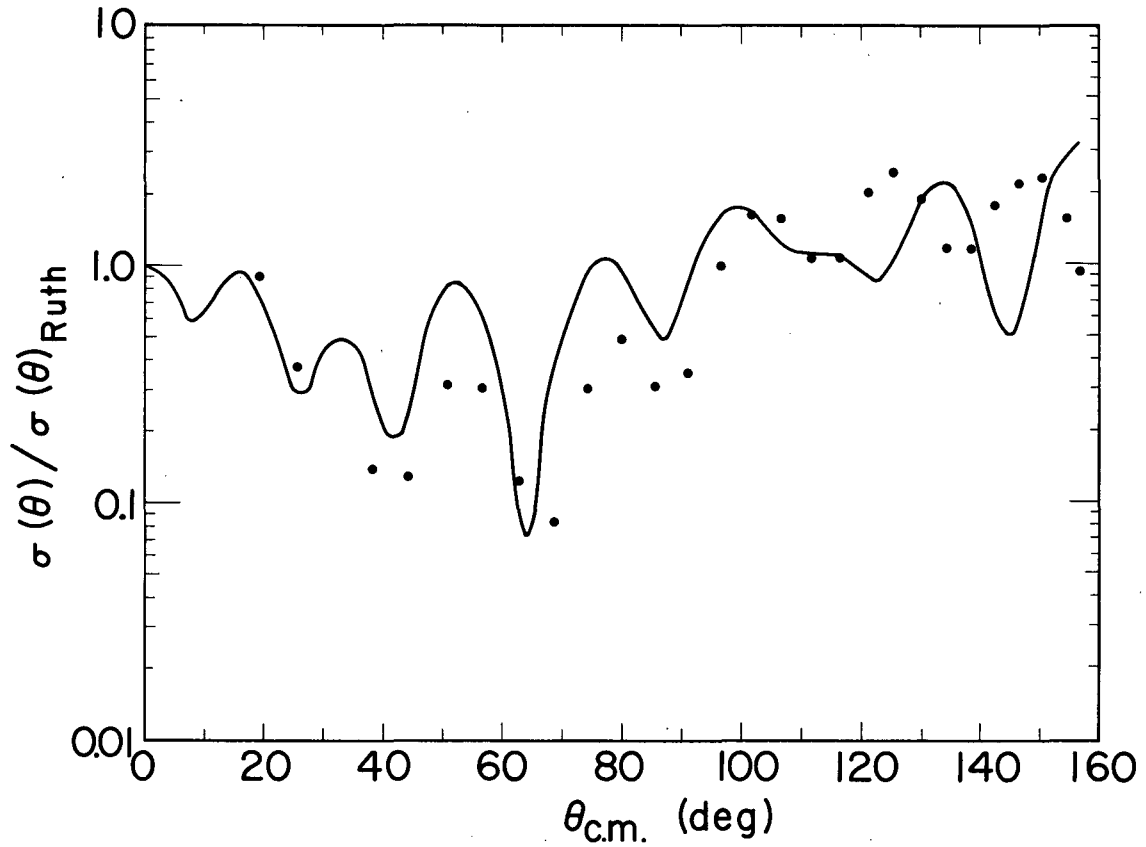
MUB-2142

MUB-2143

Fig. 53. A plot of σ/σ_{Ruth} for 25.7-MeV alpha particles scattered[107] from N^{14}. The absolute cross section of this preliminary data was not given, and the comparison involves an arbitrary adjustment of the data. The solid line is the predicted value of σ/σ_{Ruth} obtained using the optical-model parameters listed in Table $\overline{XI}$.

3. <u>Distorted-Wave Fits to the (d,α) Angular Distributions</u>

The following discussion is based on calculations made with the two-nucleon pickup or stripping program written by Dr. N. K. Glendenning for the IBM 7090 computer. These calculations are based on the approximations that the reaction occurs only at a specific radius (this position is commonly called the surface) and that the two nucleons are picked up as a lump; i.e., reference to the single-particle orbits from which the nucleons are picked up is suppressed. Therefore the reaction is characterized by the total angular momentum L that is transferred and this is the only information that can be obtained from fitting the angular distributions.

The procedure for determining the "best fit" was as follows.

(a) The optical-model parameters obtained in the preceding subsection were used to generate the distorted waves.

(b) The allowed L transfers were calculated from

$$ J_f + J_i + 1 \geq L \geq | \vec{J}_f + \vec{J}_i + \vec{1} |_{min} \qquad (9) $$

and this information given to the program.

(c) Calculations were made at a series of interaction radii to determine what radius gave the best fit. The interaction radius obtained in this manner was always approximately equal to the radius inside of which the optical-model analysis had indicated the incident particle does not penetrate and still have any chance of escaping as an elastic event. Thus elastic scattering and transfer reactions both seem to occur at approximately the same radius. However, it is probably unwise to attach a great amount of physical meaning to the parameters because the local optical-model potentials are just an approximation to a more realistic non-local potential and the non-local potentials are not so readily understood in terms of physical meaning. In addition, so as to give the proper slope to the angular distribution, changes in γ were used to

vary a damping factor $\exp(-\kappa^2/8\gamma^2)$, where $\vec{\kappa} = \dfrac{\vec{k}_\alpha}{2} - \vec{k}_d$, the momentum transferred to the incident deuteron by the picked up pair of nucleons,[*] and γ is a constant parameter defining the wave function of an alpha particle with a Gaussian form, $\exp(-\gamma^2 \Sigma r_{ij}^2)$. The value of γ used for all calculations presented here (except for the $Li^6(d,\alpha)He^4$ calculation where no damping factor was used) is 0.50×10^{13} cm^{-1}, which corresponds to an alpha particle radius of 0.75 F. If a γ corresponding to a larger alpha particle radius was used, the damping factor reduced the calculated cross sections too much at large angles. This situation is similar to other (d,α) reactions studied by using plane-wave theory.[89]

(d) The optical-model parameters were then varied to see if a better fit could be obtained. In no case was an improved fit found. Since the present theory is not capable of predicting the absolute magnitude of the cross section, the fits shown involve an arbitary normalization.

The specific fits are now discussed individually. The allowed L values for the $N^{14}(d,\alpha)C^{12*}$ (4.43-MeV) transition are 0,2, and 4. However, if p-shell nucleons are being picked up, L=4 is not allowed since two p nucleons can couple to a maximum of L=2. But since the calculation is performed without reference to the shells from which the nucleons are picked up, L=4 is included as a possibility. Hopefully L=4 will give an inferior fit. Figure 54 shows the best fit obtained. Although different relative intensities of the allowed L transfers were tried, the best fit corresponded to nearly 100% L=2. No combination of different interaction radii and optical-model parameters that were tried gave any indication that a better fit could be obtained by using an admixture of L=0 and/or L=4. Of course small admixtures, up to about 10%, could be included without definitely producing an inferior fit. However, the fit presented is for pure L=2. Figures 55, 56, and 57 illustrate how the calculated angular distribution varies as a function of

---

[*]The validity of introducing $\vec{\kappa}$ in a distorted-wave claculation is doubt-[108]ful.
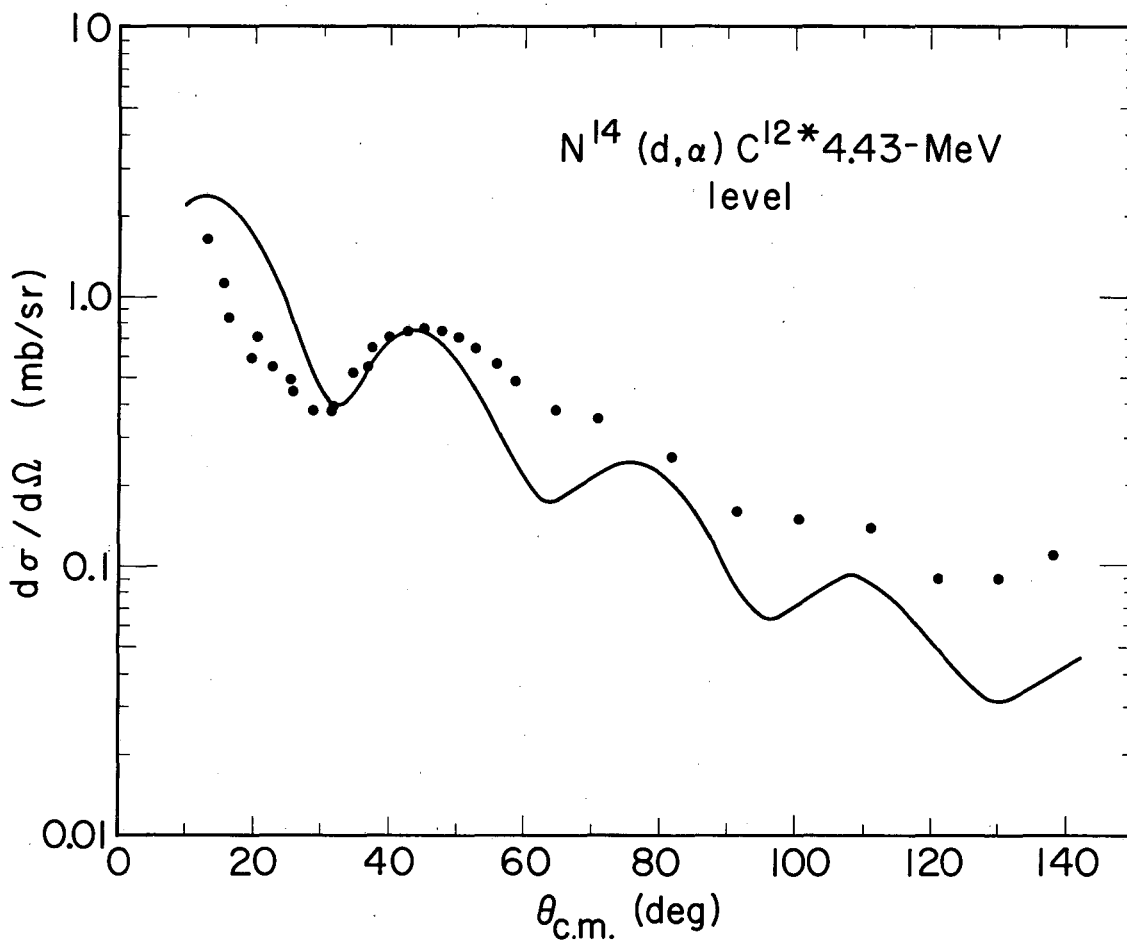
Fig. 54. Angular distribution of alpha particles from the $N^{14}(d,\alpha)C^{12*}$ (4.43-MeV) transition. The solid line was calculated for L = 2, interaction radius = 5.25 F, and the following optical-model parameters:

	V	W	a	b	r_0	r_1
deuteron	-55	-11	0.65	0.65	1.20	0.75
alpha particle	-33	- 9	0.47	0.60	1.30	1.20

Volume absorption is used for all fits shown in this section and $r_w = r_0$.
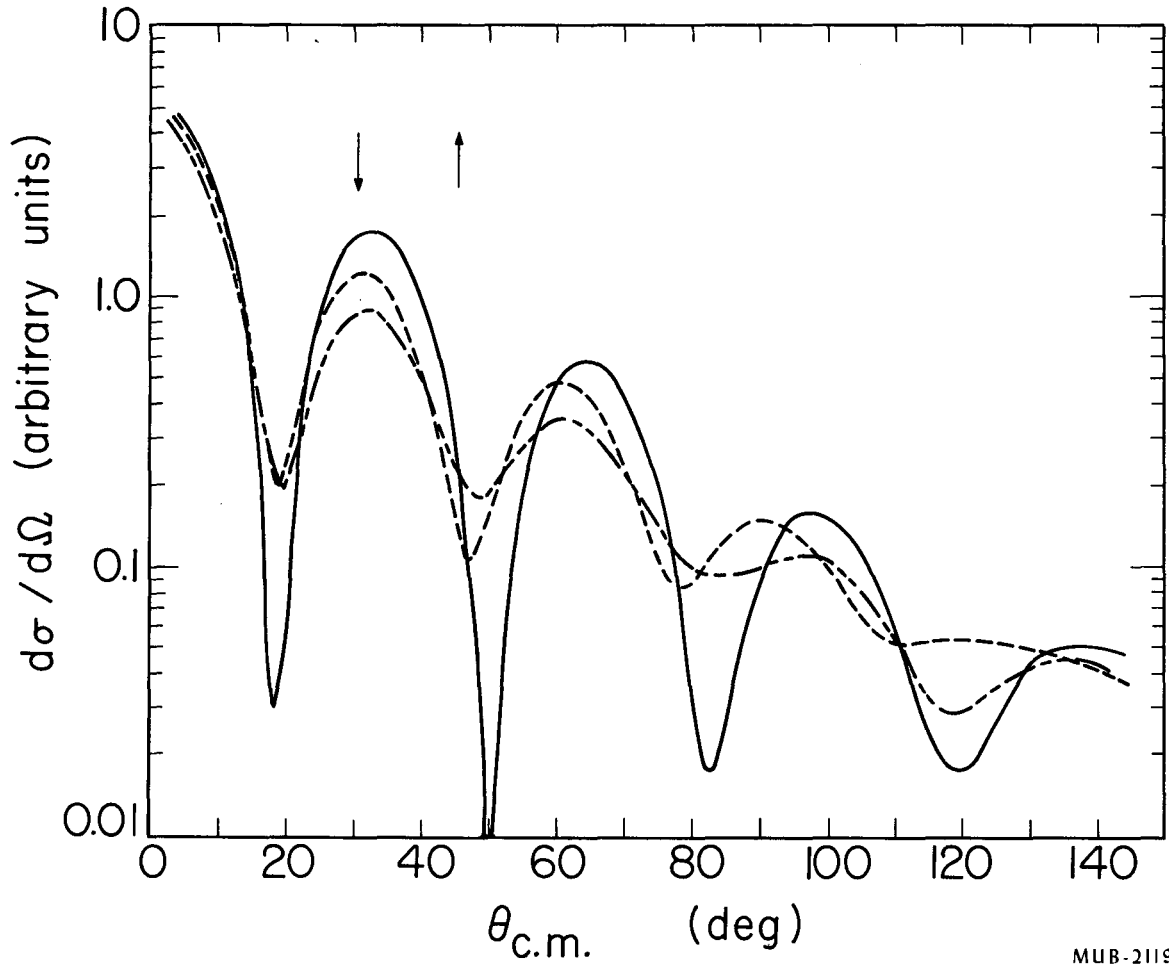
Fig. 55. Comparison of calculated angular distributions for the N^{14}(d,α)C^{12*} (4.43-MeV) transition with L = 0, as a function of interaction radius. Optical-model parameters same as in Fig. 54. Arrows indicate experimental maximum and minimum.

———————————— R = 4.50 F

- - - - - - - - - - - - R = 5.00 F

— · — - - — · — R = 5.50 F
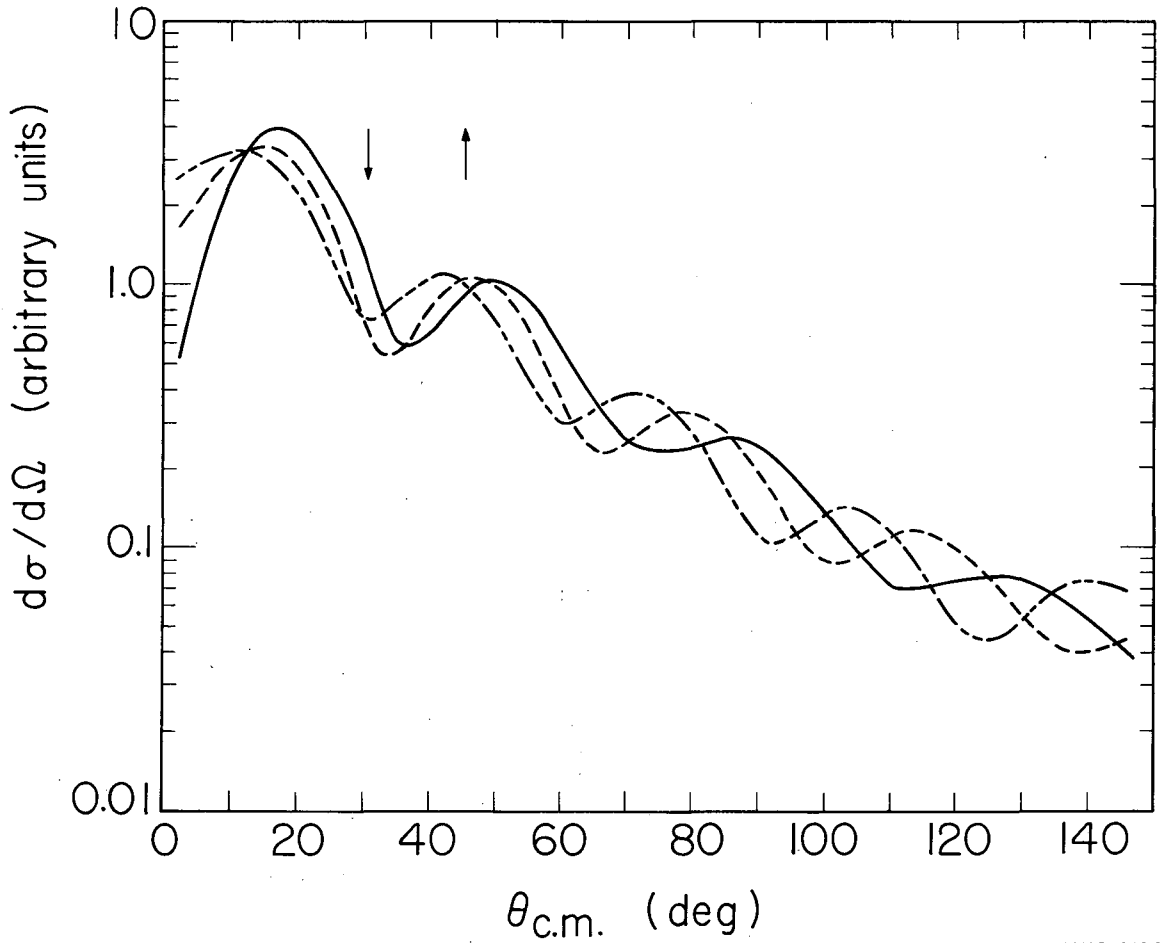
Fig. 56. Comparison of calculated angular distributions for the $N^{14}(d,\alpha)C^{12*}$ (4.43-MeV) transition with L = 2, as a function of interaction radius. Optical-model parameters same as in Fig. 54. Arrows indicate experimental maximum and minimum.

R = 4.50 F

R = 5.00 F

R = 5.50 F

Fig. 57. Comparison of calculated angular distributions for the
$N^{14}(d,\alpha)C^{12*}$ (4.43-MeV) transition with L = 4, as a function
of interaction radius. Optical-model parameters same as in
Fig. 54. Arrows indicate experimental maximum and minimum.

———————— R = 4.50 F

------------ R = 5.00 F

— — —··— — R = 5.50 F

interaction radius, and Figs. 58 through 63 show the variation as a function of different optical-model parameters. As remarked earlier the calculated angular distributions are rather insensitive to the parameters except r_0.

The allowed L values for the $N^{14}(d,\alpha)C^{12}$ ground state transition are 0 and 2, and once again the best fit corresponds to almost 100% L=2 (see Fig. 64). As in the above case and for all the other transitions analyzed, no combination of different interaction radii and optical-model parameters that was tried gave any indication that a better fit could be obtained by using an appreciable admixture of L≠2.

The fits to the $O^{16}(d,\alpha)N^{14}$ ground state and $C^{12}(d,\alpha)B^{10}$ ground state transitions also show a strong preference for L=2. Figures 65 and 66 illustrate the best fits for these reactions. The allowed L values for the first transition are 0 and 2, whereas 2 and 4 are allowed for the latter. Of course L=4 is not allowed if two p nucleons are being picked up.

Few, if any, conclusions can be drawn from the analysis of the $Li^6(d,\alpha)He^4$ transition for which an example "fit," using no damping, is shown in Fig. 67. It appears that the present code is completely incapable of fitting the plateau at small angles. Nevertheless L=2 gives better fits than does L=0.

The outstanding feature of these calculations is that L=2 transitions are strongly enhanced over L=0 transitions. A similar result was obtained by Blair and Wegner[109] for the (He^3,α) pickup reaction in that l=3 transitions were strongly enhanced relative to l=1 transitions, in contrast to the behavior of the analogous (d,t)[110] and (p,d)[111] pickup reactions.[*] The momentum-mismatch discussion given in Subsec. IV. A is

---

[*]Of course the transition to any single level by the simple pickup of one nucleon can involve only a specific l value. However, in these (He^3,α) reactions, groups of levels that could not be analyzed separately showed relatively enhanced l=3 transitions. Furthermore, l=1 transitions exhibited much larger cross sections for (p,d) and (d,t) reactions than for (He^3,α) reactions, but this difference was much less for l=3 transitions.
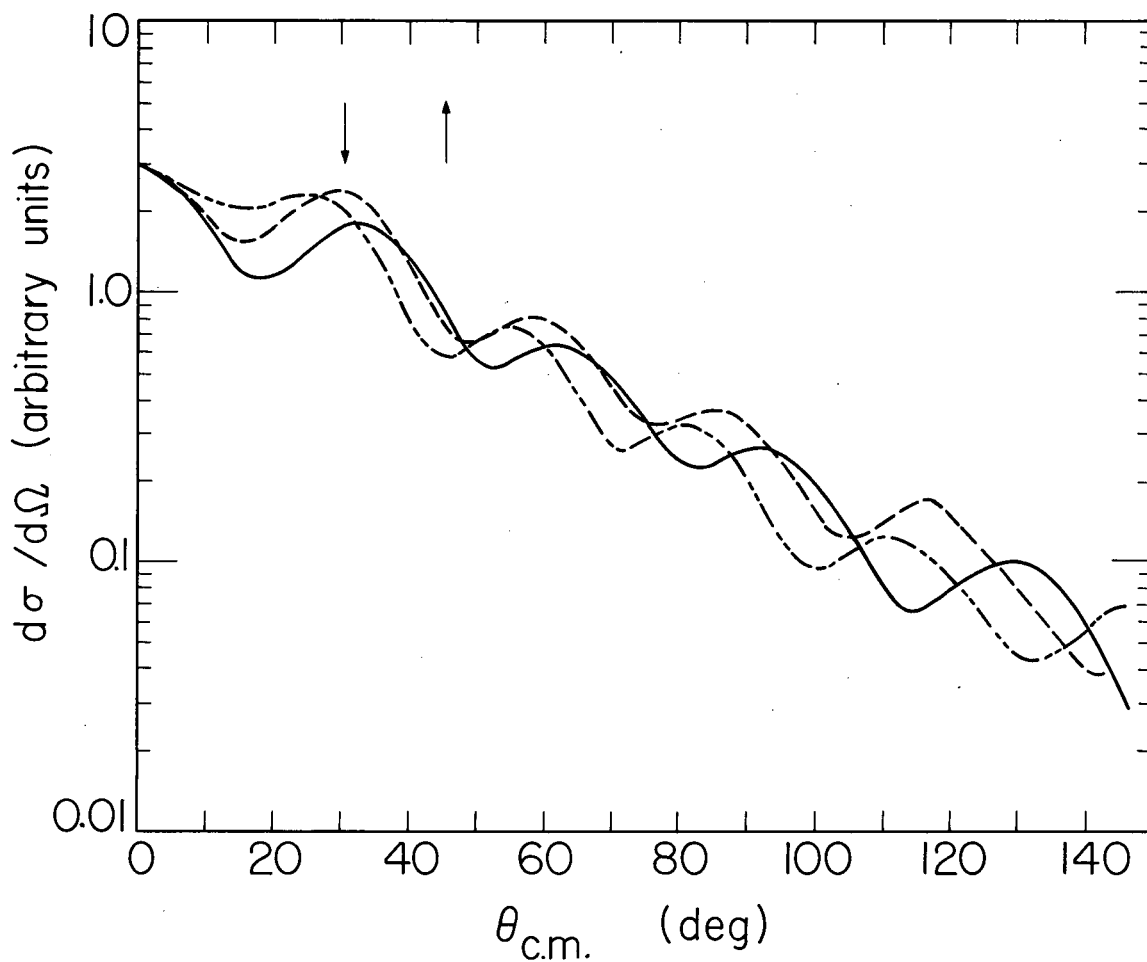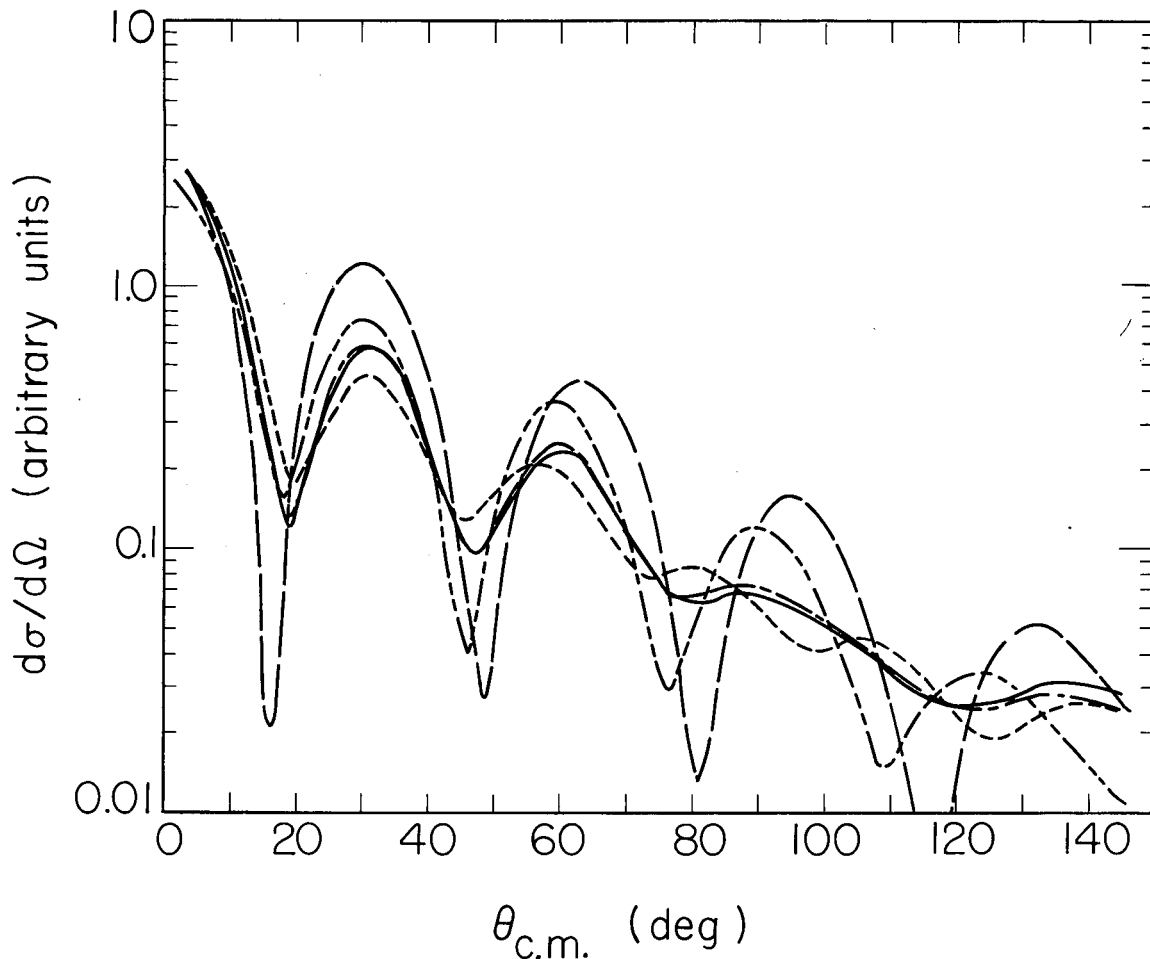
MUB-2122

Fig. 58. Comparison of calculated angular distributions for the $N^{14}(d,\alpha)C^{12*}$ (4.43-MeV) transition with L = 0, as a function of optical-model-parameter variation for the alpha particle. Optical-model parameters same as in Fig. 54 except for the perturbed parameter. Interaction radius = 5.25 F.

———————— "Standard set"

— · — · — · — V = - 60 MeV

— — — — — — W = - 6 MeV

— · · — · · — a = 0.60 F

———————— b = 0.40 F (same line as standard set)

— — — — r_0 = 0.80 F
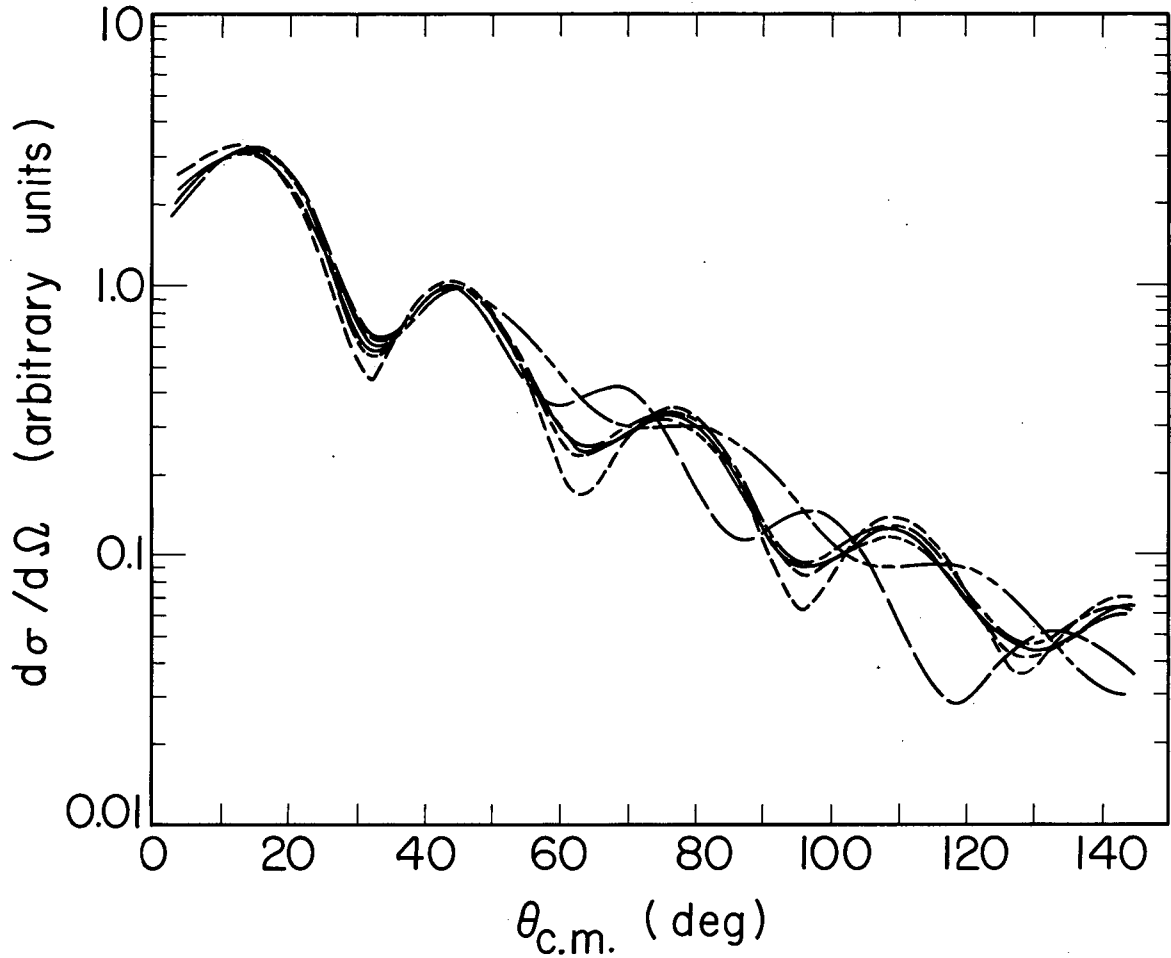
Fig. 59. Comparison of calculated angular distributions for the $N^{14}(d,\alpha)C^{12*}(4.43\text{-MeV})$ transition with L = 2, as a function of optical-model-parameter variation for the alpha particle. Optical-model parameters same as in Fig. 54 except for the perturbed parameter. Interaction radius = 5.25 F.

MUB-2146

Fig. 60. Comparison of calculated angular distributions for the
$N^{14}(d,\alpha)C^{12*}(4.43$-MeV) transition with L = 4, as a function
of optical-model-parameter variation for the alpha particle.
Optical-model parameters same as in Fig. 54 except for the
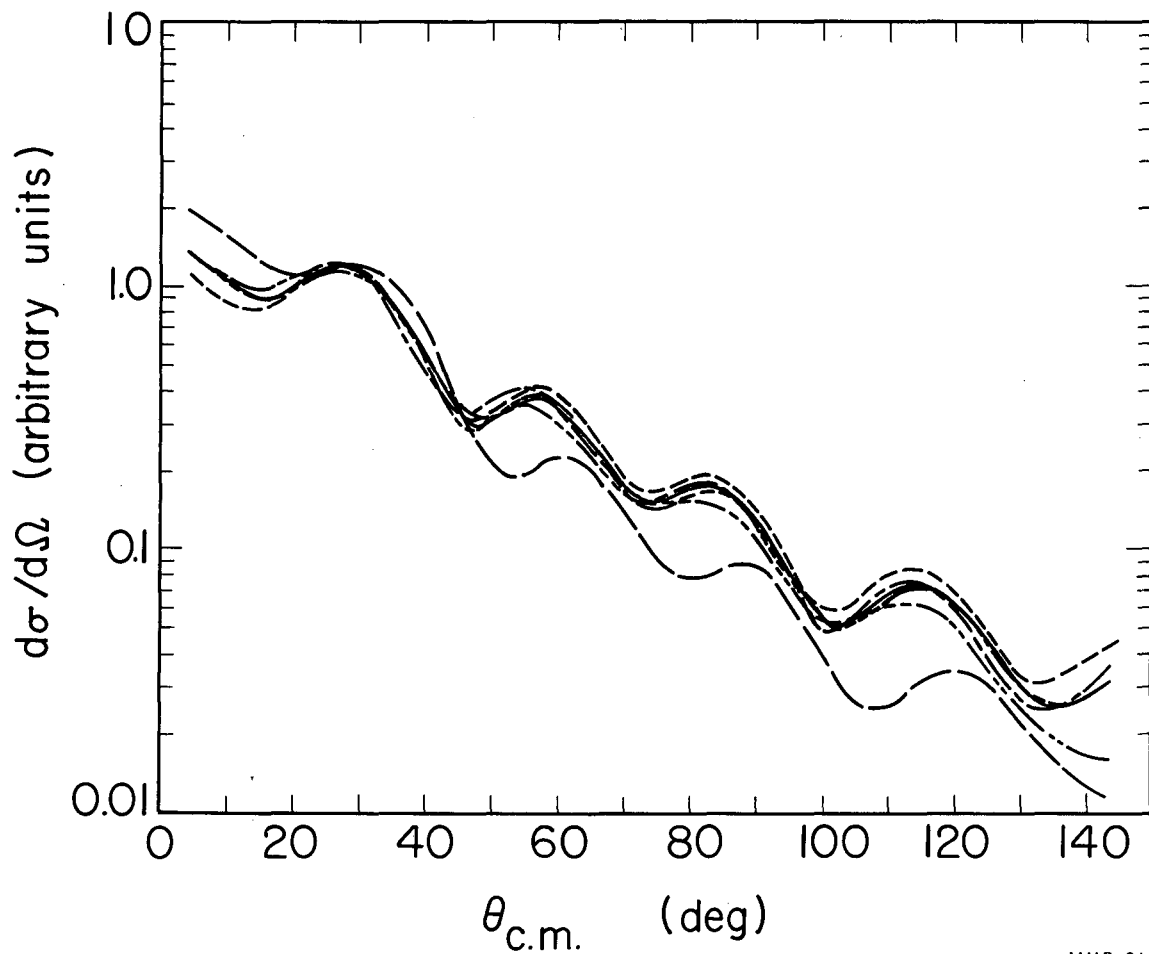perturbed parameter. Interaction radius = 5.25 F.

————————	"Standard set"
— — — — — —	$V = -60$ MeV
- - - - - - - - - - - -	$W = -6$ MeV
— — — — — — — —	$a = 0.60$ F
— — — — — — — —	$b = 0.40$ F
—— —— ——	$r_0 = 0.80$ F

Fig. 61. Comparison of calculated angular distributions for the N^{14}(d,α)C^{12*} (4.43-MeV) transition with L = 0, as a function of optical-model-parameter variation for the deuteron. Optical-model parameters same as in Fig. 54 except for the perturbed parameter. Interaction radius = 5.25 F.

————————————	"Standard set"
— — — — — —	V = - 35 MeV
- - - - - - - - - - - -	W = - 6 MeV
— - — - —	a = 0.40 F
— - — — — -	b = 0.40 F
— — —	r$_0$ = 0.80 F

Fig. 62. Comparison of calculated angular distributions for the $N^{14}(d,\alpha)C^{12*}(4.43\text{-MeV})$ transition with L = 2, as a function of optical-model-parameter variation for the deuteron. Optical-model parameters same as in Fig. 54 except for the perturbed parameter. Interaction radius = 5.25 F.

————————	"Standard set"
— ·· — — · · —	V = - 35 MeV
- - - - - - - - - -	W = - 6 MeV
— · — · —	a = 0.40 F
— ·· — — · · ·	b = 0.40 F
— — — —	r_0 = 0.80 F

MUB-2148
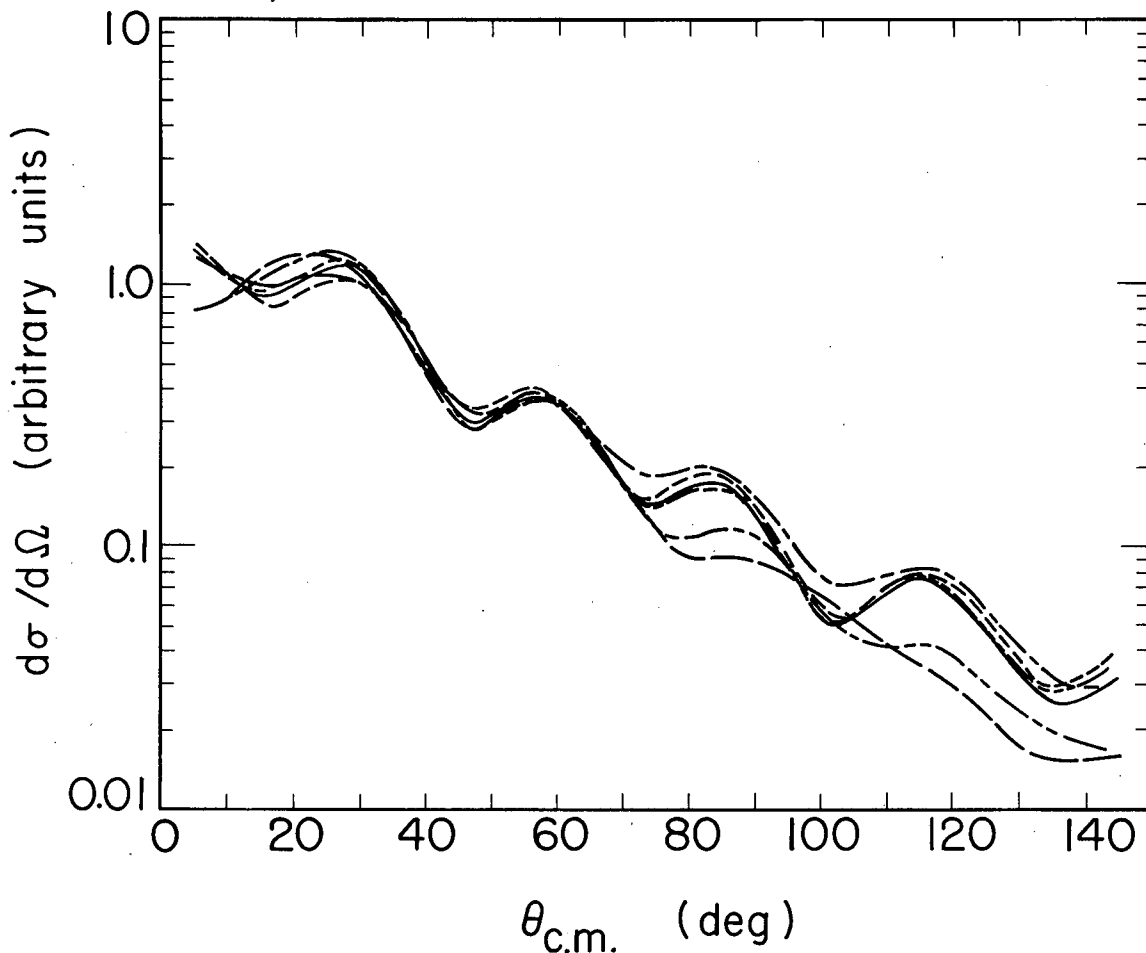
MUB-2149

Fig. 63. Comparison of calculated angular distributions for the $N^{14}(d,\alpha)C^{12*}$ (4.43-MeV) transition with L = 4, as a function of optical-model parameter variation for the deuteron. Optical-model parameters same as in Fig. 54 except for the perturbed parameter. Interaction radius = 5.25 F.
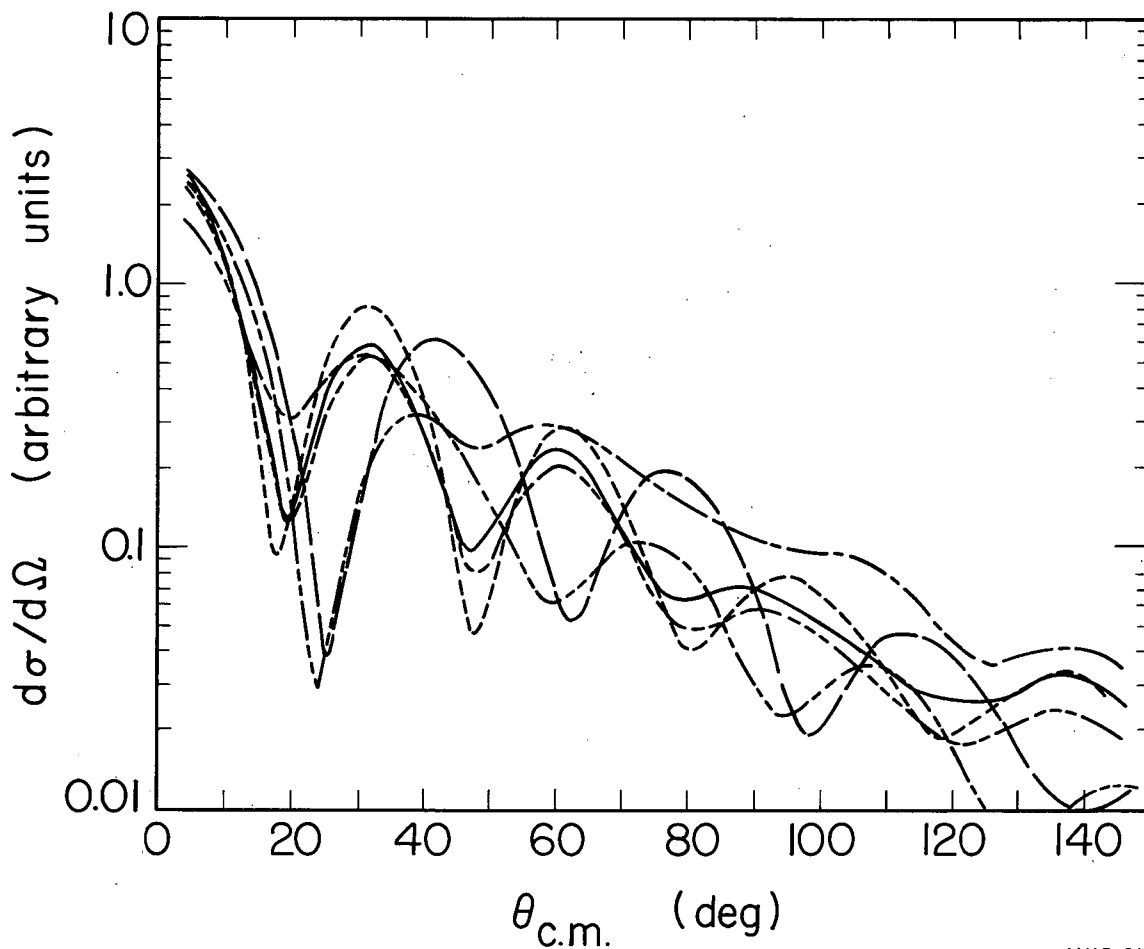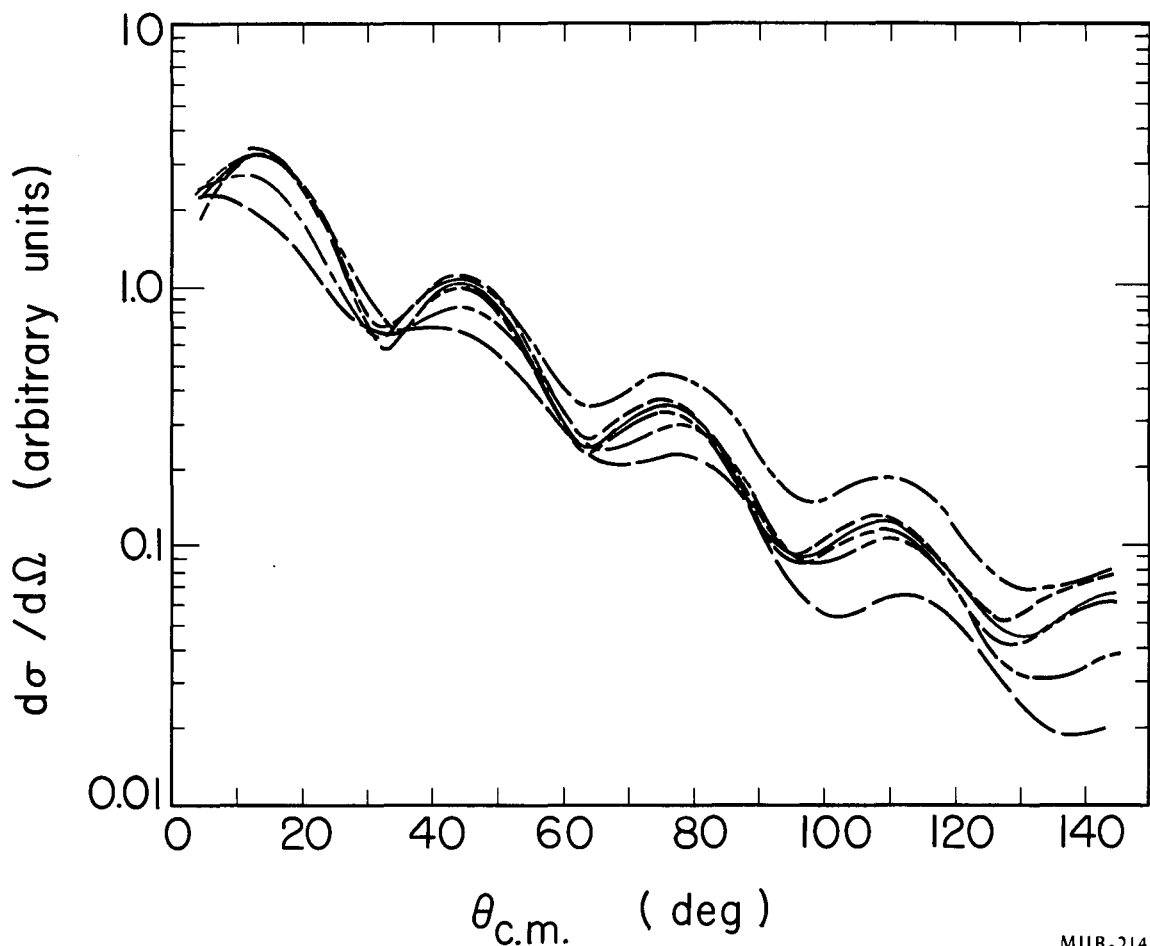
————————	"Standard set"
— — — — — —	V = - 35 MeV
- - - - - - - - - - - -	W = - 6 MeV
— — — — — —	a = 0.40 F
— — · — — · — —	b = 0.40 F
— — — — —	r_0 = 0.80 F
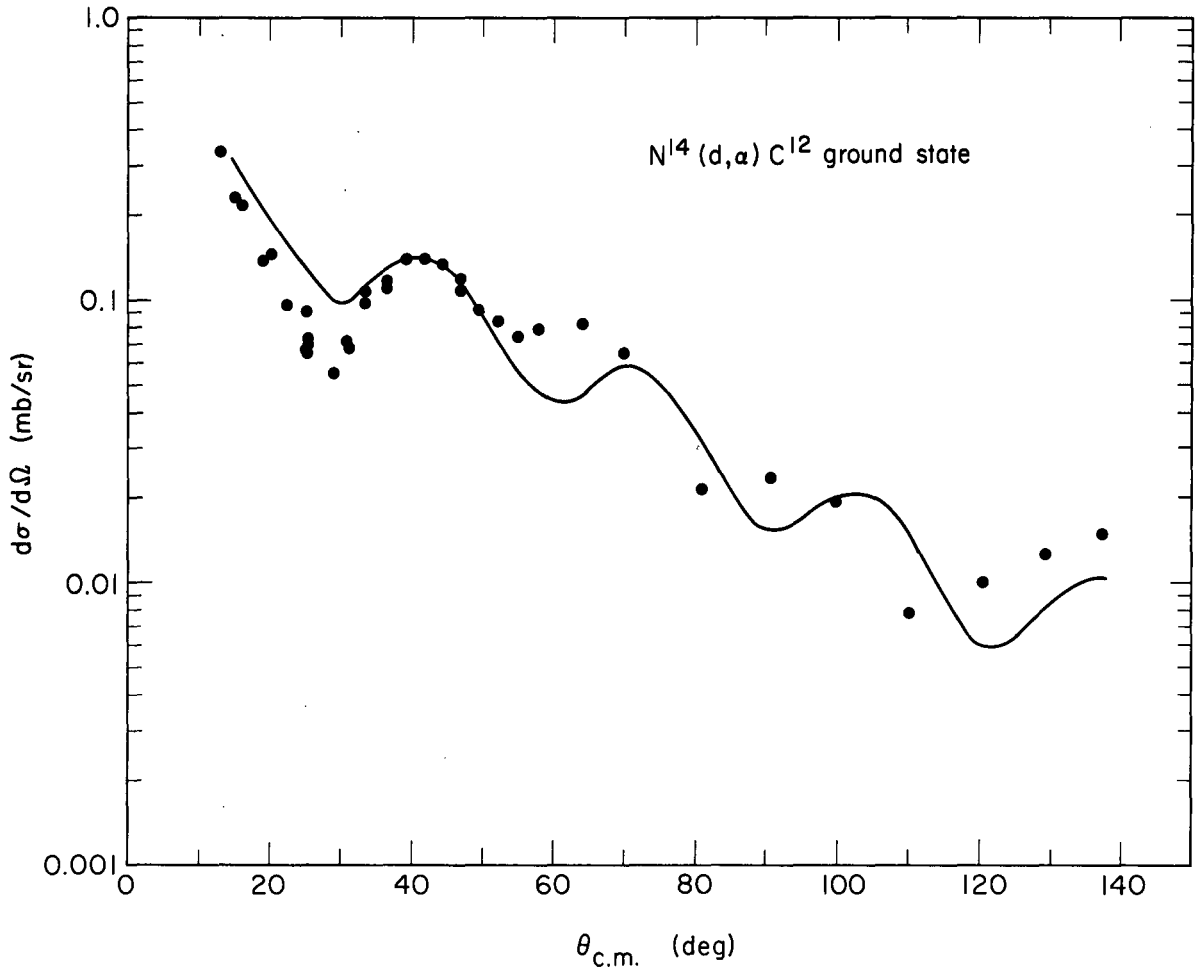
N^{14} (d,α) C^{12} ground state

Fig. 64. Angular distribution of alpha particles from the
N^{14}(d,α)C^{12} ground state transition. The solid line
was calculated for L = 2, interaction radius = 5.25 F,
and the same optical-model parameters as in Fig. 54.

MUB-2123
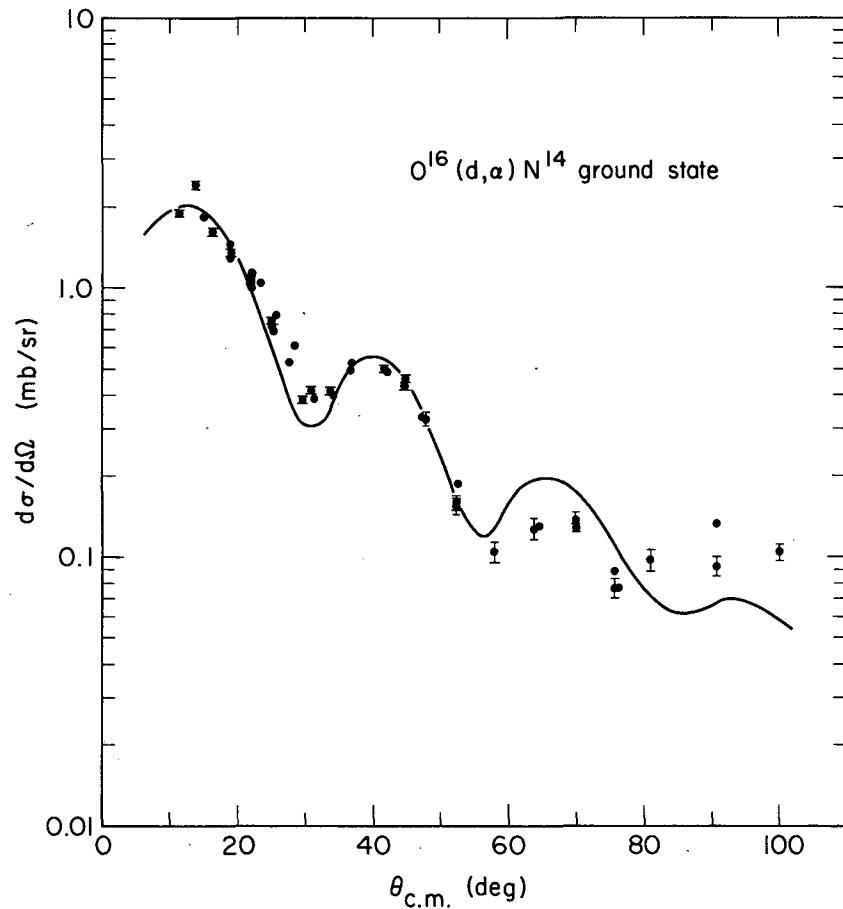
Fig. 65. Angular distribution of alpha particles from the $O^{16}(d,\alpha)N^{14}$ ground state transition. The solid line was calculated for L = 2, interaction radius = 6.00 F, and the following optical-model parameters:

	V	W	a	b	r_0	r_1
deuteron	-56	-12	0.65	0.55	1.20	0.75
alpha particle	-35	- 7	0.45	0.60	1.30	1.20
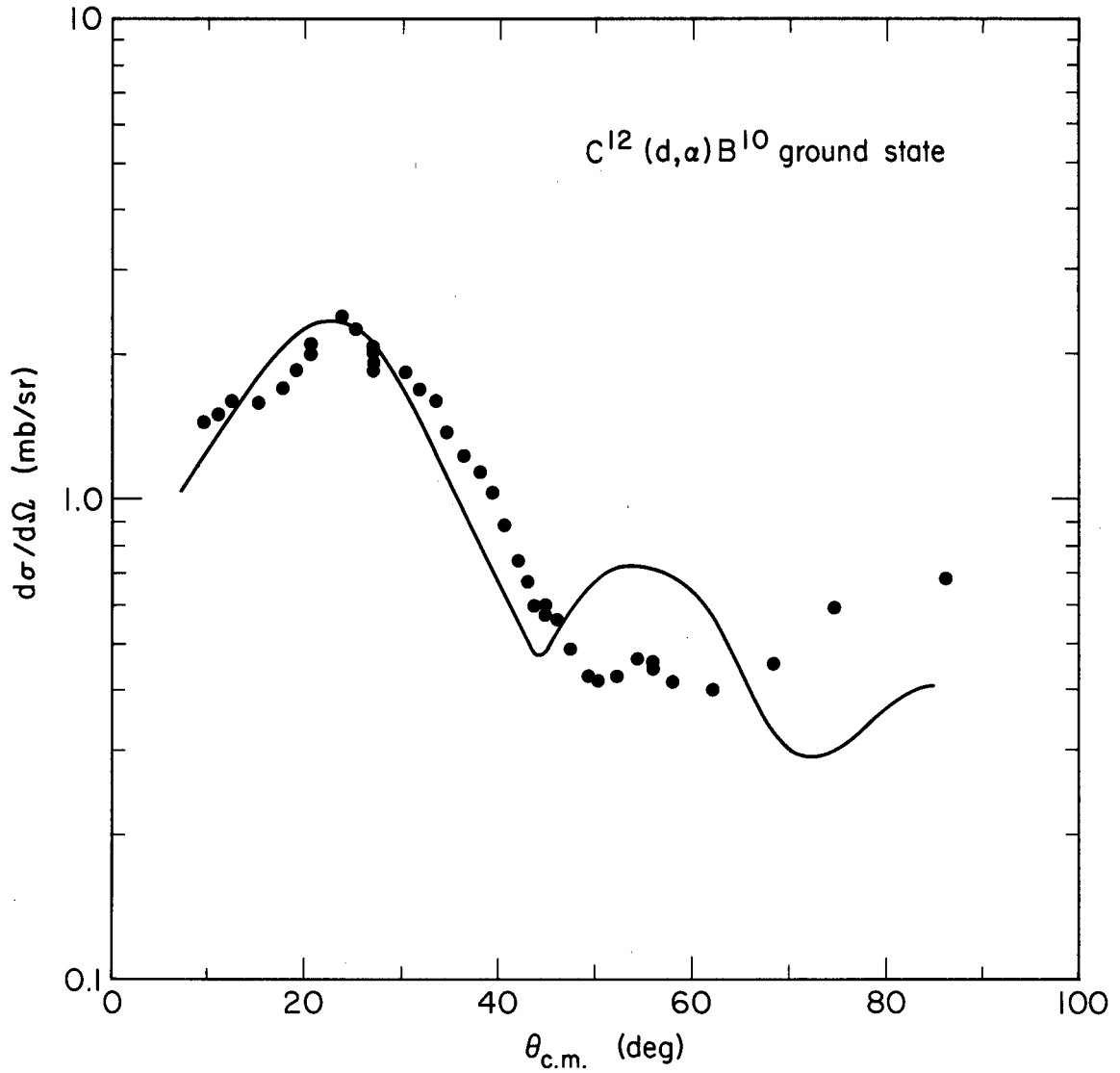
Fig. 66. Angular distribution of alpha particles from the $C^{12}(d,\alpha)B^{10}$ ground state transition. The solid line was calculated for $L = 2$, interaction radius = 4.80 F, and the following optical-model parameters:

	V	W	a	b	r_0	r_1
deuteron	-59	-13	0.60	0.60	1.20	0.75
alpha particle	-60	- 6	0.40	0.65	1.30	1.20
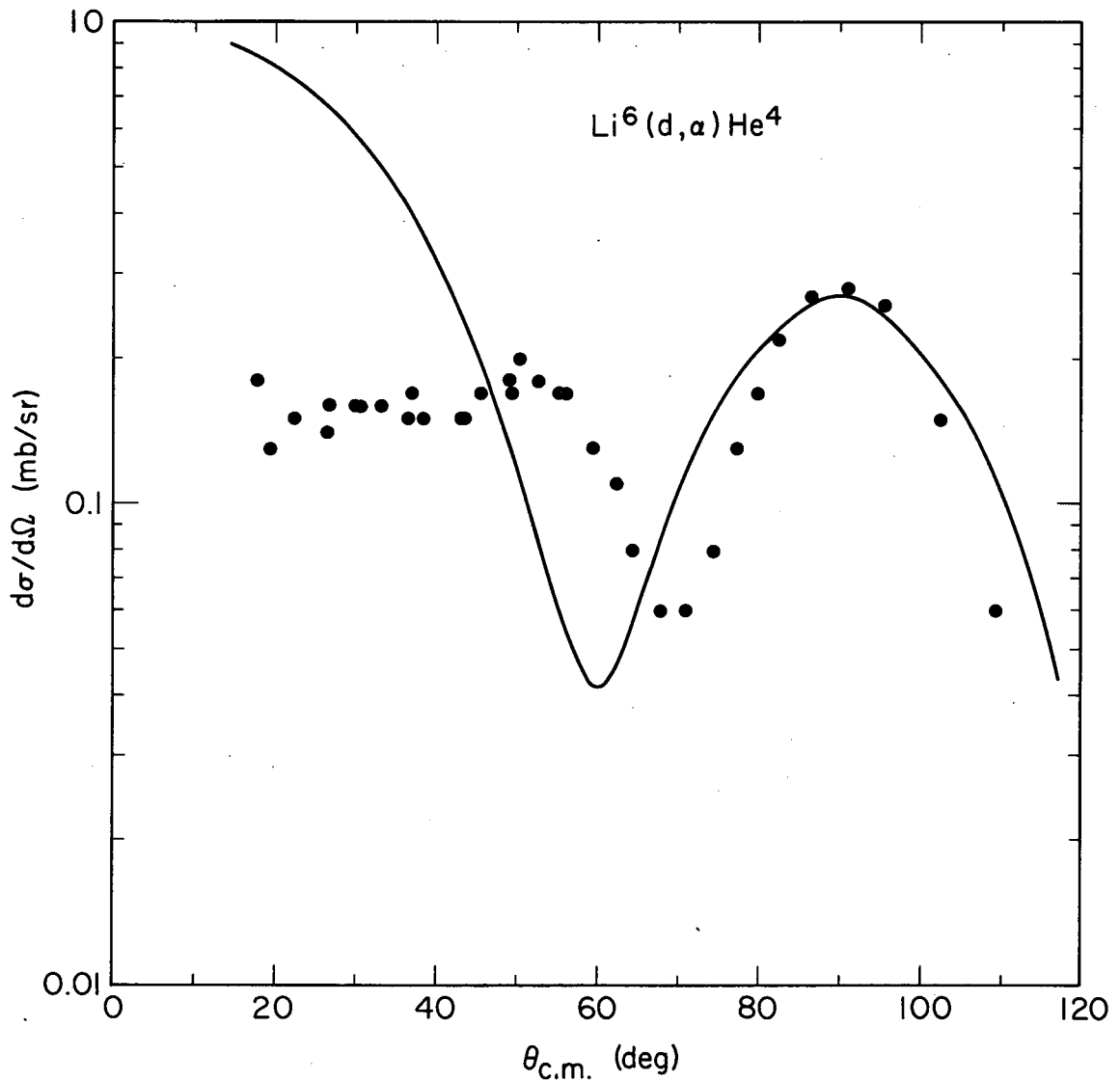
Fig. 67. Angular distribution of alpha particles from the Li^6(d,α)He^4 transition. The solid line was calculated for L = 2, interaction radius = 3.96 F, and the following optical-model parameters:

	V	W	a	b	r_0	r_1
deuteron	-47	-20	0.70	0.65	1.20	0.75
alpha particle	-50	- 1	0.30	0.50	1.14	1.00

undoubtedly pertinent to this problem also. As shown there an inhibition arises when L and $\frac{M_f}{M_i}$ $\vec{L}_d - \vec{L}_\alpha$ differ. The greater this difference the stronger will be the inhibition. Reference to Table IX illustrates that L=2 transitions would be expected to be favored, compared with L=0 transitions. Furthermore, the momentum transfer for these (d,α) reactions does not change appreciably as a function of bombarding energy, and thus L=2 should be favored at all bombarding energies. It would be interesting to analyze some of the (d,α) reactions studied at lower bombarding energies to see if L=2 is in fact favored. However, this has not been done. Another aspect that would be interesting to investigate is the following. As the value of Q is decreased, i.e., the excitation of the residual nucleus is increased, the momentum transfer diminishes. Thus L=0 transitions should account for a larger proportion of the cross section to highly excited levels. Unfortunately it is very difficult to obtain good data for such levels.

If the importance of momentum matching has not been overemphasized one should observe L=4 transitions strongly enhanced over L=2 transitions when both are allowed in reactions where two d nucleons in a triplet S configuration can be simply picked up. A study of several such reactions would yield valuable evidence in regard to the importance of momentum matching.

The enhancement of L=2 over L=0 transitions is also in accord with the predictions of the coupling scheme used by Glendenning[112] for two-nucleon transfer reactions. The nuclear structure factors arising in this model for (d,α) reactions permit only triplet S configurations for the picked-up nucleons in a scheme whereby the initial and final nuclear states are described in pure j-j coupling. These factors are defined as follows for stripping reactions.

For even-even targets

$$C_L = \left\{ a_{L1J_f} \ (j_n j_p) \right\} \tag{10}$$

where a_{LSJ} is the transformation coefficient from L-S to j-j coupling, j_n and j_p are the captured particles' total angular momenta, and the final coupling arises from $\vec{J}_f = \vec{J}_i + \vec{J}$, $\vec{J} = \vec{j}_n + \vec{j}_p$.

For odd-odd targets

$$C_L = \sum_{I=|L-1|}^{L+1} (2I+1) \left[W(J_i J_f j_n j'_p; I j_p) \ a_{L1I} \ (j_n \ j'_p) \right]^2 \tag{11}$$

where the target nucleus is considered to consist of an odd neutron and proton moving around a spin-zero core $(\vec{j}_n + \vec{j}_p = J_i)$, and one of the captured particles (j_n in the above) is required to enter the same shell-model state as one of the original pair and couple with it to zero total angular momentum; the other captured particle (j'_p) couples with j_p to form J_f.

The ratios of the structure factors obtained by using this coupling scheme are listed in Table XII. These results indicate that L=2 transitions would be strongly enhanced even if momentum-matching considerations are eliminated.

The effect produced on the calculated angular distribution by allowing the nucleons to be picked up independently has not been investigated. In the plane-wave approximation the effect does not appear to be very important.[65]

Improvements in the art of making distorted-wave calculations will undoubtedly allow one to garner more information from fitting angular distributions than is now possible. At present, however, the study of angular distributions does not appear to be as valuable as the investigation of the preferential population of final states.

Table XII. Nuclear structure factors.[a]

Reaction	Target configuration	Picked up j_n	j_p	Final configuration	Ratio of structure factors
$O^{16}(d,\alpha)N^{14}$ (g.s.)	$\left[(p_{3/2})^8_0 \ (p_{1/2})^4_0\right]_0$	$p_{1/2}$	$p_{1/2}$	$\left[(p_{3/2})^8_0 \ (p_{1/2})^2_1\right]_1$	$C_2/C_0 = 20$
$N^{14}(d,\alpha)C^{12}$ (g.s.)	$\left[(p_{3/2})^8_0 \ (p_{1/2})^2_1\right]_1$	$p_{1/2}$	$p_{1/2}$	$(p_{3/2})^8_0$	$C_2/C_0 = 20$
$N^{14}(d,\alpha)C^{12*}$ (4.43 MeV)	$\left[(p_{3/2})^8_0 \ (p_{1/2})^2_1\right]_1$	$p_{3/2}$	$p_{1/2}$	$\left[(p_{3/2})^7_{3/2} \ (p_{1/2})^1_{1/2}\right]_2$	$C_2/C_0 = 2.0$
$C^{12}(d,\alpha)B^{10}$ (g.s.)	$(p_{3/2})^8_0$	$p_{3/2}$	$p_{3/2}$	$(p_{3/2})^6_3$	Only C_2 allowed

[a] By use of coupling scheme from reference 112.

ACKNOWLEDGMENTS

-141-

APPENDIX

FORTRAN listings of the optical-model search routine GULLEY and the subroutines DIFFER and ELAS.

```
C       GULLEY 3 MAIN ROUTINE TO MINIMIZE A FUNCTION
C       WRITTEN BY R. H. PEHL AND B. D. WILKINS
        DIMENSION X(10),WT(10),G(10),EXVEC(10),XC(10),GB(10),        XB(10)
        DIMENSION DINC(10),S(10),                   XMIN(10),        XD(10),V(10)
      X   ,BB(10),D0(10),D1(10),D2(10),XBS(10)
    1 READ INPUT TAPE 2,120,NPAR,NSTEP,LMAX,LMIN,IPLOT,DEL,STEP
  120 FORMAT (5I10,2F10.5)
        READ INPUT TAPE 2,520,(X(I),I=1,10)
  520 FORMAT (4F10.6,F8.5,2F6.4,2F5.3,I2)
        READ INPUT TAPE 2,130,(WT(I),I=1,NPAR)
  130 FORMAT (7F10.5)
        WRITE OUTPUT TAPE 3,130,(WT(I),I=1,NPAR)
        NFCN = 0
        NRAT = -1
        MSTEP = -1
        WTS = WT(2)
        DMAX = LMAX
        NPARS = NPAR
        NPART = NPAR + 1
        DO 15 I = NPART,10
        XB(I) = X(I)
        XC(I) = X(I)
        XD(I) = X(I)
   15 BB(I) = X(I)
        IF (STEP) 500,20,20
   20 NPAR = NPAR - 1
        DO 200 I = 1,NPAR
        D0(I) = X(I)
        D1(I) = X(I)
  200 D2(I) = X(I)
        IF (NSTEP - 1)210,210,205
  205 CALL DIFFER (NPARS,G,F,X,DINC,NPAR,IPLOT,NSTEP,LMAX,LMIN)
  210 JPLOT = IPLOT - 1
        KPLOT = IPLOT - 2
        X(NPARS) = X(NPARS) + WT(NPARS)
  212 WT(2) = WTS*X(2)
        DO 214 I=1,NPAR
  214 DINC(I) = 0.01*ABSF(WT(I))
        CALL DIFFER (NPARS,G,F,X,DINC,NPAR,KPLOT,MSTEP,LMAX,LMIN)
        GNORM = 0.0
        DO 209 I =1,NPAR
  209 GNORM = GNORM + ABSF(G(I)/WT(I))
        GNORM = GNORM + .2
  215 WRITE OUTPUT TAPE 3,435,F,(X(I),I=1,NPARS ),(G(I), I=1,NPAR )
  219 DO 220 I = 1,NPAR
  220 EXVEC(I) = -G(I)/(GNORM*WT(I))
        DO 228 I =1,NPAR
        IF (EXVEC(I)) 223,223,224
  223 S(I) = -1.
        GO TO 225
  224 S(I) = 1.
  225 EXVEC(I) = ABSF(EXVEC(I))
  226 EXVEC(I) = SQRTF(EXVEC(I))
  228 EXVEC(I) = S(I)*EXVEC(I)
        WRITE OUTPUT TAPE 3,435,(EXVEC(I),I=1,NPAR),GNORM
        GO TO 320
  315 DO 316 I = 1,NPAR
        V(I) = 1. + ABSF(GB(I)/G(I))
  318 IF(V(I) - 10.)321,321,319
  319 V(I) = 10.
  321 IF(GB(I)/G(I))317,317,322
  317 XC(I) = (XB(I) - X(I))*(2. - V(I)) + X(I)
```

```
          GO TO 316
322 XC(I) = (XB(I) - X(I))*V(I)*1.4 + X(I)
316 CCNTINUE
          XC(NPARS) = XB(NPARS)
          GO TO 334
320 DO 330 I =1,NPAR
330 XB(I) = X(I) +        EXVEC(I)*WT(I)
          XB(NPARS) = X(NPARS)
331 CALL DIFFER (NPARS,GB,FB,XB,DINC,NPAR,KPLOT,MSTEP,LMAX,LMIN)
333 WRITE OUTPUT TAPE 3,435,FB,(XB(I),I=1,NPARS ),(GB(I),I=1,NPAR )
          GO TO 315
334 CALL DIFFER (NPARS,GC,FC,XC,DINC,NPAR,KPLOT,NSTEP,LMAX,LMIN)
          WRITE OUTPUT TAPE 3,435,FC,(XC(I),I=1,NPARS ),(V (I),I=1,NPAR )
336 RAT = (FB/FC)**2        .
          DO 340 I=1,NPAR
340 XD(I) = XB(I) + (XC(I) - XB(I))*RAT/(1.+RAT)
          XD(NPARS) = XB(NPARS)
345 CALL DIFFER (NPARS,GD,FD,XD,DINC,NPAR,IPLOT,NSTEP,LMAX,LMIN)
435 FORMAT (1P10E12.4)
          IF(F -FB)347,349,349
347 DO 348 I = 1,NPAR
348 XB(I) = X(I)
          FB = F
349 IF (FD - FC)350,352,352
350 IF (FD - FB)355,365,365
352 IF (FC - FB)360,365,365
355 DO 356 I = 1,NPAR
356 XMIN(I) =    XD(I)
          GO TO 369
360 IF(FD/FC - 1.02)358,358,359
358 NRAT = 1
359 IF(NRAT) 362,362,363
363 DO 364 I = 1,NPAR
364 XMIN(I) = XC(I)
          GO TO 369
365 IF(FD/FB-1.02)383,383,384
383 NRAT = 1
384 IF(NRAT) 372,381,381
381 DO 382 I = 1,NPAR
382 XMIN(I) = XB( I)
          GO TO 369
372 DO 373 I = 1,NPAR
373 XC(I) = 2.*XB(I) - XC(I)
          GO TO 374
362 DO 361 I = 1,NPAR
          XBS(I) = XB(I)
361 XB(I) = XC(I)
          FB = FC
371 DO 366 I = 1,NPAR
366 XC(I) = 2.*XB(I) - XBS(I)
374 WRITE OUTPUT TAPE 3,367
367 FORMAT (12H    RAT RERUN)
368 NRAT = NRAT + 1
          GO TO 334
369 IF (NSTEP - 1)1,1,370
370 DO 380 I = 1,NPAR
          DO(I) = D1(I)
          D1(I) = D2(I)
          D2(I) = XMIN(I)
          BB(I) = (D2(I) + D1(I))/2. + ((D1(I) - DO(I))-(D2(I)-D1(I)))/6.
380 X(I) = 2.*D2(I) -D1(I)+ ((D2(I)-D1(I)) - (D1(I)-DO(I)))/1.5
          BB(NPARS) = X(NPARS) - WT(NPARS)
```

```
      CALL DIFFER (NPARS,GD,FD,BB,DINC,NPAR,JPLOT,NSTEP,LMAX,LMIN)
      X(NPARS) = X(NPARS) + 2.*WT(NPARS)
      NRAT = -1
      NFCN = NFCN + 1
      DMAX = DMAX + DEL
      LMAX = DMAX + .5
      IF (NSTEP-NFCN)1,1,212
  500 STEP = 1.0
      NCYN = 1
      WT(2) = WTS*X(2)
  530 DO 532 I = 1,NPAR
  532 DINC(I) = 0.01*ABSF(WT(I))
      CALL DIFFER (NPARS,G,F,X,DINC,NPAR,IPLOT,MSTEP,LMAX,LMIN)
  534 GNORM = 0.0
      DO 521 I = 1,NPAR
  521 GNORM = GNORM + ABSF(G(I)/WT(I))
      GNORM = GNORM + .2
  535 WRITE OUTPUT TAPE 3,435,F,(X(I),I=1,NPARS ),(G(I), I=1,NPAR)
  540 DO 541 I = 1,NPAR
  541 EXVEC(I) = -G(I)/(GNORM*WT(I))
      DO 548 I =1,NPAR
      IF (EXVEC(I)) 543,543,544
  543 S(I) = -1.
      GO TO 545
  544 S(I) = 1.
  545 EXVEC(I) = ABSF(EXVEC(I))
  546 EXVEC(I) = SQRTF(EXVEC(I))
  548 EXVEC(I) = S(I)*EXVEC(I)
      WRITE OUTPUT TAPE 3,435,(EXVEC(I),I=1,NPAR),GNORM
  569 DO 570 I = 1,NPAR
      XB(I)= X(I) +         EXVEC(I) * WT(I)
  570 GB(I) = G(I)
      IF(NSTEP- NCYN)572,572,571
  572 CALL DIFFER (NPARS,GB,FB,XB,DINC,NPAR,IPLOT,NSTEP,LMAX,LMIN)
      GO TO 999
  571 CALL DIFFER (NPARS,GB,FB,XB,DINC,NPAR,IPLOT,MSTEP,LMAX,LMIN)
  573 WRITE OUTPUT TAPE 3,435,FB,(XB(I),I=1,NPARS ),(GB(I),I=1,NPAR)
  580 DO 590 I = 1,NPAR
      IF(GB(I)/G(I))585,585,590
  585 WT(I) = WT(I)/2.
  590 CONTINUE
  605 DO 610 I = 1,NPAR
      X(I) = XB(I)
  610 G(I) = GB(I)
  620 NCYN = NCYN + 1
      GO TO 534
  999 CALL EXIT
      END
```

```
      SUBROUTINE DIFFER (NPARS,G,F,X,DINC,NPAR,IPLOT,NOW,MAX,MIN)
      DIMENSION G(10),X(10),DINC(10),GF(10),XT(10),WT(10)
C     THIS SUBROUTINE COMPUTES THE DERIVATIVE VECTOR G(I) BY TAKING
C      FINITE DIFFERENCES
      DO 20 I = 1,10
   20 XT(I)=X(I)
      CALL ELAS(IPLOT,MAX,MIN,X,CHIT)
      F= CHIT
      IF(NOW)25,25,110
   25 JPLOT = 0
      DO 100 I = 1,NPAR
      XT(I)=X(I) + DINC(I)
      CALL ELAS(JPLOT,MAX,MIN,XT,CHIT)
      FD = CHIT
      XT(I)=X(I)
  100 G(I)=(FD-F )/F
  110 RETURN
      END
```

```
      SUBROUTINE ELAS(IPLOT,MAX,MIN,X,CHIT)
C     ELASTIC SCATTERING        N K GLENDENNING
C     MODIFIED BY R H PEHL  AND B D WILKINS
      DIMENSION  CR(100),CI(100),SIG(100),TH(180),CRSX(183),RUTH(183),
     X RELA(183)
     X ,RAD(180),CO(180),SO(180),GO(180),ASL(100,90)
     X ,PHIR(100),PHII(100)
     X ,CHI(100),DATA(100),WTS(100),X(10),          CHIS(100)
C
C         NOTATION
C         H1,H2      =     INTEGRATIONSTEPS,H1 FOR FIRST 20 STEPS
C         RMAX       =     MATCHING RADIUS
C         THETM      =     MAXIMUM ANGLE TO WHICH CROSS SECTION IS COMPUTED
C         DTHET      =     ANGLE INCREMENT
C         ELAB       =     LAB ENERGY OF PROJECTILE
C         CMP        =     PROJECTILE MASS IN AMU
C         CMT        =•    TARGET MASS IN AMU
C         ZZP        =     PRODUCT OF CHARGES
C         MAX        =     MAXIMUM L WAVE COMPUTED
C         VR         =     REAL WELL DEPTH
C         VI         =     IMAGINARY WELL DEPTH
C         RO         =     RADIUS PARAMETER MULTIPLYING A**1/3
C         R1         =     PROJECTILE RADIUS
C                          TOTAL RADIUS = RO * A**1/3 + R1
C                          COULOMB RADIUS = RO * A**1/3
C         AO         =     SURFACE THICKNESS OF REAL WELL
C         BO         =     SURFACE THICKNESS OF IMAGINARY WELL
C         ALPHA      =     IF = O THEN PURE SAXON IMAGINARY WELL
C                          IF = 1 THEN PURE GAUSSIAN SURFACE WELL
C                          IF = BETWEEN THEN LINEAR MIXTURE
C         BETA       =     IF = O THEN RW = RO
C                          IF = 1 THEN RW DIFFERENT FROM RO
C         MODE       =     IF POSITIVE DATA IN FM/STER
C                          IF ZERO OR NEGATIVE THEN DATA/RUTH
C         IPLOT      =     O  NO PLOT
C                          1  PLOTS START,D
C                          2  PLOTS START,D,BB
C                          3  PLOTS START,D,BB,A,B,C,RAT RERUN
C
      IF (NUFF - 37) 111,524,111
  111 NUFF = 37
    1 READ INPUT TAPE 2,490,CHECK,KIN,KEND,MODE,(DATA(JJ), JJ=KIN,KEND)
  490 FORMAT (F5.1,3I5/ (7F10.4))
      WRITE OUTPUT TAPE 3,493,(DATA(JJ), JJ = KIN,KEND)
  493 FORMAT (12F10.4)
    2 READ INPUT TAPE 2,491,(WTS(J),J=KIN,KEND)
  491 FORMAT (14F5.3)
      WRITE OUTPUT TAPE 3,494,(WTS(J), J=KIN,KEND)
  494 FORMAT (24F5.3)
   10 READ INPUT TAPE 2,500,H1,H2,RMAX,THETM,DTHET,IPLOT,MINEXP,MAXEXP
      NANGLE = THETM/DTHET + 1.001
      IF(NANGLE-180)15,15,600
   15 DO 16 K=1,NANGLE
      A=K
      TH(K)=(A-1.)*DTHET
      TH(1) = 0.10E-07
      RAD(K)=TH(K)*    0.17453295E-01
      CO(K)=COSF(RAD(K))
      SO(K)=SINF(RAD(K)/2.)**2
   16 GO(K)=LOGF(SO(K))
   20 READ INPUT TAPE 2,510,ELAB,CMP,CMT,ZZP,MAX,LMIN
  524 IF(MAX - KMAX)21,523,21
```

```
   21 KMAX = MAX
      MMAX =MAX + 1
   23 NMAX = MAX - 1
      DO 70 K = 1,NANGLE
      CO = CO(K)
      ASL(1,K) = 1.0
      ASL(2,K) = CO(K)
      DO 60 L = 1,NMAX
      CL = L
   60 ASL(L+2,K) =              ((2.*CL+1.)*CO*ASL(L+1,K) - CL*ASL(L,K))/
     X     (CL + 1.)
      DO 70 L = 1,MMAX
      CL = L - 1
   70 ASL(L,K) = (2.*CL + 1.)*ASL(L,K)
  500 FORMAT (5F10.4,3I5)
  510 FORMAT (4F10.6,2I10)
  523 VR = X(1)
      VI = X(2)
      AO = X(3)
  525 BO = X(4)
      RO = X(5)
      R1 = X(6)
      RW = X(7)
      ALPHA = X(8)
      BETA = X(9)
      KCNT = X(10)
  529 RE=   RO*CMT**0.33333333
      R=   RE + R1
      RWS= RW*CMT**0.33333333        + R1
  530 CALL OPTIC(R,ELAB,CMP,CMT,ZZP,R ,AO,BO, RE,VR,VI,ALPHA,MAX,RMAX,
     X   H1,H2,PHIR,PHII,RINTP,CR,CI,SIG,CK,ETA,RWS,BETA,LMIN)
C     LOOP ON ANGLE
  100 DO    300    K=1,NANGLE
      Y=ETA*GO(K)
      Z= ETA/2./SO(K)
      SUM1 = -Z * COSF(Y)
      SUM2 =  Z * SINF(Y)
      RUTH(K) =    (Z / CK)**2
C     LOOP ON L WAVE
      DO  200    M=1,MMAX
      Y=ASL(M,K)
      Z     =    2.*(SIG(M)-SIG(1))
      SI= SINF(Z)
      CS= COSF(Z)
      SUM1 = SUM1 + ( CS *CR(M) - SI *CI(M) ) * Y
  200 SUM2 = SUM2 + ( CS *CI(M) + SI *CR(M) ) * Y
      CRSX(K) = (SUM1 **2 + SUM2 **2 )/CK**2
  300 RELA(K) = CRSX(K)/RUTH(K)
      IF (MODE)305,305,301
  301 DO 303 K = KIN,KEND
  303 DATA(K) = DATA(K)/RUTH(K)
      WRITE OUTPUT TAPE 3,493,(DATA(JJ), JJ = KIN,KEND)
      MODE = 0
  305 WRITE OUTPUT TAPE 3,700
      WRITE OUTPUT TAPE 3,710,ELAB,CMP,CMT,ZZP,VR,VI,ALPHA,BETA,RO,R1,
     X   RW,AO,BO,ETA,CK
      WRITE OUTPUT TAPE 3,720
  400 MM=(NANGLE+2)/3
  420 DO  430 K =1,MM
      I= MM+K
      J= I+MM
  430 WRITE OUTPUT TAPE 3,730,TH(K),CRSX(K),RELA(K),TH(I),CRSX(I),
```

```
      X     RELA(I),TH(J),CRSX(J),RELA(J)
            WRITE OUTPUT TAPE 3,750
            REAC=0.
            DO 440 M=1,MMAX
            L=M-1
            TAN= 2.*CR(M)/(1.-2.*CI(M))
            TRANS =4.*(CI(M)-CI(M)**2-CR(M)**2)
            C=L
            REAC=REAC+ (2.*C+1.)*TRANS
  440 WRITE OUTPUT TAPE 3,760,L,CR(M),CI(M),SIG(M),PHIR(M),PHII(M)
      2   ,TAN,TRANS
            REAC=REAC*3.14159/CK**2
            WRITE OUTPUT TAPE 3,770       ,REAC
            WRITE OUTPUT TAPE 3,740,MAX,RMAX,H1,H2   ,RINTP
  800 CHIM = 0.0
            CHIST = 0.0
  810 K = 1
  815 GO TO 820
  817 K = K + 1
  820 AA = K
  830 TH(K) = (AA -1.)*DTHET
  848 IF(TH(K) -CHECK)817,850,850
  850 DIV = (RELA(K) + RELA(K+1))*(DATA(K) + DATA(K+1))
            REL = RELA(K) - RELA(K+1)
            DAT = DATA(K) - DATA(K+1)
            CHI(K) = ((RELA(K) + RELA(K+1) - (DATA(K) + DATA(K+1)))/
      X     WTS(K))**2/DIV/25.
            IF (DAT/REL)860,870,870
  860 CHIS(K) = ((REL-DAT)/WTS(K))**2/DIV/2.
            GO TO 890
  870 CHIS(K) = (REL -DAT)/WTS(K)/SQRTF(DIV)
  890  CHIS(K) = ABSF(CHIS(K))
            IF(CHIS(K) -   50.)900,900,903
  903 CHIS(K) = 50.
  900 IF(CHI(K) -   50.)906,906,907
  907 CHI(K) = 50.
  906 CHIM = CHIM + CHI(K)
            CHIST = CHIST + CHIS(K)
  901 IF(K - KEND)817,902,902
  902 CHIT = CHIM           + CHIST
  905 WRITE OUTPUT TAPE 3,910,CHIT            ,CHIM,     CHIST
  910 FORMAT( 7H CHIT=F12.4,  7H  CHIM=F12.4,  7H CHIST=F12.4 /1H1)
            IF( IPLOT)590,590,450
  450 DO 470 K=1,NANGLE
            Y = RELA(K)
            CYCLE=MAXEXP-MINEXP
            NPLOT=  100./CYCLE *0.4343 *LOGF(Y/10.**MINEXP)+0.5
            CALL GRAPH(NPLOT,0,0)
            Y = DATA(K)
            NPLOT=  100./CYCLE *0.4343 *LOGF(Y/10.**MINEXP)+0.5
            CALL GRAPH (NPLOT,44,-1)
  470 WRITE OUTPUT TAPE 3,780,TH(K)
  700 FORMAT(      39H1    ELASTIC SCATTERING CROSS SECTION I ///)
  710 FORMAT(       9H    ELAB=F10.6,    8H     CM =F10.6,    8H    CMT=
      XF10.6,         8H    ZZP=F10.6//  7H   VR=F10.6,    7H    VI=
      XF10.6,        10H  ALPHA=F5.3,    8H   BETA=F3.1// 7H   RO=F10.6,
      X  7H    R1=F10.6,      7H    RW=F6.3,
      X  7H    A0=F10.6,      7H    B0=F10.6//
      X  8H   ETA=F10.6,      6H    K=F10.6//)
  720 FORMAT(    113H       THETA         CRSX       CRSX/RUTH          THETA
      X    CRSX       CRSX/RUTH        THETA       CRSX       CRSX/RUTH//)
  730 FORMAT( 3(0PF12.1,1P2E13.4))
```

```
740 FORMAT(9H0    LMAX=I3, 9H    RMAX=F10.4, 7H    H1=F10.4, 7H    H2=
   X F10.4,   10H   RINTP=F10.4//)
750 FORMAT(    110H0           L           CR           CI           SIG
   X         PHIR          PHII          TAN          T(L)//)
760 FORMAT(I10,7E15.5)
770 FORMAT(    28H0   REACTION CROSS SECTION =1PE15.5)
780 FORMAT(1H+F8.4)
590 GO TO (10,20,591),KCNT
591 RETURN
600 CALL EXIT
    END
```

REFERENCES

1. M. H. MacFarlane and J. B. French, Rev. Mod. Phys. 32, 567 (1960).

2. S. Hinds and R. Middleton, Proc. Phys. Soc. (London) 74, 762 (1959).

3. B. G. Harvey and J. Cerny, Phys. Rev. 120, 2162 (1960).

4. A. A. Jaffe, F. S. Barros, P. D. Forsyth, J. Huto, J. J. Taylor, and S. Ramavataram, Proc. Phys. Soc. (London) 76, 914 (1960).

5. W. Tobocman, Phys. Rev. 115, 98 (1959).

6. N. K. Glendenning (Lawrence Radiation Laboratory, Berkeley, California), private communication.

7. This point was first discussed by R. K. Adair, Phys. Rev. 87, 1041 (1952).

8. B. L. Cohen and A. G. Rubin, Phys. Rev. 114, 1143 (1959).

9. J. B. Mead and B. L. Cohen, Phys. Rev. Letters 5, 105 (1960).

10. R. E. Ellis, R. G. Summers-Gill, and F. J. Vaughn (private communication to Homer E. Conzett, Lawrence Radiation Laboratory, Berkeley, California).

11. H. Bichsel, R. F. Mozley, and W. A. Aron, Phys. Rev. 105, 1788 (1957).

12. R. E. Ellis and L. Schecter, Phys. Rev. 101, 636 (1956).

13. G. E. Fischer, Phys. Rev. 96, 704 (1954).

14. R. G. Summers-Gill, Phys. Rev. 109, 1591 (1958).

15. See, for example, J. W. Mayer, J. Appl. Phys. 30, 1937 (1959).

16. W. L. Briscoe, Rev. Sci. Instr. 29, 401 (1958).

17. R. H. Stokes, J. A. Northrup, and K. Boyer, Rev. Sci. Instr. 29, 61 (1958).

18. M. S. Livingston and H. A. Bethe, Rev. Mod. Phys. 9, 263 (1937).

19. H. E. Wegner, Semiconductor Nuclear Particle Detectors, in Proceedings on an Informal Conference, Asheville, North Carolina, September 1960; National Academy of Sciences, National Research Council, Nuclear Science Series Report 32 (1961), p. 74 (NAS, NRC Pub. No. 871).

20. These standard counters were developed by W. L. Hansen, Lawrence Radiation Laboratory, Berkeley, California.

21. P. T. Andrews, Thin Silicon Surface Barrier Counters, in Proceedings of the Symposium on Nuclear Instruments, Harwell, September 1961 (Academic Press, Inc., New York, 1962).

22. Bruno Rossi, High-Energy Particles (Prentice-Hall, Inc., Englewood Cliffs, New Jersey, 1952), Chap. 2.

23. J. H. Elliott, Nucl. Instr. Methods 12, 60 (1961).

24. R. J. Silva, Mechanism of the (α, pn) Reaction (Ph.D. Thesis) Lawrence Radiation Laboratory Report UCRL-8678, March, 1959 (unpublished).

25. J. Cerny, Two-Nucleon Transfer Reactions in the Light Elements (Ph.D. Thesis), Lawrence Radiation Laboratory Report UCRL-9714, May, 1961 (unpublished).

26. W. A. Aron, B. G. Hoffman, and F. C. Williams, Range-Energy Curves, Atomic Energy Commission Report AECU-663, May 1951 (unpublished).

27. B. G. Harvey, J. Cerny, R. H. Pehl, and E. Rivet, Nucl. Phys. 39, 160 (1962).

28. Y. Nagahara, J. Phys. Soc. Japan 16, 133 (1961).

29. H. E. Conzett, Phys. Rev. 105, 1324 (1957).

30. D. Halliday, Introductory Nuclear Physics, (John Wiley and Sons, Inc., New York, 1955), p. 315.

31. K. B. Mather and P. Swan, Nuclear Scattering, (Cambridge University Press, New York, 1958), Chap. 2.

32. F. Ajzenberg-Selove and T. Lauritsen, Nucl. Phys. 11, 1 (1959).

33. J. M. F. Jeronymo, G. S. Mani, F. Picard, and A. Sadeghi, Nucl. Phys. 38, 11 (1962).

34. E. W. Hamburger and J. R. Cameron, Phys. Rev. 117, 781 (1960).

35. B. Zeidman (Argonne National Laboratory, Argonne, Illinois), private communication.

36. V. J. Ashby and H. C. Catron, Tables of Nuclear Reaction Q Values, Lawrence Radiation Laboratory Report UCRL-5419, Feb. 1959 (unpublished).

37. N. A. Vlasov, S. P. Kalinin, A. A. Ogloblin, L. N. Samoilov, V. A. Sidorov, and V. I. Chuev, J. Exptl. Theoret. Phys. U.S.S.R. 28, 639 (1955) [translation: Soviet Phys. JETP 1, 500 (1955)].

38. H. B. Willard, J. K. Bair, and J. D. Kingston, Phys. Rev. 90, 865 (1953).

39. G. F. Bogdanov, N. A. Vlasov, S. P. Kalinin, B. V. Rybakov, and V. A. Sidorov, Physica $\underline{22}$, 1150 (1956).

40. H. Tyrén, G. Tibell, and Th. A. J. Maris, Nucl. Phys. $\underline{4}$, 277 (1957).

41. J. Sawicki, Acta Phys. Polon. $\underline{15}$, 71 (1956).

42. H. E. Conzett, G. Igo, H. C. Shaw, and R. J. Slobodrian, Phys. Rev. $\underline{117}$, 1075 (1960).

43. B. H. Flowers, in Proceedings of the International Conference on Nuclear Structure, Kingston, Canada, 1960, edited by D. A. Bromley and E. W. Vogt (University of Toronto Press, Toronto, 1960), p. 417.

44. T. Lauritsen and F. Ajzenberg-Selove, "Energy Levels of Light Nuclei-May 1962," Nuclear Data Sheets, National Academy of Sciences - National Research Council, Washington, D. C.

45. K. Wildermuth, in Proceedings of the International Conference on Nuclear Structure, Kingston, Canada, 1960, edited by D. A. Bromley and E. W. Vogt (University of Toronto Press, Toronto, 1960), p. 418.

46. Y. C. Tang, K. Wildermuth, and L. D. Pearlstein, Phys. Rev. $\underline{123}$, 548 (1961).

47. A. B. Clegg, Nucl. Phys. $\underline{33}$, 194 (1962).

48. H. E. Gove and J. A. Harvey, Phys. Rev. $\underline{82}$, 658 (1951).

49. S. H. Levine, R. S. Bender, and J. N. McGruer, Phys. Rev. $\underline{97}$, 1249 (1955).

50. F. C. Khanna, Y. C. Tang, and K. Wildermuth, Phys. Rev. $\underline{124}$, 515 (1961).

51. T. A. Tombrello and G. C. Phillips, Phys. Rev. $\underline{122}$, 224 (1961).

52. P. D. Kunz, Ann. Phys. (N.Y.) $\underline{11}$, 275 (1960).

53. F. Pellegrini, Nucl. Phys. $\underline{24}$, 372 (1961).

54. J. Catalá, A. Bonet, and E. Villar, Anales Real Soc. Espan. Fis. Quim (Madrid) $\underline{A54}$, 241 (1958).

55. A. M. Lane and R. G. Thomas, Rev. Mod. Phys. $\underline{30}$, 257 (1958).

56. E. L. Sprenkel, J. W. Olness, and R. E. Segel, Phys. Rev. Letters $\underline{7}$, 174 (1961).

57. D. Kurath, Phys. Rev. $\underline{101}$, 216 (1956).

58. W. W. True and E. K. Warburton, Nucl. Phys. $\underline{22}$, 426 (1961).

59. D. R. Inglis, Phys. Rev. $\underline{87}$, 915 (1952).

60. D. R. Inglis, Rev. Mod. Phys. 25, 390 (1953).

61. K. Ono and K. Kuroda, Phys. Rev. 117, 214 (1960).

62. C. D. Zafiratos, A Study of Two Nucleon Stripping and Two Nucleon Pickup Reactions in Light Nuclei (Ph.D. Thesis), University of Washington, Seattle, May 1962 (unpublished).

63. W. A. Schier, C. P. Browne, and I. F. Wright, Bull. Am. Phys. Soc. 6, 416 (1961).

64. I. Talmi and I. Unna, Ann. Rev. Nucl. Sci. 10, 390 (1960).

65. N. K. Glendenning, Nuclear Stripping Reactions, Ann. Rev. Nucl. Sci. (1964) (to be published).

66. M. A. Nagarajan (Department of Physics, Case Institute of Technology, Cleveland, Ohio), private communication.

67. F. J. Vaughn, Elastic and Inelastic Scattering of 48 MeV Alpha Particles by Carbon and Magnesium (Ph.D. Thesis), University of California Radiation Laboratory Report UCRL-3174, October 1955 (unpublished).

68. E. Rivet and J. Cerny (Lawrence Radiation Laboratory, Berkeley, California) private communication.

69. E. K. Warburton and W. T. Pinkston, Phys. Rev. 118, 733 (1960).

70. I. Talmi and I. Unna, Ann. Rev. Nucl. Sci. 10, 353 (1960).

71. W. W. True, Phys. Rev. 130, 1530 (1963).

72. B. G. Harvey and E. Rivet (Lawrence Radiation Laboratory, Berkeley, California), private communication.

73. E. Kashy, R. R. Perry, R. L. Steele, and J. R. Risser, Phys. Rev. 122, 884 (1961).

74. D. H. Wilkinson, in Proceedings of the International Conference on Nuclear Structure, Kingston, Canada, 1960, edited by D. A. Bromley and E. W. Vogt (University of Toronto Press, Toronto, 1960), p. 23.

75. R. J. Van de Graaff, A. Sperduto, W. W. Buechner, and H. A. Enge, Phys. Rev. 86, 966 (1952).

76. C. Hu, J. Phys. Soc. Japan 15, 1741 (1960).

77. T. Yanabu, J. Phys. Soc. Japan 16, 2118 (1961).

78. W. M. Macdonald, <u>Nuclear</u> <u>Spectroscopy</u>, <u>Part B,</u> edited by F. Ajzenberg-Selove (Academic Press, Inc., New York, 1960), p. 932.

79. D. H. Wilkinson, Phil. Mag.[8] $\underline{1}$, 379 (1956).

80. G. E. Fischer and V. K. Fischer, Phys. Rev. $\underline{114}$, 533 (1959).

81. Ibid. $\underline{121}$, 1863 (1961).

82. Y. Hashimoto and W. Parker Alford, Phys. Rev. $\underline{116}$, 981 (1959).

83. T. H. Braid and B. Zeidman, Bull. Am. Phys. Soc. $\underline{7}$, 300 (1962).

84. S. T. Butler, N. Austern, and C. Pearson, Phys. Rev. $\underline{112}$, 1227 (1958).

85. M. K. Bannerjee, <u>Nuclear</u> <u>Spectroscopy</u>, <u>Part B,</u> edited by F. Ajzenberg-Selove, (Academic Press, Inc., New York, 1960), p. 703.

86. J. Cerny, B. G. Harvey, and R. H. Pehl, Nucl. Phys. $\underline{29}$, 120 (1962).

87. R. J. Wilson, Investigation of (d,α) Reactions on Be^9, N^{14}, F^{19}, and P^{31} (Ph.D. Thesis) Washington University, St. Louis, June 1963 (unpublished).

88. J. B. Ball, C. B. Fulmer, and C. D. Goodman, Phys. Rev. $\underline{130}$, 2342 (1963).

89. K. Takamatsu, J. Phys. Soc. Japan $\underline{17}$, 896 (1962).

90. S. Yoshida, Phys. Rev. $\underline{123}$, 2122 (1961).

91. S. Yoshida, Nucl. Phys. $\underline{33}$, 685 (1962).

92. A. E. Glassgold and A. Galonsky, Phys. Rev. $\underline{103}$, 701 (1956).

93. G. E. Owen and L. Madansky, Phys. Rev. $\underline{105}$, 1766 (1957).

94. W. Tobocman and W. R. Gibbs, Phys. Rev. $\underline{126}$, 1076 (1962).

95. E. M. Henley and B. A. Jacobsohn, Phys. Rev. $\underline{108}$, 502 (1957).

96. E. M. Henley and B. A. Jacobsohn, Phys. Rev. $\underline{113}$, 225 (1959).

97. A. M. Baldin, V. I. Gol'danskii, and I. L. Rozenthal, <u>Kinematics of Nuclear Reactions,</u> translated by W. E. Jones, (Pergamon Press, Ltd., New York, 1961), p. 141.

98. J. C. Legg, Phys. Rev. $\underline{129}$, 272 (1963).

99. B. D. Wilkins, Total-Reaction Cross-Section Measurements for Charged Particles (Ph.D. Thesis), Lawrence Radiation Laboratory Report UCRL-10783, May, 1963 (unpublished).

100. M. A. Melkanoff, D. S. Saxon, J. S. Nodvik, and D. G. Cantor, <u>A FORTRAN Program for Elastic-Scattering Analyses with the Nuclear Optical Model</u> (University of California Press, Berkeley, 1961).

101. J. S. Nodvik and D. S. Saxon, Phys. Rev. 117, 1539 (1960).

102. R. J. Slobodrian, Phys. Rev. 125, 1003 (1962).

103. H. J. Erramuspe and R. J. Slobodrian, Nucl. Phys. 34, 532 (1962).

104. S. Mayo and J. E. Testoni, Nucl. Phys. 36, 615 (1962).

105. J. C. Jodogne, P. C. Macq, and J. Steyaert, Phys. Letters 2, 325 (1962).

106. J. Aguilar, W. E. Burcham, J. Catalá, J. B. A. England, J. S. C. McKee, and J. Rotblat, Proc. Roy. Soc. (London) A254, 395 (1960).

107. T. Mikumo (private communication to George Igo, Lawrence Radiation Laboratory, Berkeley, California).

108. J. S. Blair (University of Washington, Seattle, Washington), private communication.

109. A. G. Blair and H. E. Wegner, Phys. Rev. 127, 1233 (1962).

110. B. Zeidman, J. L. Yntema, and B. J. Raz, Phys. Rev. 120, 1723 (1960).

111. C. D. Goodman, J. B. Ball, and C. B. Fulmer, Phys. Rev. 127, 574 (1962).

112. N. K. Glendenning, Nucl. Phys. 29, 109 (1962).